Composites of Lyotropic Lamellar Systems and Micro-Particles

Von der Fakultät für Naturwissenschaften
Department Chemie
der Universität Paderborn

zur Erlangung des Grades eines
Doktors der Naturwissenschaften
–Dr. rer. nat.–
genehmigte Dissertation

von

Shahram Shafaei

aus Tabriz (Iran)

Paderborn 20.07.2007

Die vorliegende Arbeit wurde in der Zeit von Januar 2004 bis Juni 2007 im Fachgebiet Physikalische Chemie am Department Chemie der Fakultät für Naturwissenschaften der Universität Paderborn unter Anleitung von Prof. Dr. Claudia Schmidt angefertigt.

Referent:	Prof. Dr. Claudia Schmidt
Korreferent:	Prof. Dr. Wolfgang Bremser

Eingereicht am:	29.06.2007
Mündliche Prüfung am:	20.07.2007

Acknowledgements

There are many people, in different ways, who have contributed to the realization of this thesis.

First of all, I wish to express my thanks to my supervisor *Prof. Dr. Claudia Schmidt,* who gave me the opportunity to obtain my PhD at Paderborn University. Thank you very much for your scientific guidance, invariable support, patience and always being open for discussions.
Prof. Dr. W. Bremser, for scientific insight and open discussions about micro-particles.

Dr. A. Imhof, from Utrecht University, for providing the PMMA micro-particles.
Prof. Dr. U. Olsson, who gave me the opportunity to work in the Department of Physical Chemistry 1 at Lund University.
Bruno Medronho from Coimbra and Lund University for scientific curiosity, fruitful collaboration, it was a real pleasure to work with you! I am grateful to have you as a friend.
Dr. H. Egold and *Prof. Dr. Marsmann* for NMR measurements.
Dr. S. Herres-Pawlis for reading my thesis.
Prof. Dr. N. Sinyavsky for helping with analysis of the NMR data with the Mat.Lab program.
Houman Shirzadi, for helping with analysis of the data using the Origin program.

I want to thank everyone involved at the department of Physical Chemistry:
Prof. Dr. H. Kitzerow, *Dr. K. Hiltrop* for helping to do the SAXS measurements, *Richard Szopko*, for the invaluable help to install Windows XP and other administrative works, *Dr. S. Benning* and *Dr. A. Hoischen,* for their support in our department, *Dr. T. Kramer*, for giving me interesting ideas about synthesis of the nano-particles, *Gisela Jünnemann*, for helping to synthesize the particles, I also learnt a lot about German culture from her. *Claudia Stehr* helped me in performing AFM measurements, *Frau Koralewicz,* for the fast handling of bureaucratic works.

I would like to take the opportunity to thank these friends who also helped in one way or another: *Y. Wang, M. Blaschke, Dr. L. Majoros, M. Perez, G. Ar, H. Matthias, K. Hillmann, S. Lages, F. Klama, H. Behling* and *R. Nouroozi.*

Frank Imgrund, my best friend, who was cheering me up while in Germany.

Finally, I extend my warmest thanks to **my family**, who always provided me with love and encouragement and supported me through all the years.

Presentations and Publications

- B. Medronho, S. Shafaei, M. G. Miguel, U. Olsson, C. Schmidt, "*From Layers to Onions and Vice-versa: Continuous versus Discontinuous Shear-Induced Transformations of the L_α Phase*", Poster, **International Soft Matter Conference**, Eurogress Aachen, Germany, 1-4 October 2007.
- B. Medronho, S. Shafaei, R. Szopko, M. G. Miguel, U. Olsson, C. Schmidt, "*Shear-induced structural transformations of the lyotropic lamellar phase: Continuous or discontinuous transition?"*, Poster, **21th Conference of the European Colloid and Interface Society,** Geneva, Switzerland, 10-14 September 2007.
- S. Shafaei, B. Medronho, C. Schmidt, M. G. Miguel, U. Olsson, "*Transition from Lamellar phase to Multi-lamellar Vesicles and Vice-Versa",* Poster, **6th Annual Surface and Colloid Symposium**, Lund, Sweden, 15-17 November, 2006.
- S. Shafaei, C. Schmidt, "*Rheo-NMR Study of the Shear-Induced Formation of Multi-lamellar Vesicles in Lamellar System Filled with Micro Particles",* Poster, **26th Annual GDCh Meeting on Magnetic Resonance "Novel Applications of Magnetic Resonance to Condensed Matter"**, Tübingen, Germany, 28-30 September 2006.
- S. Shafaei, M. Blaschke, C. Schmidt, "*Influence of Spherical Particles on the Shear-Induced Orientation States of a Lamellar Phase"*, Poster, **3rd Zsigmondy-Kolloquium**, Berlin, Germany, 6-7 April 2006.
- S. Shafaei, C. Schmidt, "*Mixtures of Colloidal Spheres and Lamellar Surfactant Phases*", Poster, **42th Meeting of the German Colloid Society**, Aachen, Germany, 24-28 September 2005.
- S. Shafaei, C. Schmidt, "Hybrid Systems of Bilayer Membranes and Colloid Particles", Oral, **NMR Spring Workshop**, Pottenstein, Germany, 12 March 2006.
- B. Medronho, S. Shafaei, C. Schmidt, M. G. Miguel, U. Olsson, "*Transition from L_α phase to MLVs and Vice-Versa: Coexistence versus Incomplete Transformation",* in preparation
- S. Shafaei, C. Schmidt, "*Identification of the nematic phase in the lecithin/water/n-decane system*", in preparation
- S. Shafaei, C. Schmidt, "*Influence of Micro-Particles on the Shear-Induced Formation of Multi-lamellar Vesicles in Lamellar System",* in preparation.

Content

1 Introduction

The self assembly of amphiphilic molecules (surfactants) in solution has been the subject of intensive research in the past decades. It is well known that aqueous solutions of amphiphilic molecules tend to form different types of aggregates such as spherical aggregates, rod-like aggregates, packed bilayers (lamellar or L_α phase) and various other liquid crystalline structures. The richness of these phenomena is used in many applications, including foods, animal feeds, pharmaceuticals, cosmetics, detergents and mineral processing.[1]

Surfactants at high concentrations in water often form lamellar phases with bilayers packed together to give a regular interlayer spacing as shown in Figure 1.1. The bilayers are separated from each other by water layers. The lamellar phase can be stabilized by a low spontaneous curvature of the water-oil interface[2], by long-range repulsive interaction forces such as electrostatic repulsion resulting from ionic charges, or by thermal fluctuations of the membranes.[3]

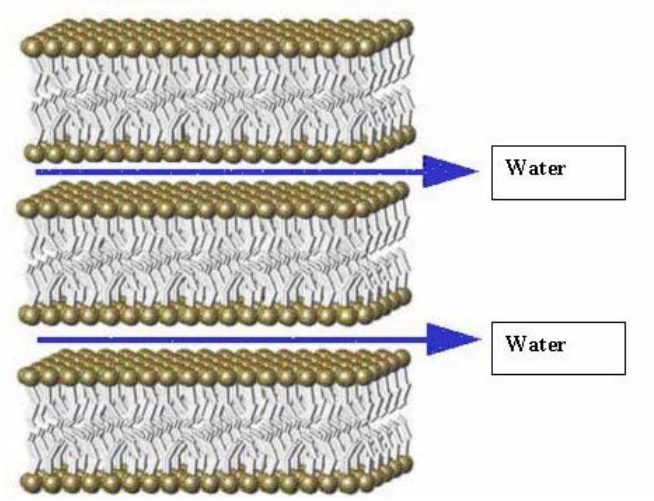

Figure 1.1 Representation of a stack of lamellar aggregates separated by water channels.

The phase behaviour of lyotropic liquid crystals has been investigated in numerous amphiphilic systems.[4] Phase transitions, as indicated in the phase diagram, can be observed by variation of the temperature or the concentration, and by the addition of a co-surfactant or a salt.[5-10] Shear flow can also induce transitions to other structures.[11] The lecithin, water and oil system is a representative example forming different types

of lyotropic liquid crystals. The isothermal quasi-ternary-phase diagram and the phase properties of several systems of the type lecithin, water and oil have been investigated by Angelico and co-workers.[12] These authors published a still incomplete study of the lecithin/water/n-decane system; a complete investigation of the phase transitions especially in the multiphase region close to the decane corner and the L_α phase in the phase diagram is still missing. Therefore, it is one of the aims of this thesis to provide some more details about the phase behaviour of the lecithin/water/n-decane system.

The behaviour of lamellar phases under shear has been investigated in different amphiphilic systems and followed by various techniques in recent years.[13-15] Shear flow is known to have a strong influence on the structure and orientation of lamellar phases. Different orientation states can be characterized by specifying the orientation of the layer normal (director) with respect to the direction of velocity, the direction of the velocity gradient and the vorticity direction, respectively.[16] The three principal orientations of the layer normal, that is, if the director points parallel to the neutral (vorticity) direction, the velocity direction and the velocity gradient direction are denoted as perpendicular, transverse, and parallel, respectively. In lyotropic surfactant lamellar phases the parallel[13,15,17-20] and perpendicular[15,18,20,21] orientations as well as mixtures of the parallel and perpendicular[20,22] orientations have been observed. In addition, a unique shear-induced defect structure, consisting of close-packed, almost monodisperse, multi-lamellar vesicles, also called “onions”, first investigated by Roux and co-workers[13] was found for many different systems. The size distribution of shear-induced multi-lamellar surfactant vesicles depends on the applied shear rate (see Figure 1.2). Escalante et al.[23] interpreted their rheology results as an irreversible transformation to onions with the increase of shear rate. Panizza et al.[24] found two different regimes that differ in the size of the onions that depends on the initial and final shear rates. Müller and collaborators[16] reported reversibility in non-ionic surfactant systems. Medronho et al.[25] investigated the reversibility in the onion size distribution during stepwise cycling of the shear rate.

Different orientations of the lamellar n-decane-based lecithin organogel under shear have been found by Burgemeister[26] and Blaschke.[27] The orientation diagram shows different states including parallel and perpendicular orientations as well as onions, depending on shear rate, composition and temperature.

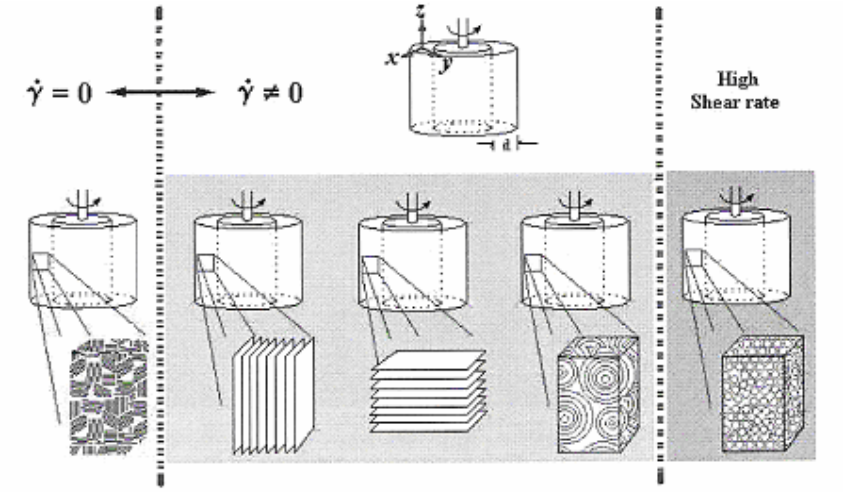

Figure 1.2 Schematic process of the different orientation of bilayers on the lamellar phase under shear. Not only different orientation of layers in the Couette cell, but also the size distribution of shear-induced MLVs depends on the applied shear rate.

For the investigation of the influence of micro-particles on the lamellar phase, the synthesis of spherical particles is necessary. The preparation of spherical particles via heterophase polymerization has developed into a mature technique in macromolecular chemistry.[28] The control of particle size, size distribution and shape, or the incorporation of functional groups in the particles or on their surfaces is a central topic in preparative colloid chemistry. The result is an ever-growing number of new functional materials. The accessibility of highly monodisperse colloids within a tunable size range is a crucial prerequisite for the generation of photonic band gap materials.[29] During the last decade, dye-labelled spherical particles have been of interest for industrial applications as well as academic research. They are used as calibration kits for optical methods, e.g., confocal microscopy[30] or flow-cytometry.[31] Their widespread use is based on the stability of the particles and the dyes. Furthermore, their well determined shape, size and narrow distribution is advantageous.

The equilibrium phase behaviour of mixtures of lyotropic bilayers (not onion) and small spherical particles has been investigated. A low concentration of magnetic[32] or nonmagnetic solid particles with a size smaller than 20 % of the bilayer spacing can be incorporated into the lamellar phase.[33,34] The behaviour of mixtures of lyotropic lamellar phases and spherical particles of micrometer size under shear was investigated by Poon and co-workers.[35] Depending on the size of the particles, their volume fraction, and the stage during the preparation process at which the particles

are added, they have found different structures of the composite, such as stuffed onions in which the particles are encapsulated at the centre of the onions, decorated onions in which, as well as replacing the onion core, the particles decorate the polyhedral lattice of edges between the onions, and so-called onion-particle alloys. The latter are formed when the particles are added late in the shearing procedure, in which case the onions remain intact and the particles reside entirely in the interstitial regions between them. They found that the rheological properties of a lamellar phase in the presence of a small amount of submicron-size solid particles are not very different from those of the pure lamellae.[36]

The addition of colloidal particles can modify the rheological properties of a variety of complex fluids.[37,38] Zapotocky and et al.[39] reported that the addition of a small volume fraction of colloidal particles to lamellar systems can efficiently control their rheology and they obtained optical visualization of both the lamellae orientation and the structure of any defects induced by the addition of colloidal particles. Basappa et al.[40] reported that the addition of spherical micro-particles to a lamellar system enhanced the moduli (storage and loss) and retarded the decay of the defect network under shear treatment.

The structure of the lamellar phase with a layer spacing of several nanometers is not compatible with spherical particles of micrometer size. In mixtures, the particles prefer defect regions of the lamellar phase as can be seen in Figure 1.3. One question addressed in this study is whether defects of the layer structure of lyotropic lamellar phases generated by adding micro-particles may enhance the nucleation of vesicles and lead to faster transformation to this orientation state of the L_α phase under shear.

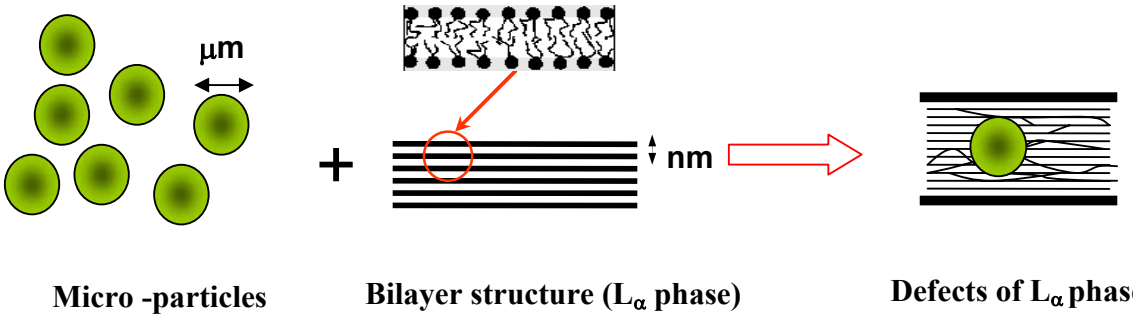

Figure 1.3 Representation of influence of micro-particles on the lamellar phase.

This thesis is divided in seven chapters: Following this introduction, in the second

chapter the theoretical aspects related with the aggregation of surfactants in solution and the different orientations of the lamellar phase under shear, a brief review of colloids, as well as the background of the different techniques used for the characterization of the samples are described. The materials and utilized chemicals, sample preparation techniques and a brief outline of the experiments and the employed techniques are presented in the third chapter. Chapter four contains the salient results of the temperature-dependent phase behaviour at one specific composition of the n-decane based lecithin organogel system. The fifth chapter summarizes the results of the characterization of the nano- and micro-particles which have been synthesized. In the sixth chapter the influence of micro-particles on the lamellar phase and its behaviour under shear is discussed. The conclusions of this thesis and a brief outlook are given in the seventh chapter.

2 General Aspects of Surfactants and Colloidal Particles

2.1 Surfactants and Lyotropic Liquid Crystals

2.1.1 Surfactants

Surfactants (SURFace ACTive AgeNTS) are amphiphilic molecules which combine two distinctive parts; one part is solvent soluble and the other part is insoluble. For the most commonly used solvent, water, the two parts of the surfactant molecule are referred to as hydrophilic (water-loving) and hydrophobic (water-hating). The hydrophilic part (the head), is a polar group which can be charged or uncharged. The hydrophobic part (the tail) is constituted by one or more hydrocarbon chains, linear or branched, with varying length. The number of chains, their length and the degree of branching are important parameters which determine the physico-chemical properties of amphiphiles.[41]

Surfactants are usually classified according to the charge of the headgroup. In this way, it is common to divide them into cationic, anionic, non-ionic, and zwitterionic.[42]

Cationics. The most important surfactants in this class are the amines, which can be obtained in the primary, secondary or ternary forms. Practically all metals, minerals, plastics, fibers, cell membranes, etc. are negatively charged, allowing for the use of these surfactants as anticorrosion agents, dispersants, antistatic agents, bactericides, etc.

Anionics. Sulphates, sulphonates, carboxylates and phosphates represent the majority of the polar groups found in anionic amphiphiles. These are the most used surfactants mainly because of their cheap and easy manufacture. They are also used in most detergent formations.

Non-ionics. These surfactants contain an uncharged head group, usually polyetheric or polyhydroxylic. They are used in liquid and solid detergents and in a variety of other industrial applications, being particularly useful in the stabilization of oil-water emulsions.

Zwitterionics. In this class, the surfactant head group is constituted by two charged groups of opposite signs. The ammonium group usually forms the positively charged group, while the negative group is often phosphate or carboxylate. Since these surfactants exhibit excellent dermatological properties and low eye irritation they are

often used in shampoos and other cosmetic products. Lecithin (1,2-diacyl-*sn*-glycero-3-phosphocholine) is a representative example of this category of surfactants. It is made up of a mixture of natural phospholipids account for more than 50 % of the lipid matrix of biological membranes in most organisms.

In Table 2.1 examples of surfactants belonging to the different classes are given.

Table 2.1 Examples of surfactants from the different described classes.

Surfactant type	Symbol	Example
Cationic	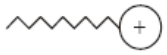	Amine: $R_4N^+X^-$
Anionic	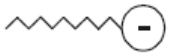	Sulphonate: $RSO_3^-Na^+$
Non-ionic		Ethylenoxide: $RO(CH_2CH_2O)_nH$
Zwitterionic		Lecithin: $RPO_4^-CH_2CH_2NR_3^+$

2.1.2 Surfactant Aggregates in Solution

The hydrophilic-hydrophobic nature of amphiphilic molecules leads to their self-assembly into a variety of structures in aqueous solution. The energy of the amphiphile is lowest when it can find a place at the interface; therefore such molecules are also referred to as surfactant. The simplest surfactant aggregate is the *micelle*. Micelles are formed at low concentrations of surfactant molecules. They can have the shape of a sphere, ellipsoid or rod, depending on the surfactant parameter (see below). The concentration at which micelles start to form is called the critical micelle concentration, or CMC, and is an important characteristic of a surfactant. The critical micelle concentration at a fixed temperature is observed as amphiphile concentration increases from very low values. The precise location of the CMC depends on the technique used to measure it. Many physical properties exhibit abrupt changes at the CMC, as illustrated in Figure 2.1. The most widely used technique to obtain the CMC is surface tension measurement.[4,42]

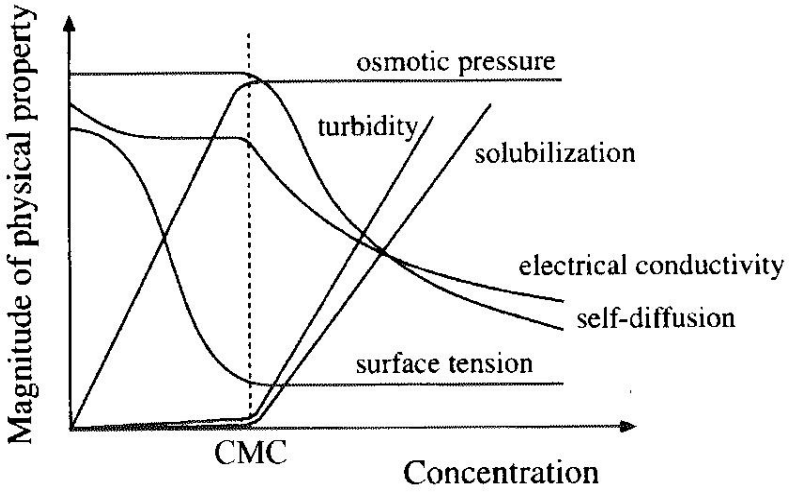

Figure 2.1 Schematic representation of some physical properties which exhibit a sudden change or discontinuity near the critical micelle concentration (CMC). Reproduced from Ref. [42].

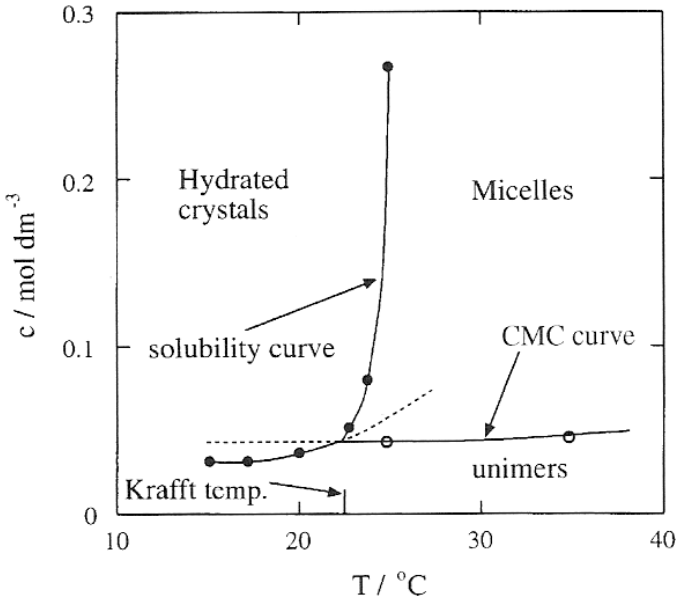

Figure 2.2 Temperature dependence of surfactant solubility in the region of the Krafft point. Reproduced from Ref. [42].

Another important characteristic of surfactants is the *Krafft temperature,* T_k. The solubility of a surfactant varies with temperature. Most surfactants are highly water-soluble at high temperatures, but a temperature decrease implies a decrease in solubility. At a certain point the surfactant precipitates from the solution as a hydrated crystal in which the hydrocarbon chains are ordered and densely packed. The solubility of the surfactant as a function of temperature is called the *Krafft boundary.* For many surfactants the crystallization appears in the concentration range of the *CMC*. A commonly used term is the *Krafft point*, which can be understood as the intersection between the Krafft boundary and CMC curve. The solubility of the system below the Krafft point is determined by the solubility of the surfactant monomers, whereas the solubility of the system above the Kraft point is determined by the solubility of the micelles, which is much higher (see Figure 2.2).[42]

One of the intriguing properties of oil-water-surfactant systems is their ability to self-assemble into a large variety of complicated structures. All these can be understood from the simple fact that the hydrophilic head of the amphiphile tries to avoid contact with hydrocarbons, either oil or the hydrophobic tail of other surfactants, whereas the hydrophobic tail tries just the opposite.

The *hydrophobic effect* which is mainly entropic in origin[43] leads to a variety of different aggregates. In many cases, the molecules form globular, rod-like or worm-like micelles, hexagonal phases, sponge phases and membranes, i.e., monolayers and bilayers (see Figure 2.3). However, this hydrophobic effect does not explain why the surfactants associate in well characterized structures with particular types or shapes of aggregates. In this aggregation process there are several contributions: the hydrophobic interactions, in which the water-water interactions are more favorable than those between water and the alkyl chains; the head group repulsions due to hydration or steric hindrance and, for ionic surfactants, also due to electrostatic repulsions, and finally packing considerations. System variables such as the surfactant concentration, temperature and the presence of salt contribute to the formation of different aggregates.

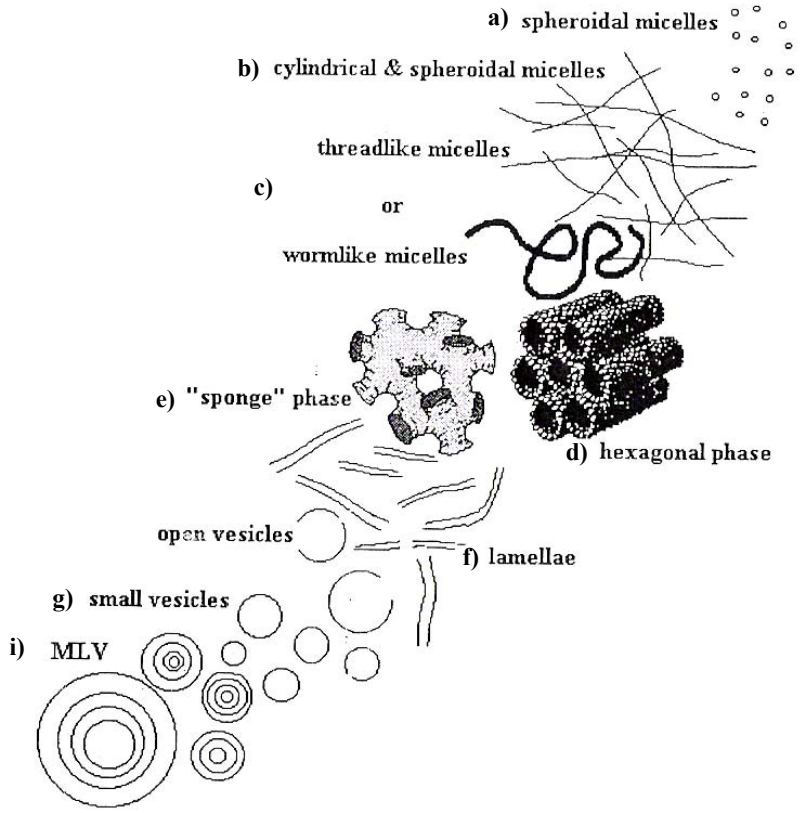

Figure 2.3 Several micellar structures that can be formed by surfactants. a) spherical micelle, b) cylindrical micelle, c) threadlike or wormlike micelles, d) hexagonal phase, e) sponge phase, f) lamellar phase, g) uni-lamellar vesicles, and i) multi-lamellar vesicles (MLV).

The *surfactant number* or *surfactant parameter,* N_s, (also called *critical packing parameter, CPP*) directly relates the structure of the amphiphilic molecule to the aggregate architecture. N_s is obtained as[44]

$$N_s = \frac{\upsilon}{l a_0}, \qquad (1)$$

where υ and l represent the volume and length of the hydrocarbon chain, respectively, and a_0 is the area per head group. The volume of a surfactant hydrocarbon chain (in nm^3) is obtained by[44]

$$\upsilon = 0.027(n_C + n_{Me}), \qquad (2)$$

where n_C is the number of carbon atoms in the chain and n_{Me} the number of methyl groups. The length of the fully stretched alkyl chain (in nm) is calculated as[44]

$$l = 0.15 + 0.127\, n_C. \qquad (3)$$

The area per head group, a_0, is not determined by the actual size, but by the electrostatic repulsions between the head groups. Usually, the trends in the changes of the head group area are sufficient for the interpretation of data when using the surfactant parameter model.

The surfactant parameter is a measure of the balance between the hydrophobic and the hydrophilic parts of the amphiphile molecule and so it relates the properties of the amphiphiles to the preferred curvature of the aggregate. A small value of N_s means that the head group is large, which leads to highly curved aggregates (spherical micelles). If the surfactant presents a larger N_s value, by addition of salt, or increasing of the surfactant alkyl chain, the aggregates present a lower curvature, going from spheres to rod-like micelles, and finally, when $N_s \approx 1$, to planar (lamellar) structures (see Figure 2.4). For surfactant parameters above unity reverse structures are more favorable.

Another way to analyse the surfactant aggregate structure is by using the curvature concept explicitly. In this approach the *mean curvature, H,* is used instead of the surfactant number. The mean curvature is defined as[42]

$$H = \frac{1}{2}\left(\frac{1}{R_1} + \frac{1}{R_2}\right) \qquad (4)$$

Where R_1 and R_2 are the principal radii of curvature for a surface. For a sphere, $R_1 = R_2 = R$ and the mean curvature is equal to $H = 1/R$; for a cylinder, $H = 1/(2R)$ ($R_1 = R$, $R_2 = \infty$), and for a planer bilayer, $H = 0$.

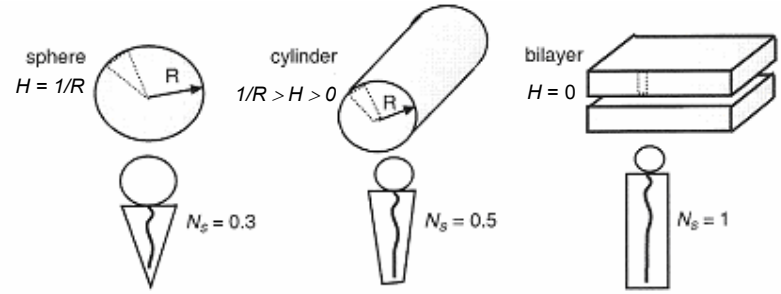

Figure 2.4 Illustration of the mean curvature, H, and the surfactant parameter, N_s, for three common surfactant aggregate shapes: the sphere, the cylinder and the bilayer. Reproduced from Ref. [44].

2.1.3 The Lamellar Phase

Aqueous solutions of many surfactants are known to form lamellar liquid crystalline phases with bilayers packed together to give a regular interlayer spacing, as shown in Figure 2.5 (a). Such phases can be formed in mixtures of surfactant with water and primary n-alkyl alcohols and forms the main matrix of biological membranes that contain phospholipids as lyotropic compounds. The ordered bilayer structure is formed by amphiphilic molecules disposed in bidimensional infinite layers, delimited by water layers, all of them having a parallel disposition. The lamellar phase exhibits a rich structural polymorphism which, as for any system of condensed matter, is controlled by thermodynamical variables (concentration, temperature, pressure) the variations of which induce symmetry changes of the organizations at phase transitions.[45]

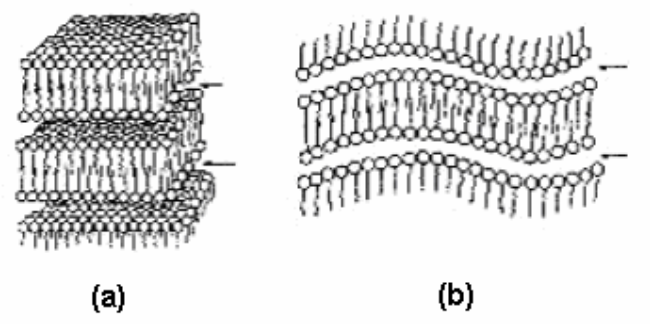

Figure 2.5 Lamellar structures: a) bilayer, b) rippled bilayer; arrows indicate water layer location. Reproduced from Ref. [45].

The lamellar phases can be stabilized by low spontaneous curvature of the water-oil interface[2], by the composition of long-range (10-500 nm) repulsive interaction forces such as electrostatic repulsion resulting from ionic charges or steric repulsions resulting from thermal fluctuations of the membranes.[3] The lamellar phase can be swollen in some cases by adding either oil or water, until the separation of the monolayers reaches several thousand angstrom.[46,47] In this case, the lamellar phase is stabilized by the undulation of the surfactant sheets. Undulation forces dominate when the membranes are flexible or, in terms of the bending modulus κ, when $\kappa \sim k_B T$, and electrostatic forces are absent or screened out. Uncharged bilayers of single chain surfactants and co-surfactants with a short chain length are rather flexible and the bilayers are therefore not flat but rippled. The hydrophilic and hydrophobic parts of

the molecule are balanced and the surfactant parameter has a value of 1. The lamellar phase is birefringent when viewed between crossed polarizers. It is less viscous than the hexagonal and cubic phases and may even flow in certain systems. The properties of lamellar phases can be of importance in many areas: such as the formulation of concentrated detergents, properties of foods and behaviour of cosmetic preparations.

2.1.4 The Nematic Phase

Certain solutions of lyotropic surfactants present nematic structures, similar to thermotropic nematics, which orient themselves in an external magnetic field or under mechanical stress and show typical Schlieren textures when observed in polarized light. Lyonematic structures were discovered by Lawson and Flaut.[48] Many ionic ternary solutions and some nonionic surfactants in binary aqueous solution form nematic structures in a relatively narrow concentration/temperature range. Surfactants that give nematic phases usually have the polar head group of the type SO_4^-, CO_2^-, $N(C_5H_{10})_4^+$ or $N(CH_3)_4^+$, their alkyl tails have more than eight carbon atoms.

Aggregates of the nematic phase are finite and anisotropic, due to the one-dimensional ordering characterized by the director $\vec{n}$, and present an important translational disorder. Three types of nematic phases are implied, the nematic discotic phase N_D, the nematic calamitic phase N_C and the nematic biaxial phase N_{BX} (see Figure 2.6). The discotic phase is formed by planar disc micelles and is related to the lamellar phase. Micelles may be built like rounded bricks or ruler shaped, rather than circular discs. The calamitic phase is formed by rod-like micelles, and is related to the hexagonal phase. In a concentration/temperature representation, the biaxial nematic phase, if present, always occurs between N_D and N_C phases.

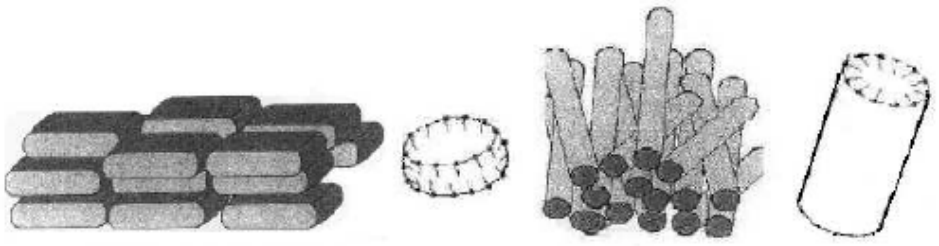

Figure 2.6 Representation of nematic phases: a) discotic micelles shaped like rounded bricks, b) schematic of a discotic micelle showing distribution of amphiphilic molecules, c) rod-like calamitic micelles, d) schematic of a cylindrical micelle showing distribution of amphiphilic molecules. Reproduced from Ref. [45].

Lyotropic nematic structures are located between the well ordered phases (lamellar, cubic, and hexagonal) and the completely disordered phases (micellar isotropic solution). [45,49]

2.1.5 Vesicles

Vesicles typically occur for phospholipid and other double-tailed surfactants. There are two types of vesicles. Unilamellar vesicles consist of a single bilayer sphere enclosing aqueous solution. Multi-lamellar vesicles have an onion structure as shown in Figure 2.7. They are made of several uni-lamellar vesicles formed one inside the other in diminishing size, creating a multi-lamellar structure of concentric spheres separated by layers of water. Vesicles are of great industrial importance as encapsulating agents for the controlled release of drugs, as micro-reactors for artificial photosynthesis (among other reactions), and as substrates for a variety of enzymes and proteins and perfumes in formulations.

a) b)

Figure 2.7 Vesicle structures: a) uni-lamellar vesicle, b) multi-lamellar vesicle (onion).

Vesicles, or synonymously liposomes, are one type of self organizing structure of amphiphiles in water.[44] The chemical structures of vesicle-forming amphiphiles show a great variety. Some of these substances are isolated from natural products like egg yolk,[50] while other chemicals are synthetically accessible.[51] One of the general ways to form phospholipid vesicles is by the method of sonication of an aqueous dispersion of the lipid.

Vesicle systems are usually not a distinct thermodynamic phase but a non-equilibrium state of the lamellar phase. If extra energy is dissipated in a lamellar system, the bilayers start to separate from each other, they are cut in small pieces, start to bend and eventually close to form vesicles.[52,53] Often vesicles are formed by dispersing lamellar bilayers where this dispersion may take place by dilution or by the input of

external energy. It should be noted that the size distribution of the vesicular dispersion is strongly affected by the method of preparation.[42]

Shear has a profound influence on the formation of vesicles. As mentioned above, in order to observe the formation of vesicles, it is often necessary to have an external force acting on the planar lamellar bilayers. Such shear-induced transitions from stacked bilayers to vesicles have been subject of a large number of investigations.[54-57] It has been shown that planar lamellae which are originally present become first oriented by the shear field at low shear rate, while the transformation to vesicles takes place at high shear rate. Moreover, it has been observed that the size of the onions can scale with the inverse of the square root of the shear rate. The transformation of planar lamellae to vesicles does not necessarily depend on the shear rate, but in many situations it is controlled by the strain.[19,58,59]

2.1.6 Lamellar Phase under Shear

The influence of shear on the structure and orientation of complex fluids has attracted much interest in recent years.[56,60] Especially samples with lamellar phases can undergo a variety of morphological transitions, which have been characterized in terms of an orientation diagram.[17] The three principal states of orientation, in which the normal of the layer is parallel to the vorticity (neutral), velocity or velocity gradient axis, are shown in Figure 2.8. The different orientations of the lamellar phase in a flow field are called perpendicular (a), transverse (b), and parallel (c). [15,61,62]

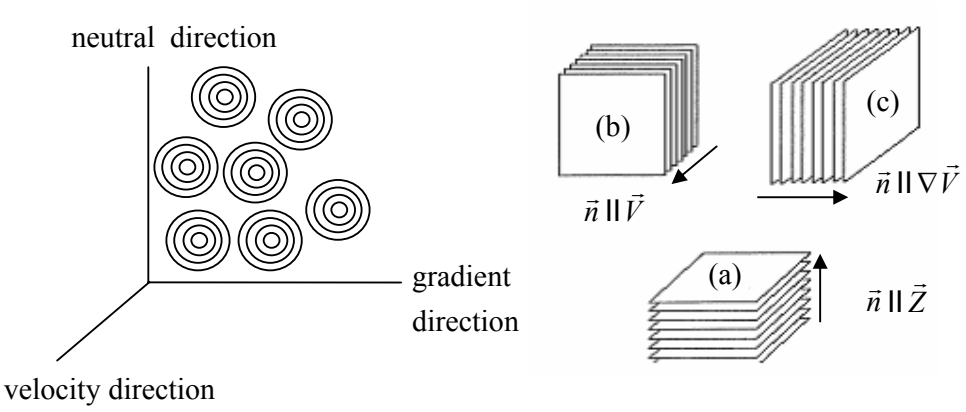

Figure 2.8 Schematic representation of the simple orientations of a lamellar phase in a flow. The different states are labelled as (a) perpendicular, (b) transverse, (c) parallel, and onions.

Recently, there was a report on two transitions from parallel-to-perpendicular-to-parallel orientation.[63,64] In addition to these orientation states, close-packed monodisperse multi-lamellar vesicles, called “onions”, can be found in many systems of lyotropic lamellar phases.[14,16,18-20,24,61,65-73] The detailed mechanism of onion formation remains unclear at present but there are theoretical investigations for the mechanisms of onion formation.[74-79] Up to now, steady state structures under shear are well studied for a variety of surfactant systems.[54,56] Nevertheless, the transition between different steady state structures, and even from the equilibrium structure at rest, remains elusive.

2.2 Colloids

The word "colloid" was derived from the Greek "kolla" for glue, as some of the original organic colloidal solutions were glues. This term was first coined in 1862 to distinguish colloids from “crystalloids” such as sugar and salt. In the early 19th century, Michael Faraday showed that when a strong beam of light passes through a colloidal solution, it is scattered. This method to study colloids was further developed by John Tyndall and became known as the "Tyndall effect".

In general, a colloid or colloidal dispersion is a heterogeneous mixture that visually appears to be a homogeneous solution. A heterogeneous mixture is a mixture of two phases whereas a solution is one phase. In a colloid, the dispersed phase is made of tiny particles or droplets that are distributed evenly throughout the continuous phase. There are no strict boundaries on the size of colloidal particles, but they tend to vary between 10^{-9} m to 10^{-6} m in size. Due to colloidal particles being so small, their individual motion changes continually as a result of random collisions with the molecules of the dispersion medium. This random, zig-zagging movement is called Brownian motion after the man who discovered it. This motion helps to keep the particles in suspension. Colloidal particles are found naturally in blood, bones and food products as well as in industrial applications like paints and pharmaceutical products.[80]

2.2.1 Types of Colloids

The particles are normally distributed in a dispersion medium, where both the particles and the medium can be in the gas, liquid or solid state. Such mixtures are called colloidal dispersions. Table 2.2 lists examples of various types of such colloids. The classical research in colloid science was performed on liquid solutions containing solid particles.

Table 2.2 Different types of colloidal dispersions and the usual classification according to the original states of their constituent parts.

Dispersing medium	Dispersed phase	Name
Solid	Solid	Solid sol
Solid	Liquid	Gel
Solid	Gas	Solid foam
Liquid	Solid	Sol
Liquid	Liquid	Emulsion
Liquid	Gas	Foam
Gas	Solid	Solid aerosol
Gas	Liquid	Aerosol

Amphiphiles in solution are known as association colloids. Macromolecules in solution can also have sizes of 1 nm or larger. These can be classified as macromolecular colloids.

There are two main ways of forming a colloid; reduction of larger particles to colloidal size or condensation of smaller particles, e.g. molecules, into colloidal particles. This latter approach generally makes use of chemical reactions such as hydrolysis or displacement. Laboratory and industrial methods make use of several techniques.

A method of forming an aerosol is to tear away a liquid spray with a gas jet. The process can be enforced by separating the liquid into droplets with electrostatic repulsions, done by applying a charge to the liquid.

Emulsions are usually prepared by vigorously shaking the two constituents together, often with the addition of an emulsifying agent, e.g. a surfactant such as soap, in order to stabilize the product formed. Polymeric particles which are prepared easily by emulsion polymerization, form a nearly monodisperse suspension of colloidal spheres.

Colloids are often purified by dialysis, a very slow process, where the aim is to remove a large part of any ionic material that may have accompanied their formation. A membrane is selected that will not allow colloid particles to pass through but will let the solvent and ions permeate through. The method relies on diffusion, osmosis and ultrafiltration.[42,80]

2.2.2 Charge and Steric Stabilization

Colloidal particles in a fluid dispersion medium always show Brownian motion and hence collide with each other frequently. The stability of colloids is thus determined by the interaction between the particles during such a collision. There are two basic interactions: one being attractive and the other repulsive. When attraction dominates, the particles will adhere to each other and finally the entire dispersion may coalesce. When repulsion dominates, the system will be stable and remain in a dispersed state. Stabilization serves to prevent colloids from aggregating. Steric stabilization and electrostatic stabilization are the two main mechanisms for colloid stabilization. Electrostatic stabilization is based on the mutual repulsion of electrical charges. Different phases generally have different charge affinities, so that a charge double-layer forms at any interface. Small particle sizes lead to enormous surface areas, and this effect is greatly amplified in colloids. In a stable colloid, the mass of a dispersed phase is so low that its buoyancy or kinetic energy is too little to overcome the electrostatic repulsion between charged layers of the dispersing phase.

The surface of a colloidal particle can develop a charge through a number of mechanisms. For example, ionization of surface acid or base groups in aqueous solution can create a charged surface. Ion adsorption or desorption or adsorption/desorption of ionic surfactants leads to the development of an electrical double layer in many colloidal dispersions. The charge on the dispersed particles can be observed by applying an electric field on a concentrated electrolyte. In this case all particles migrate to the same electrode and therefore must all have charge of the same sign.

Steric stabilization of colloidal particles is achieved by attaching (grafting or chemisorption) macromolecules to the surfaces of the particles (Figure 2.9). The stabilization due to the adsorbed layers on the dispersed particle is generally called steric stabilization. Steric stabilization has several distinct advantages over electrostatic stabilization. First, the interparticle repulsion does not depend on electrolyte concentration, in contrast to charge stabilized colloids where the electric doublet layer thickness is very sensitive to ionic strength. Second, steric stabilization is effective in both non-aqueous and aqueous media, whereas charge stabilization is usually exploited in aqueous solutions. Finally, steric stabilization operates over a wide range of colloid concentrations, in contrast to charge stabilization which is most effective at low concentrations. The most effective steric stabilizers are block or graft

copolymers where one type of block is soluble in the dispersion medium and the other is insoluble so that it attaches to the colloid particles.[42]

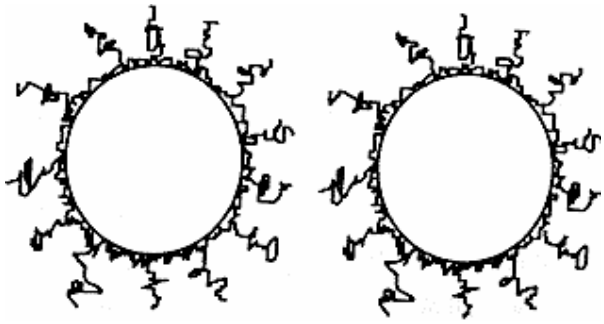

Figure 2.9 Schematic representation of the steric stabilization of a colloidal particle. The contact of colloidal particles is prevented by attached long-chain molecules.

2.2.3 Emulsion Polymerization

A typical conventional emulsion polymerization recipe will consist of water, emulsifier, monomer and initiator. Water serves as both a transport and heat transfer medium. An emulsifier is a hydrocarbon chain with one hydrophobic end and one hydrophilic end. If the concentration of emulsifier is high enough, the hydrophobic ends of several emulsifiers (usually about 50 to 100) form aggregates known as micelles. The emulsifier serves as a stabilizer for polymer particles and monomer droplets. The hydrophobic ends will attach to the particles while the hydrophilic ends will remain in the water phase. The charges on these emulsifiers form what is known as an electrical double layer which prevents the particles from coagulating. In other words, the emulsifier serves to keep the particles suspended in the water. The micelles can also be the location of particle nucleation. Monomer is present in the reaction in the form of large droplets. These droplets act as a reservoir of monomer. The monomer in the droplets diffuses through the water phase and into the micelles due to thermodynamic reasons. Initiator is added to the reaction mixture and dissociates into two radicals in the presence of heat. The initiator radicals are extremely reactive and readily react with any monomer in the water phase. The monomer in the water phase continues to add to the radical until the chain grows long enough such that its solubility in water is exceeded. The oligomeric radical chain (multiple monomeric units) is now hydrophobic enough to enter a polymer particle or enter a micelle to nucleate a new particle. This is known as micellar nucleation. The conventional emulsion polymerization will occur in three stages. The first stage involves the nucleation (birth) of polymer particles. This can occur by either micellar or homogeneous nucleation. The second stage involves

the growth of the particles until the monomer droplets disappear. The third and final stage begins with the disappearance of the monomer droplets and continues until the end of the reaction.[42,81]

2.3 Techniques

2.3.1 ^{2}H-NMR

Deuteron NMR spectroscopy is an extremely powerful technique for investigating molecular order and dynamics. The motivation for acquiring ^{2}H NMR spectra of solids and liquid crystals is to determine the local electric environment of the deuteron and to use this to obtain information about molecular order and dynamics. Many NMR active nuclei have a spin I greater than ½ and are termed quadrupolar (e.g. ^{14}N, ^{2}H). The deuterium nucleus has a spin 1, which means that in the presence of a magnetic field there are three quantized energy levels with magnetic quantum numbers, +1, 0, and −1. The NMR experiment consists of causing transitions between these levels by the application of energy in the radiofrequency (rf) range. Since the deuterium nucleus is quadrupolar and there is a nonspherical charge distribution at the nucleus. The interaction of the quadrupole moment eQ with the electric field gradient (EFG) at the nucleus causes a substantial perturbation of the Zeeman splitting (H_z = 46 MHz) at a magnetic field of 7 T. This perturbation is so large that the other NMR nuclear spin interactions, such as the scalar J coupling, the chemical-shift anisotropy (H_σ = 0.5 KHz) and the dipole-dipole interaction (H_D = 10 KHz), are negligible. Therefore, deuterium solid-state NMR spectra are dominated completely by the quadrupole coupling (H_Q = 250 KHz). The time independent Hamiltonian operator for deuterons in a static magnetic field, B_o, is given by:

$$H = H_z + H_Q + H_\sigma + H_D \qquad (5)$$

The Zeeman Hamiltonian is:

$$H_z = - \omega_o I_z. \qquad (6)$$

The Larmor frequency $\omega_o = \gamma B_o$ is expressed in rad s^{-1}, and I_z is the operator of the z component of the deuteron spin angular momentum.

The combined Hamiltonian of the Zeeman and quadrupolar interaction is:

$$H^o = H_z + H_Q \qquad (7)$$

The NMR frequencies of the two transitions are given by:

$$\omega = \omega_0 \pm \delta(3\cos^2\theta - 1 - \eta \sin^2\theta \cos 2\gamma) \qquad (8)$$

where δ is 3/8 times the quadrupolar coupling constant $e^2 q_{zz} Q/\hbar$ (expressed in rad s^{-1})

and the asymmetry parameter η of the electric field gradient tensor is defined as

$$\eta = (q_{yy} - q_{xx})/q_{zz} \quad (9)$$

The asymmetry parameter is usually zero for C–D bonds, meaning that the electric field gradient tensor is axially symmetric. In addition, the z axis of the electric field gradient tensor is along the C–D bond direction. The polar angles θ and γ specify the orientation of the magnetic field with respect to the principal axes system of the electric field gradient tensor.

If η is taken as zero ($q_{xx} = q_{yy}$), the NMR angular frequencies of the two transitions are given by:

$$\omega = \omega_0 \pm \delta(3\cos^2\theta - 1). \quad (10)$$

The energy diagram and the allowed transitions for these frequencies are shown in Figure 2.10. The quadrupole term lifts the twofold degeneracy of transitions between the Zeeman levels at the Larmor frequency, υ_0, and results in two transitions at frequencies, $\upsilon_0 \pm \upsilon_Q$, with:

$$2\upsilon_Q = 2\,\omega_Q/2\pi = \tfrac{3}{4}(e^2 q_{zz} Q/h)\,[(3\cos^2\theta - 1) - \eta \sin^2\theta \cos\gamma] \quad (11)$$

Fast molecular motions on the NMR time scale average out the quadrupolar interactions and the time-averaged quadrupolar Hamiltonian becomes zero if the motion is isotropic. This occurs in an isotropic liquid, where only the Zeeman splitting with a single line is obtained. If the molecular motions have correlation times slower than the NMR time scale, which is given by the inverse of the width of the spectrum (i.e. the quadrupole splitting), the quadrupolar interaction does not vanish. This leads to a splitting in the NMR spectrum. The two resonance lines are then separated by a frequency difference.[82,83]

The magnitude of the observed splitting reflects not only the quadrupolar averaging due to fast but non-isotropic reorientational motions, which results in a reduction of the splitting. It has also an angular dependence, which opens the possibility to gain information of the relative orientation of the molecules with respect to the magnetic field. This is particularly simple if $\eta = 0$, which is found, for example, in uniaxial liquid crystalline phases. In this case motional averaging results in a residual quadrupole interaction with $\eta = 0$.[84]

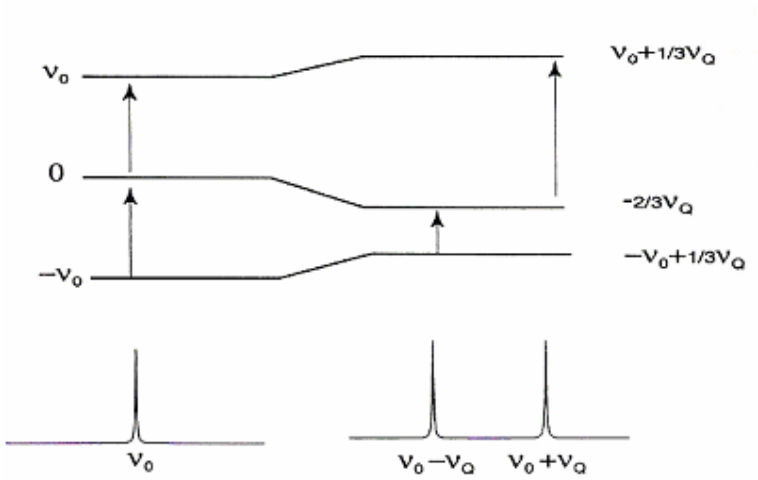

Figure 2.10 The energy level diagram for a deuteron (spin 1) in a magnetic field. On the left the allowed transitions in the absence of a quadrupole interaction are indicated and the single line NMR spectrum is sketched. On the right the allowed transitions in the presence of a quadrupole interaction give a two line spectrum, with a separation of $2\upsilon_Q$ by the first order quadrupole interaction. Reproduced from Ref. [82].

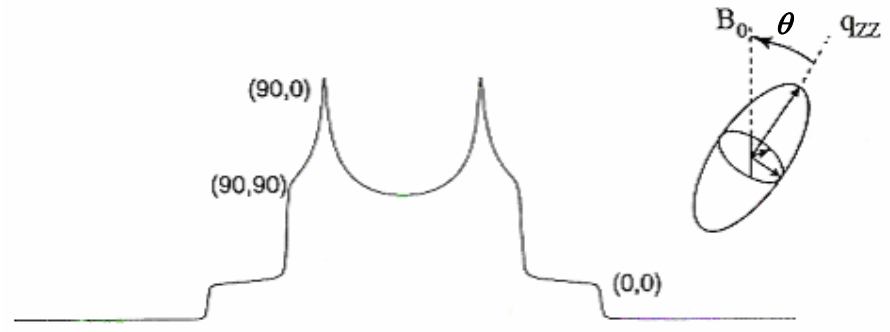

Figure 2.11 The deuterium NMR powder lineshape of orientations results in an isotropic distribution. The discontinuities in the lineshape correspond to the (θ,γ) values indicated. Reproduced from Ref. [82].

In the uniaxial case the splitting is dependent only on the angle θ between the principal z-axis of the EFG tensor and the axis of the external static magnetic field B_o. If a single crystal or an oriented system is rotated in the magnetic field, different resonance lines are predicted for each orientation. For a single deuteron with the principal z-axis of the EFG tensor along the magnetic field direction (θ = 0), the spectrum consists of two sharp lines, while for a polycrystalline power, which has an

isotropic distribution of angles θ and γ, the spectrum is a superposition of doublets and the overall line shape is the characteristic powder pattern. As shown in Figure 2.11 for the general case of $\eta \neq 0$ three singularities occur in the spectrum corresponding to specific orientations: for $\theta = 0°$ at $\pm$ 3/4 $(e^2q_{zz}Q/h)$, for ($\theta = 90°$, $\gamma = 0$) at $\pm$ 3/8 $(e^2q_{zz}Q/h)(1 + \eta)$ and for ($\theta = 90°$, $\gamma = 90°$) at ($\pm$ 3/8$(e^2q_{zz}Q/h)(1 - \eta)$. For $\eta = 0$ the latter two singularities coincide. [82,84]

2.3.1.1 Quadrupole Echo

The deuterium NMR lineshapes are very broad and the free-induction decay signal therefore dies away very rapidly. This decay is very fast, so that most of the signal is lost during the receiver dead time. The standard procedure for avoiding distortions due to this dead time is to use a quadrupole echo pulse sequence (QE), 90_x-τ-90_y, and record the echo signal occurring at time τ after the second pulse. The term "echo" refers to an increase in the NMR signal after a certain time interval, following the application of an intense radiofrequency pulse to an ensemble of spins in a constant magnetic field. The creation of an echo usually requires the application of *two exciting pulses*. The first pulse at t = 0 generates coherence which defocuses under the influence of an inhomogeneous interaction, e.g. caused by an inhomogeneous magnetic field or a quadrupole interaction. A second pulse, applied at t = τ, inverts the accumulated effects of the inhomogeneous interaction and initiates the refocusing which leads then to an echo at t = 2τ. The pulse sequence is shown in Figure 2.12. The crosshatched areas schematically represent the time required for the receiver to recover.[82,85]

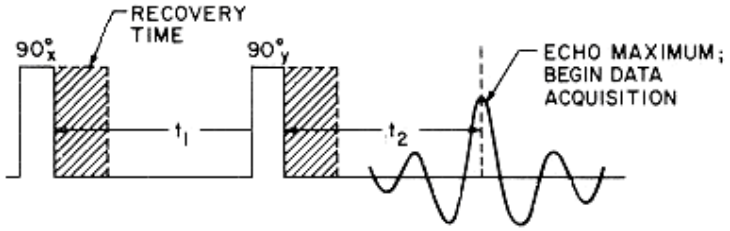

Figure 2.12 The quadrupole echo pulse sequence, used to refocus inhomogeneously broadened lines, such as the solid-state deuterium NMR powder pattern. Reproduced from Ref. [85].

2.3.1.2 ^2H NMR of Lyotropic Liquid Crystals

Deuteron NMR is a standard method for investigating the structure and dynamics of membranes, phospholipid bilayers and related model system. The ^2H NMR spectrum of a liquid crystalline anisotropic phase containing D_2O confined in the water layer exhibits a quadrupolar splitting characteristic of the water molecules. Despite the rapid motion of water molecules, a small degree of orientational order remains enforced by the orientation of the anisotropic liquid crystalline phase. Spectra of isotropic phases like, for example, cubic liquid crystalline phases exhibit zero splitting. Both lamellar and hexagonal phases produce splittings. Figure 2.13 shows the powder patterns obtained for an isotropic phase (iso), a hexagonal phase (hex), and a lamellar phase (lam). The lamellar and hexagonal spectrum can be distinguished because the ^2H powder pattern for the hexagonal phase of amphiphilic rods has a splitting that is roughly half of that for the corresponding lamellar phase.[86] This is due to lateral diffusion about the rod generating one more axis of symmetry for further averaging of the quadrupolar interaction.

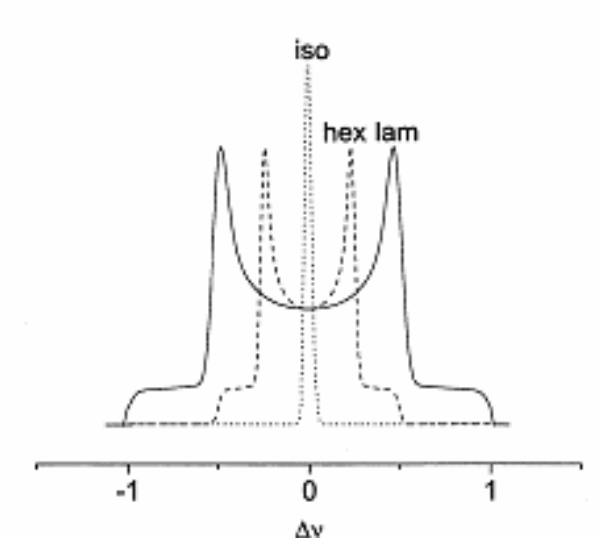

Figure 2.13 Illustration of the powder patterns obtained for isotropic (iso), hexagonal (hex), and lamellar (lam) liquid crystalline phases.

The diffusion about this extra axis provides one more term ½ ($3\cos^2\alpha$ -1) to the interaction averaging. In this case α = 90° (the angle between the surface normal and the cylinder axis), so the term counts as ½, making the quadrupolar splitting for hexagonal array of cylinders smaller in absolute magnitude by a factor of 1/2

compared to that of the lamellar system. [87]

2.3.2 Rheology

Rheology (from the Greek words "ρεἶν ", flow, "λογια ", study) is the science of the deformation and flow of matter. It provides information on the mechanical response to a dynamic stress or strain. Stress (σ) is the force per unit area and so has the units Nm^{-2} or Pa. Strain (γ) is the deformation of the sample, for example, its relative change in length, and is dimensionless. A schematic of a shear deformation is shown in Figure 2.14, where the liquid is filled between parallel plates. The bottom plate is fixed but the top plate is moved at a speed v_x in the *x* direction. The shear stress is proportional to the velocity gradient $\frac{dv_x}{dy}$:

$$\sigma = \eta \frac{dv_x}{dy} \ , \qquad (12)$$

where η is called the coefficient of viscosity, and is expressed in kg m^{-1} s^{-1} or Pa s.

We can define $\dot{\gamma} = \frac{dv_x}{dy}$ as the shear rate in units of s^{-1}. The shear stress is:

$$\sigma = \eta\dot{\gamma} \ . \qquad (13)$$

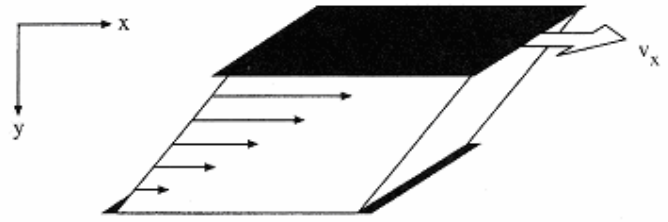

Figure 2.14 Schematic of a shear experiment between parallel plates. The top plate is moved at constant speed v_x, causing a steadily increasing strain. Reproduced from Ref. [42]

In principle there are two categories of materials, either Newtonian fluids where the viscosity is independent of the shear rate or non-Newtonian fluids where the viscosity is a function of shear rate. Many everyday materials like paint or yogurt get thinner as the shear rate is increased, this is termed *shear thinning*. Some things become thicker with increasing shear rate and are *shear thickening* (e. g. whipped cream). Other substances are plastic above a certain shear stress, meaning that the fluid does not

exhibit plastic flow until a yield stress, σ_o, is reached. Such fluids are called Bingham fluids and the stress is given by [42]

$$\sigma = \eta\dot{\gamma} + \sigma_0 . \qquad (14)$$

In contrast to liquids, solids have an elastic response to applied stress or strain, at least for small deformations. At low strains, the stress is proportional to the strain (Hooke's law) and independent of the deformation rate. One of the most important characteristics of soft materials is the dependence of their mechanical behaviour on the rate of deformation. Since at low rates of deformation most soft materials exhibit viscous behaviour whereas at high rates of deformation they behave elastically, they are called viscoelastic materials.

The viscoelasticity of soft materials is probed via several types of experiments. In dynamic or oscillatory tests the complex modulus of a sample at small angles of deformation is determined. The tests are called microscale experiments compared to macroscale tests like rotational or viscometry tests. The complex modulus describes the total resistance of the sample to oscillatory shear: $\sigma = G^*\dot{\gamma}$; similar is the resistance to flow in rotational tests ($\sigma = \eta\dot{\gamma}$). The complex modulus *G** is:

$$G^* = G' + iG'' \qquad (15)$$

where *G′* is the elastic or storage modulus and *G″* is the viscous or loss modulus and $\tan\delta = G''/G'$ is the phase angle or loss angle.

A structured system will gain energy from the oscillatory motion as long as the motion does not disrupt the structure. This energy is stored in the sample and is described by the elastic modulus. The magnitude of the storage modulus is depending on the number of interactions between the ingredients in the sample. The strength of each interaction *G′* is the sum of all interactions multiplied with the strength in the interaction. The higher the number of interactions, the higher is G'. The stronger the interaction the higher is the *G′* value. *G′* is a measure of the structure of the sample. Oscillatory shear will also create motion between the ingredients of the sample, i.e. friction. This friction will cause energy to be lost as viscous heating. The loss modulus describes the part of the energy which is lost as viscous dissipation. The loss modulus is only related to the number of interactions but is virtually independent of the strength of the interaction. The greater the number of interactions in which friction can be created, the larger is *G″*. The *G″* value is a measure of the flow properties for the sample in the structured state. The viscosity associated with the loss modulus is the

dynamic viscosity $\eta' = G''/\omega$, where ω is the angular frequency of the imposed oscillating stress or strain.[42,88]

The phase angle $tan\delta$ is associated with the viscoelasticity of the sample. A low value in $tan\delta$ or δ indicates a higher degree of elasticity (more solidlike). The phase angle δ can be used to describe the viscoelastic properties of a sample as shown in 2.2.

Table 2.2 Overview of the relation between phase angles and the viscoelastic properties of samples.

$\delta = 90°$	$G^* = G''$ and $G' = 0$	viscous sample
$\delta = 0°$	$G^* = G'$ and $G'' = 0$	elastic sample
$0° < \delta < 90°$		viscoelastic sample
$\delta > 45°$	$G'' > G'$	semi-liquid sample
$\delta < 45°$	$G' > G''$	semi-solid sample

3 Experimental

The purpose of this chapter is to describe the materials and experimental techniques used for this study. The description of materials will include the lecithin system, the investigation of which has formed the basis of this work, and furthermore many other materials used for the synthesis of particles. The major experimental techniques which have been used for this work, including rheo-polarizing microscopy, rheo-^{2}H NMR, and rheological measurements will be described.

3.1 Materials

The pseudo-ternary surfactant system investigated in this thesis consists of lecithin as a surfactant, water as solvent and n-decane as oil. The surfactant soybean lecithin (Epikuron 200) was supplied by Degussa Bioactives AG. It consists of 92 % soybean phosphatidylcholine (PC) and other minor compounds which are listed in Table 3.1. The average molecular weight is 772 g mol^{-1}. n-Decane ($C_{10}H_{22}$) of 95 % purity and a molecular weight of 142.29 g mol^{-1} was obtained from Merck and D_2O was purchased from Deutero GMBH with 99.96 % purity and a molecular weight of 20.028 g mol^{-1}.

Table 3.1 Composition of soybean lecithin "Epikuron 200".

Chemical name	Percentage
Phosphatidylcholine	Min. 92 %
Lyso-phosphatidylcholine	Max. 3 %
Other Phospholipids	Max. 2 %
Water	Max. 0.8 %
Oil	Max. 2 %
α-Tocopherol	Max. 0.2 %

The influence of micro-particles on the flow behaviour of the lamellar phase was

studied on samples of the lecithin system, mixed with spherical particles. The PMMA particles used were surface-modified with poly(12-hydroxystearic acid) and labelled with the fluorescent dye (Rodamine RITC) and had a diameter of 2 µm. These particles were provided by Dr. Imhof, Utrecht University.[89]

For the synthesis of SiO_2 and PMMA nano-particles and melamine-formaldehyde micro-particles the chemicals listed in table 3.2 were used.

Table 3.2 Specification of chemicals used for the synthesis of nano- and micro-particles

Chemical	**Formula**	**Purity**	**Supplier**
Ammonia	NH_3+H_2O	-	Lancaster
Ethanol	C_2H_5OH	≥ 96 %	Lancaster
Tetraethyl orthosilicate	$C_8H_{20}O_4Si$	≥ 98 %	Lancaster
Methyl methacrylate	$C_5H_8O_2$	> 99 %	Lancaster
Glycidyl methacryalt	$C_7H_{10}O_3$	≥ 95 %	Lancaster
Ethylen glycol dimethacrylate	$C_{10}H_{14}O_4$	≥ 98 %	MERCK
Aluminum oxide	Al_2O_3	-	Woelm Pharma
Toluene	$C_6H_5CH_3$	> 99 %	MERCK
Potassium peroxodisulfate	$K_2S_2O_8$	≥ 98 %	MERCK
Sodium sulphite	Na_2SO_3	≥ 98 %	Lancaster
n-Dodecylamine	$C_{12}H_{27}N$	≥ 98 %	Lancaster
2,4,6-Triamino-1,3,5-triazine	$C_3H_6N_6$	≥ 99 %	Fluka
Tetramethylammonium hydroxide	$C_4H_{13}NO$	-	MERCK
Formaldehyde	CH_2O	-	MERCK
Hydrogen peroxide	H_2O_2	-	Fluka
Sodium bis (2-ethylhexyl) sulphosuccinate	$C_{20}H_{37}O_7S$	-	SIGMA
Sodium Chloride	NaCl	-	MERCK

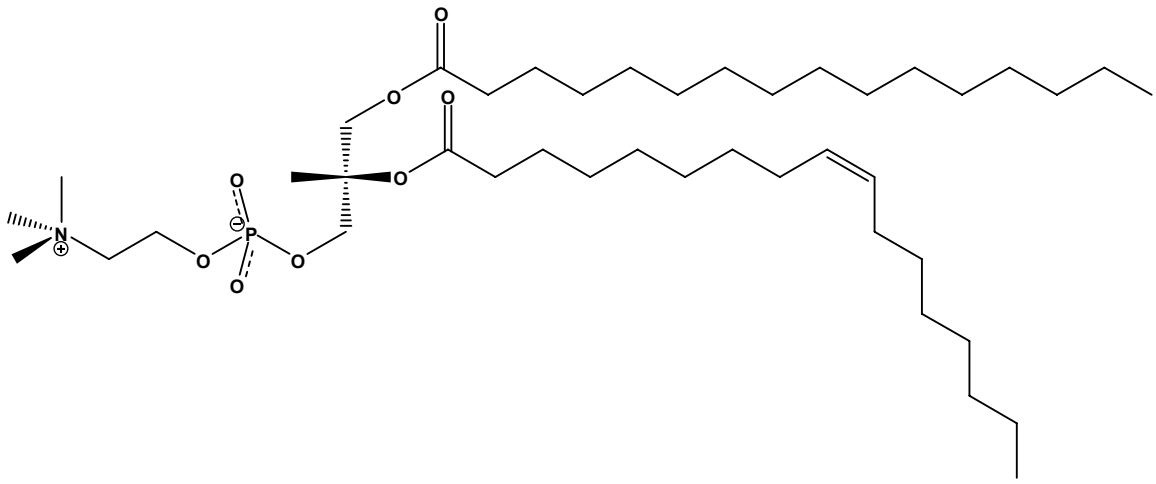

Figure 3.1 Phosphatidylcholine (PC), the main component of the lecithin used.

3.1.1 Sample Preparation

For all experiments of this work, two different types of samples were prepared, on the one hand, samples of lecithin/D_2O/n-decane forming an L_α phase, and on the other hand samples of the same system, but mixed with spherical particles of PMMA. The samples were prepared by adding the desired mass of lecithin to the solutions of D_2O and n-decane. For the preparation of samples with particles, the micro-particles of PMMA were added to the desired amount of n-decane and the composite was mixed using an ultrasonic bath for 1 min, followed by the addition of the surfactant and D_2O. All samples were mixed by slow rotation on a *Staudinger* wheel for two days at 40 °C. The air bubbles introduced in the mixing process were subsequently removed by brief centrifuging, in the case of samples without particles. The samples were stored in darkness. The compositions of all samples used are listed in table 3.3.

Table 3.3 Composition of the samples of lecithin/decane/D_2O system, m_L: mass of lecithin, m_D: mass of D_2O, m_n: mass of n-decane m_p: mass of particles and n_w: molar ratio of D_2O/ lecithin.

Sample	m_L/g	m_D/g	m_n/g	m_p/g	n_w
1	0.9998	0.1423	0.8555	0.0020	5.496
2	0.9998	0.1348	0.8442	0.0201	5.197
3	0.9997	0.1155	0.8221	0.0597	4.453
4	0.9507	0.1368	0.8220	0.1000	5.547
5	0.9879	0.1408	0.8520	0.0403	5.494
6	0.9701	0.1398	0.8376	0.0810	5.555
7	1.0131	0.1436	0.8679	0.0202	5.464
8	1.0145	0.1445	0.8583	-	5.490
9	0.9981	0.1423	0.8560	-	5.496
10	0.9500	0.1356	0.8084	0.1010	5.501
11	1.9962	0.2847	1.7109	-	5.498
12	0.9917	0.1422	0.8492	0.0201	5.527
13	1.9969	0.2857	1.7122	-	5.515
14	0.9494	0.1364	0.8147	0.1000	5.538
15	0.9910	0.1434	0.8496	0.0201	5.578
16	1.9978	0.2967	1.738	-	5.729
17	2.9943	0.4270	2.9949	-	5.546
18	1.9963	0.2878	1.7117	-	5.557
19	1.0004	0.1428	0.8569	-	5.502
20	1.0005	0.1427	0.8574	0.1010	5.498
21	2.0041	0.2079	1.7927	-	3.999
22	0.9996	0.0828	0.9172	-	3.193
23	0.8001	0.0730	0.7259	-	3.517
24	1.0007	0.0958	0.9034	-	3.690
25	1.0000	0.1038	0.8996	-	4.001

26	0.4984	0.0554	0.4402	-	4.285
27	1.0007	0.1170	0.8938	-	4.507
28	0.9993	0.1296	0.8752	-	4.999
29	0.9999	0.1424	0.8570	-	5.494
30	0.9993	0.1572	0.8641	-	6.064
31	1.0603	0.1423	0.8445	-	5.998
32	1.0001	0.1687	0.8315	-	6.502
33	1.0001	0.1813	0.8185	-	6.988

3.1.2 General Procedures of Particle Synthesis

3.1.2.1 Synthesis of SiO_2 Particles

A solution of ammonia (195 g, 25 % in water, Riedel-de Haën) and ethanol (1000 g, 99.9 %) was stirred for 10 minutes at room temperature to give a homogeneous solution. Tetraethoxysilane (13.1 g, 99 %, ABCR) was carefully added to this solution and then the mixture was stirred for 24 hours at room temperature. After a few more minutes, the transition to a turbid white suspension occurred regularly. The solvent was removed, and the residue dissolved in ethanol, washed with ethanol (3 x 30 ml). The particles were redispersed after centrifugation (for 15 minutes at 3000 rotations per minute) in four total steps.

3.1.2.2 Synthesis of PMMA Particles

In a three-necked round bottom flask (250 ml), 140 ml of distilled water were heated to 80 °C and degassed with a gentle stream of argon during 1 hour. A mixture of 16 g of methyl methacrylate (MMA, 99 % Lancaster), 10 wt % (2 ml) glycidyl-methacrylate (functionalized comonomer) and 10 wt % (2 ml) ethylene glycol-di-methacrylate (cross-linker) were destabilized using basic aluminum oxide (Al_2O_3). The mixture was added to 16 g of toluene. The resulting solution was added to the degassed water and stirred for 10 minutes at 80 °C to give an

emulsion. The polymerization was initiated by adding a solution of 0.8 g of potassium peroxodisulfate in 20 ml of degassed water. The progress of the polymerization was monitored by observing the interference colour of a dried sample taken from the reaction vessel (see Table 3.4). After 40 to 60 minutes the reaction was stopped by fumigating with air for at least 5 min. Then the reaction vessel was opened and heated up to 80 °C and stirred for at least 1 hr. Stirring was continued to remove the toluene and unreacted monomers at ambient temperature overnight. Particles of large size were removed by centrifugation for 10 min at 3000 rpm. Further purification was performed by repeated (4 times) centrifugation for 120 min at 3000 rpm, decanting of the solvent, and resuspension of the particles in distilled water after each cycle.

The surface of the particles was chemically modified by stirring the resulting aqueous particle suspension at 50 °C for 24 hr with the dissolved nucleophile. In the case of dyes, 10 mg and in the case of dodecylamine 500 mg were added. The unreacted nucleophile was removed by repeated centrifugation and washing with water, until no reactant was found in the water phase. The principle of the preparation of modified PMMA particles is shown in Figure 3.2.

Table 3.4 The colour of PMMA particles as a function of reaction time.

Time/min	Colour of particles	Remark
0	Colourless	Start of reaction
5	Violet-blue	-
10	Green-yellow	Centre was light blue
15	Green-red	-
20	Red (deep red)	-
30	White-red	-
40	red	The reaction was stopped

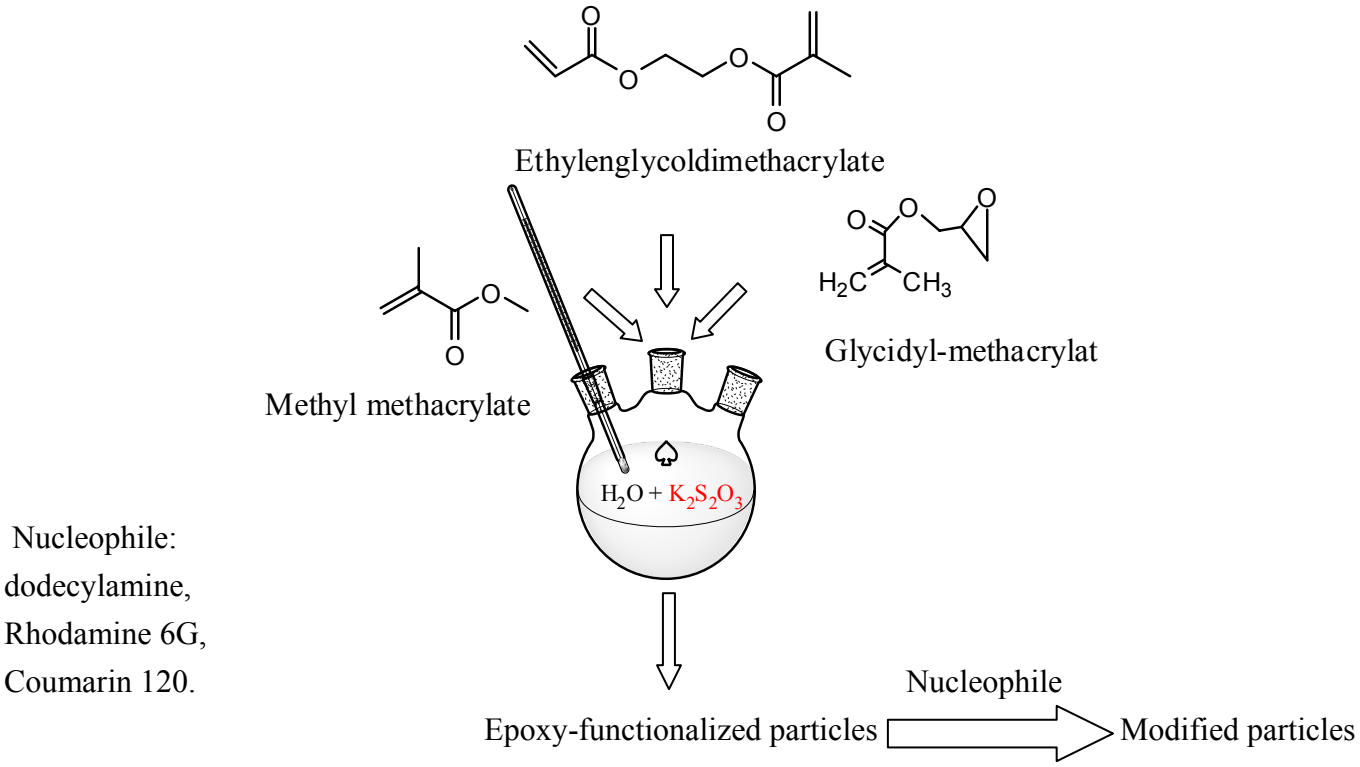

Figure 3.2 Flow diagram of reaction steps.

3.1.2.3 Synthesis of Melamine-Formaldehyde Particles

In a three-necked round bottom flask (250 ml), 0.63 g (0.05 ml) of 2,4,6-triamino-1,3,5-triazine (melamine) and 0.05 ml of tetramethylammonium hydroxide 25 % were added to 50 ml of distilled water. The mixture was stirred for 10 – 12 min at 70 °C until all of the melamine was dissolved. A solution of 2.43 g (0.3 mol) of formaldehyde was added to the mixture after stirring for 60 min at 70 °C. When 0.3 ml of hydrogen peroxide (30%) were added to the mixture to start the polymerization the colour changed to white. Stirring was continued for 26 min at 70 °C, then the solvent was removed and the residue was washed with distilled water and centrifuged for 30 min at 4500 rpm.

3.2 Methods

3.2.1 Polarizing Microscopy

The microscopy experiments were performed in transmission mode under crossed polarizers using a Leitz ORTHOLUX 2 POL microscope. Different lenses with L10, L25 and L32 magnification were used. The pictures were recorded with a JVC TK-C1381 colour video camera. Steady-state shear flow conditions were generated using a CSS450 Linkam shear cell. Images in the velocity-vorticity plane are taken with crossed polarizers oriented at 45° to the flow direction. The samples were placed between parallel plates with diameter 15 mm and 500 µm gap. A heating/cooling rate of 0.5 °C/min was used for temperature scans, in order to allow time for temperature equilibration.

3.2.2 ^{2}H NMR

For the NMR experiments under shear a cylindrical Couette cell of 14 and 15 mm inner and outer diameter respectively, was used. This cell is integrated into an NMR probe for a superconducting magnet. Its axis is aligned parallel to the external magnetic field. Shear is applied by rotating the outer cylinder with an external motor located below the NMR magnet. A photograph and a schematic drawing of the experimental setup for the rheo-NMR experiments are shown in Figure 3.2. The spectra were recorded on a Tecmag Apollo NMR spectrometer at the resonance frequency of 46.073 MHz for deuterons. A quadrupole echo sequence with a pulse separation of 60 µs was used. With the saddle-shaped NMR coil surrounding the shear cell, pulse durations of 22 µs for a 90° pulse were obtained. Typically, 128 scans were accumulated for each spectrum, and a recycle delay (last delay) of 500 ms was used. The temperature of the sample was controlled to an accuracy of ±0.2 °C using an airflow system. The temperature of the air was regulated by using a HAAKE Phoenix II P1 thermostat filled with Silicon oil.

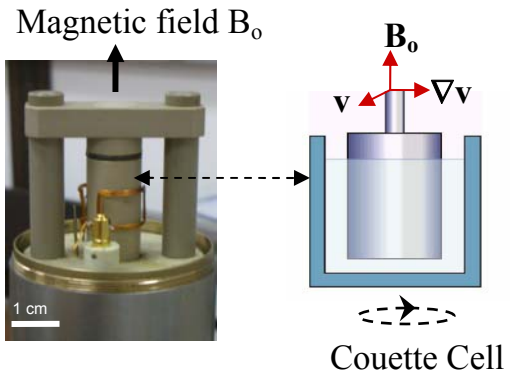

Figure 3.2 Experimental setup for rheo-NMR experiments.

For the investigation of the phase behaviour of the lecithin system by NMR the samples were filled in 4 cm long glass tubes of 5 mm diameter which were sealed with a Teflon plug. The tubes were inserted into a home-built goniometer probe such that the tube axis was perpendicular to the static magnetic field. The sample can be rotated about the tube axis allowing for the measurement of orientation-dependent spectra. Spectra were measured with a quadrupole echo pulse sequence, and 128 scans were averaged before Fourier transformation. The sample was pre-equilibrated in the isotropic phase at ca. 60 °C for every measurement. Slow cooling from the isotropic to the anisotropic phase was sufficient to achieve a uniform alignment of the L_α phase by the magnetic field.

3.2.3 Rheology

The rheology experiments were performed in Lund University with a Physica UDS 200 rheometer using a cone and plate cell made of stainless steel (MK20/M, 1º cone angle). The instrument is equipped with a temperature control unit that was calibrated to give a temperature in the sample chamber within 0.1°C of the set value. Evaporation of the solvent was reduced by a solvent trap on the top of the cell. All samples were pre-sheared at 35 °C to align the L_α phase.

The viscoelastic properties, i.e. the dynamic moduli, were determined by small frequency oscillatory tests where the linear regime was previously verified by stress sweep tests. Shear controlled experiments at a constant shear rate were

performed as a function of time in order to follow the kinetics of MLV formation. A temperature sweep (0.5 °C/min) at a constant shear stress and frequency was used to determine the transition from the lamellar to nematic phase.

3.2.4 SAXS

SAXS measurements on lecithin samples were performed in Lund University with a Kratky compact small angle system equipped with a position sensitive detector (OED 50 M from M Braun, Graz Austria) containing 1024 channels of a width of 53.6 µm. Cu K_α radiation with a wavelength of 1.54 Å was provided by a Seifert ID-300 X-ray generator operating at 50 kV and 40 mA. To minimize background scattering, the camera volume was kept under vacuum. A 10 µm thick Ni filter was used to remove K_β radiation and a 1.55 mm W filter was used to protect the detector from the primary beam. The distance between sample and detector was 277 mm. The samples from the phase diagram determination were used. The sample holder was a 1 mm quartz capillary and samples were transferred to the capillary using a syringe. The samples were transferred at high temperatures (isotropic phase) and then cooled very slowly into the anisotropic phases. A Peltier element controlled the temperature within ± 0.1 °C.[90]

SAXS measurements for sample 13 of lecithin/D_2O/n-decane were carried out at Paderborn University with approximately the same equipment as described above. In this case, the SAXS setup was calibrated using cholesterylmyristate as a reference (see appendix, Figure A.8).[91]

The measurements give intensity versus channel number as primary data. For the physical interpretation the channel number has to be converted to a scattering vector q. The known constants of wavelength (λ), sample-detector distance (l), and channel width (c_w) are listed in Table 3.4. The scattering vector of a peak is given by: $q = 2\pi\ c_w\ \Delta c\ /\lambda\ l$, where $\Delta c = c_p - c_{pb}$ with the channel numbers c_p and c_{pb} of the current peak and the primary beam, respectively.

Table 3.4 The constant parameters of SAXS, required for the conversion of the channel number to a scattering vector.

SAXS measurement	λ / nm	c_w /μm	l / mm
Lund University	0.1542	53.6	277
Paderborn University	0.1542	53.3	230

3.2.5 Other Techniques

The particle characterization was performed with a scanning microscope (Model Alpha, WiTec). The instrument was operating in pulsed force mode AFM using silicon cantilevers (pointprobe-FM, Nanosensors). All samples were prepared on glass substrates.

Light scattering experiments were performed with a model 5000e compact goniometer system (ALV-Laser Vertriebsgesellschaft), which allows the simultaneous recording of static and dynamic light scattering (SLS/DLS). A Nd:YAG laser with 200 mW operating at a wavelength of 532 nm was used as a light source. Cylindrical quartz glass cuvettes with an outer diameter of 20 mm served as scattering cells. The scattering intensity was observed under 13 different scattering angles reaching from 30° to 150°. All measurements were performed at 25 °C. The particles were characterized via SLS/DLS in water and toluene solutions. All suspensions were filtered with a 1.2 μm PET syringe filter (Mecherey-Nagel).[29,92]

4 Phase Behaviour of the Lecithin Organogel

Extensive research on lyotropic liquid crystals over the last few decades has allowed the phase diagrams, the most common structures, and the specific properties of these nanostructured materials to be established in great detail.[41,49,93-95] Systems formed by lecithin, water and oil are representative examples of this category of materials and are of interest for a multitude of different applications such as dispersion technology, cosmetics, pharmaceutical products, food and encapsulation systems.[96-102]

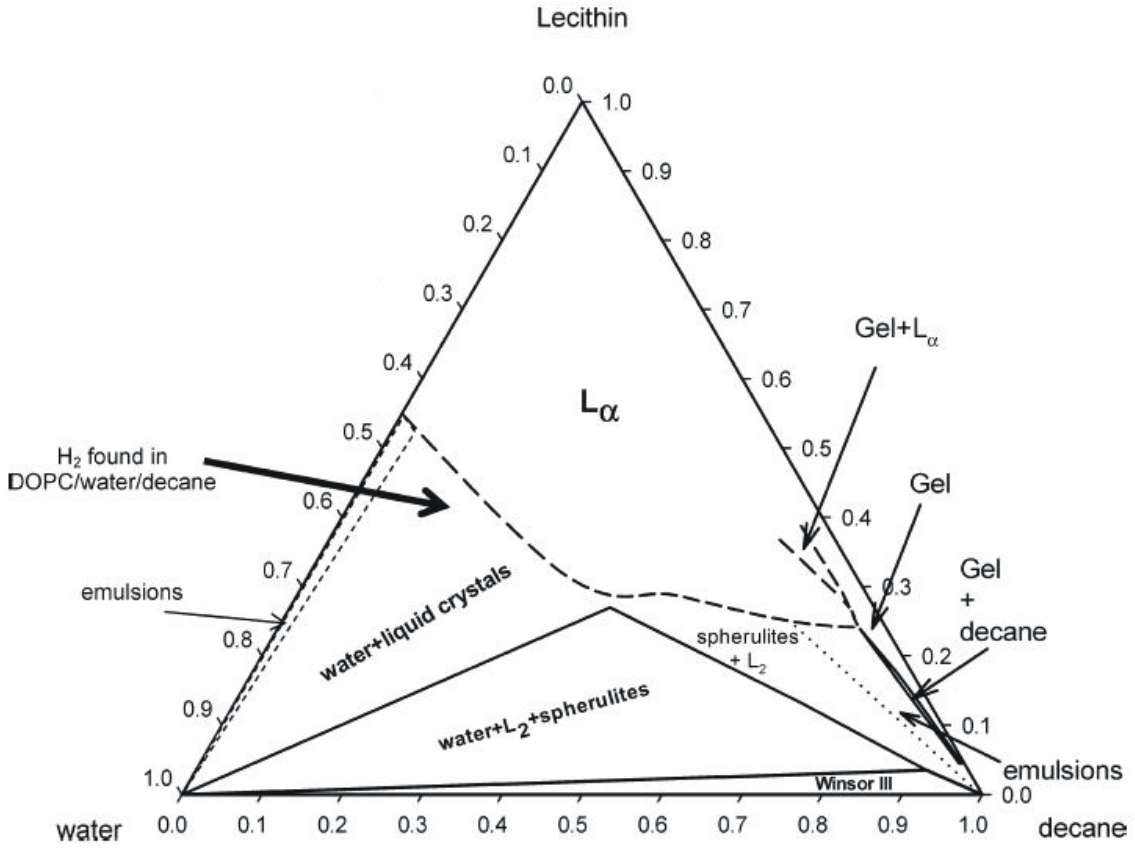

Figure 4.1 Phase diagram for the system lecithin/water/decane at 25 °C with single and multiphase areas which has been obtained by Angelico and co-workers. Phase abbreviations are as follows: L_2, reverse micellar solution phase, L_α, lamellar phase and H_2 reverse hexagonal phase. Reproduced from Ref. [12].

The isothermal quasi-ternary-phase diagrams and the phase properties of several systems of the type lecithin, water, and oil (where the oil is cyclohexane, isooctane or n-decane) have been investigated by Angelico and co-workers (see Figure 4.1).[12,103] As can be seen in the phase diagram of the system lecithin/water/n-decane, several liquid crystal phases and emulsions exist. Angelico et al. found that upon addition of water to the lecithin/n-decane system, first a gel is formed. When more water is added, pure decane is expelled and the system undergoes a phase separation, resulting in a coexistence of gel with pure oil (low lecithin content). At high lecithin content a lamellar phase is observed. As shown in Figure 4.1, a large part of the phase diagram is occupied by this lamellar phase. In addition, a coexistence of reverse micelles, water and spherulites close to a stable Winsor II phase equilibrium are seen in a large range of water and decane concentration. The bold arrow in Figure 4.1 indicates the region where a reverse hexagonal phase was found.

As reported in Reference 12 the multiphase region close to the decane corner and the gel phase of the L_α + gel, was not investigated in detail. Therefore, it is the aim of the present work to provide some more details of the phase behaviour of the system lecithin/water/decane. The shear-induced orientation states of the lamellar phase of this system have been investigated by Burgemeister and later on by Blaschke[26,104] Blaschke[104] observed two distinct splittings in the ^{2}H NMR spectra during temperature dependence experiments, indicating that a second liquid crystalline phase exists close to the L_α phase. Following his work a specific region of the phase diagram (lamellar phase) will be explored and the phases and phase properties at various temperatures will be investigated, extracting the characteristic parameters of different structures by using polarizing microscopy, SAXS, ^{2}H NMR and rheological measurements.

4.1 Identification of Phase Transitions by Polarizing Microscopy

Polarizing microscopy is commonly used to detect the birefringence phenomena and to distinguish different types of mesophases by their characteristic textures. If the sample is anisotropic and shows strong birefringence, the intrinsic coloured

texture based on the structure of the phase can be observed through crossed polarizers. In contrast with this, dark regions of the texture mean that there is no birefringence (isotropic structure) or a rather weak birefringence.

In this thesis, the phase behaviour of lecithin/D_2O/n-decane system with sample n_w = 5.5 have been characterized by polarizing microscopy. The lamellar phase develops a typical oily streak texture which occurs only in lamellar phases, as can be seen in Figure 4.2. This texture was obtained after loading a fresh sample with 50 % lecithin and n_w = 5.5 (sample 9 in Table 3.2) between the plate-plate shear cell with 500 µm gap, at 16 °C.

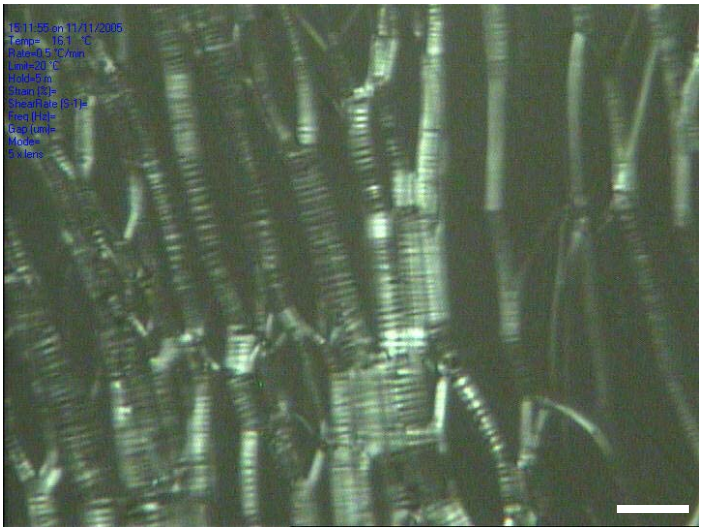

Figure 4.2 Light microscope textures of the system lecithin/D_2O/n-decane with n_w = 5.5. The oily streak texture characteristic of lamellar phase was observed between crossed polarizers at 16 °C. Bar = 100 µm

The phase penetration experiment involves placing the pure lecithin between two microscope slides and contacting it with an aqueous phase as shown in Figure 4.3. This experiment also was performed for the system of AOT/brine (see appendix, Figure A.1). The metastable myelin state was obtained upon contact of the water with lecithin. The figure on the right indicates that the tubules are twisted. This myelin state was only observed for a short time before the typical lamellar phase appeared. The myelinic figures represent classical myelinic

instabilities at the interface. These instabilities were first observed in lipids by Virchow in 1854 and are the subject of several studies.[105-110] There is no complete understanding of the myelin formation process; we do know that the myelin textures of water-lipid appear as a consequence of the swelling by increasing water contact and dissolution of the bulk lamellar phase. The physical reason why a lamellar phase should swell in this bizarre fashion still remains unknown.

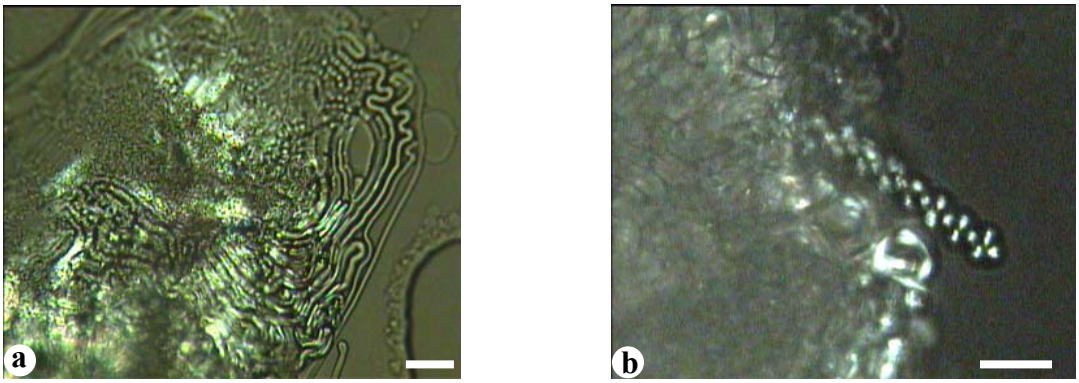

Figure 4.3 An optical microscope texture of the system lecithin/D_2O was taken between crossed polarizer and shows a typical contact experiment. Pattern (a) shows the myelin texture observed after contacting water with lecithin at the interface. Bar = 100 μm. Pattern (b) shows large magnification of tubules which are twisted. Bar = 50 μm.

An attempt to identify phase transitions for a sample of lecithin/D_2O/n-decane with n_w = 5.5 increasing the temperature by using polarizing microscopy was made. When microscopically observed between crossed polarization filters different textures characteristic of lamellar, nematic and isotropic phases are found, but a clear distinction between pure anisotropic phases and a two-phase region was not possible. The temperature dependent experiments were performed by loading a fresh sample of lecithin/D_2O/n-decane into the plate-plate cell with 500 μm gap of the CSS450 Linkam shear cell connected to a polarizing microscope. The sample temperature was controlled by a heating/cooling rate of 0.5 °C/min. Figure 4.4 shows a sequence of optical micrographs of different textures observed with increasing of temperature. Two phase transition

temperatures (39°C and 50 °C) were observed. As will be shown later, the lower transition temperature at 39 °C corresponds to the phase transition from L_α to N_D + L_α. At 50 °C there is the transition from the anisotropic region to the isotropic phase.

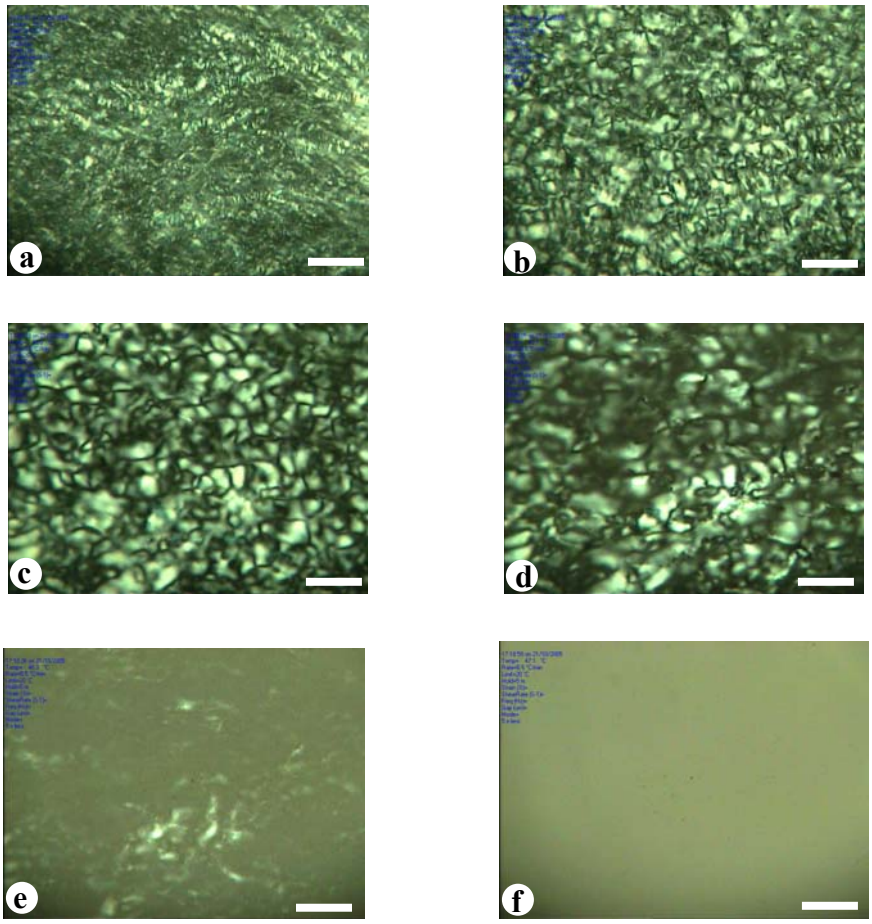

Figure 4.4 The evolution of the liquid crystalline structures of lecithin/D_2O/n-decane with n_w = 5.5 as imaged by polarizing microscopy with increasing temperature. (a) Optical micrograph of L_α phase at 25 °C. (b) Pattern of the biphasic region L_α + N_D at 39 °C. (c) Same system at 40 °C. (d-e) Coexistence of anisotropic and isotropic phases at 46-47 °C. (f) Isotropic phase at 50 °C. The width of the bar on the images corresponds to 150 μm.

4.2 Identification of Phase Transitions by SAXS

Small angle X-ray scattering (SAXS) has been recognized as a powerful technique for the study of phase transitions in liquid crystalline phases. The samples 13, 17 with n_w = 5.5, and 21 with n_w = 4.0 of the lecithin/D_2O/n-decane system were used. X-ray small angle diffraction patterns are recorded during slow cooling after pre-equilibrating of the samples in the isotropic phase at around 60 °C. As the temperature is decreased from 60 to 16 °C, the SAXS pattern of sample 21 with n_w = 4 shown in Figure 4.6 does not change. Only a small decrease of the intensity at the Bragg peak was observed at high temperatures. The sharp peak indicates the existence of the lamellar phase in this temperature range.

The experiment was repeated for sample 17 with n_w = 5.5 and the results were compared with the SAXS results of a similar sample (13) which have been obtained in the Department of Chemistry of Paderborn University. As shown in Figure 4.7 different SAXS patterns compared to Figure 4.6 are obtained.

At 60 °C an isotropic phase is expected showing one single broad peak. The observed structure of the scattering function at high temperature could result from a superposition of an isotropic and nematic peak. At lower temperatures, three features can be recognized. The one at the highest q value is assigned to the lamellar phase. The origin of the broad pattern with multiple peaks at lower q, however, remains unclear. A similar feature has been observed by Angelico et al.[12] for the system lecithin/iso-octane/water. Demixing may have occurred during the sample preparation, resulting in a non-equilibrium multi-phase sample.

This experiment was also carried out for sample 13 with similar composition (n_w = 5.5), using the SAXS technique at the University of Paderborn. In this case, the sample was heated to 60 °C in the isotropic phase, the temperature was slowly decreased to 30 °C, and then measurements were performed at increasing temperature. As shown in Figure 4.8 two peaks were obtained between 30 to 49 °C. The sharp line indicates the lamellar phase and the second broad peak at lower q shows the presence of another phase. This second phase probably is a nematic phase. The two phases coexist over a large range of temperatures.

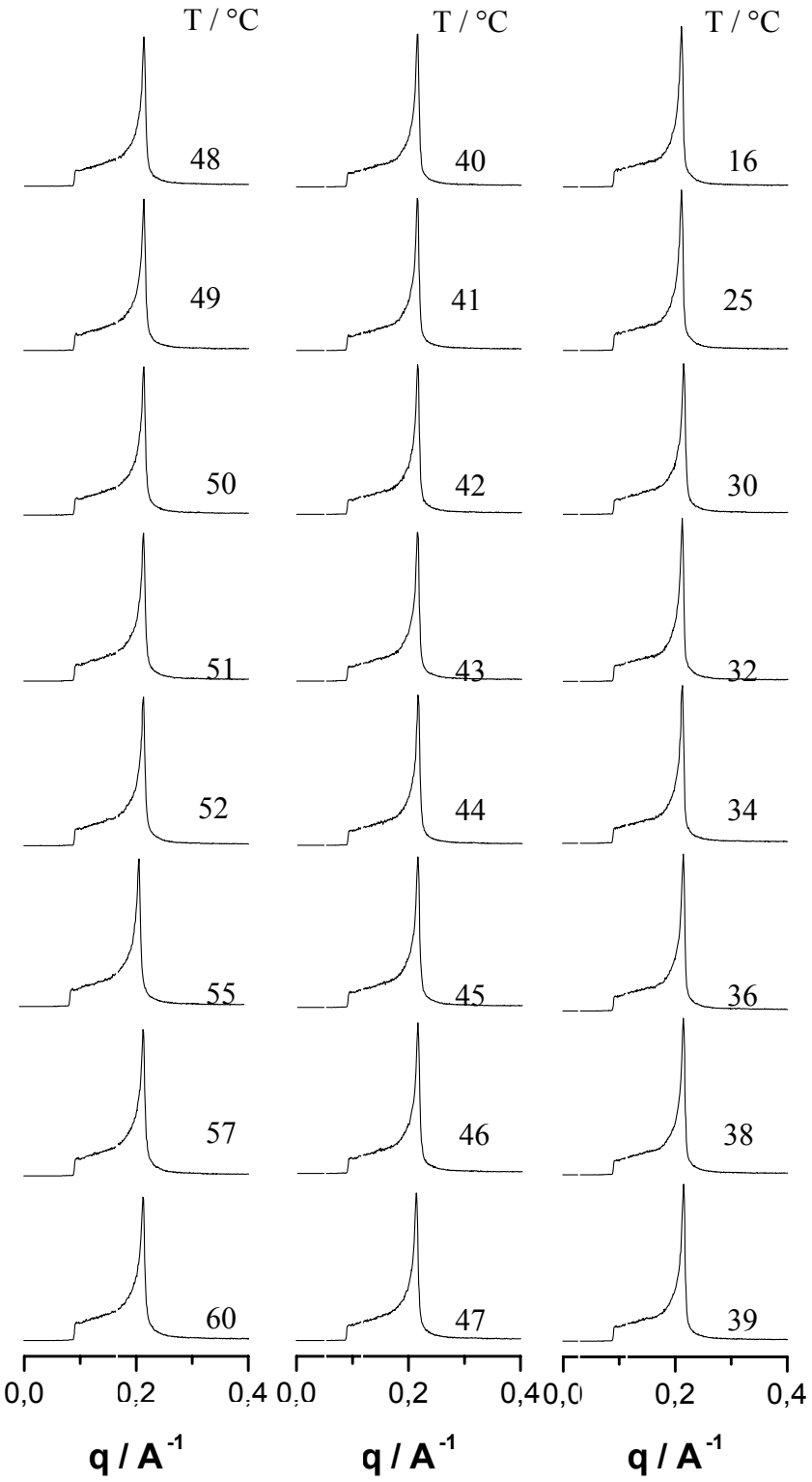

Figure 4.6 SAXS diffraction patterns obtained by scanning temperatures for sample 21 (n_w = 4) of the system lecithin/D_2O/n-decane in Lund University.

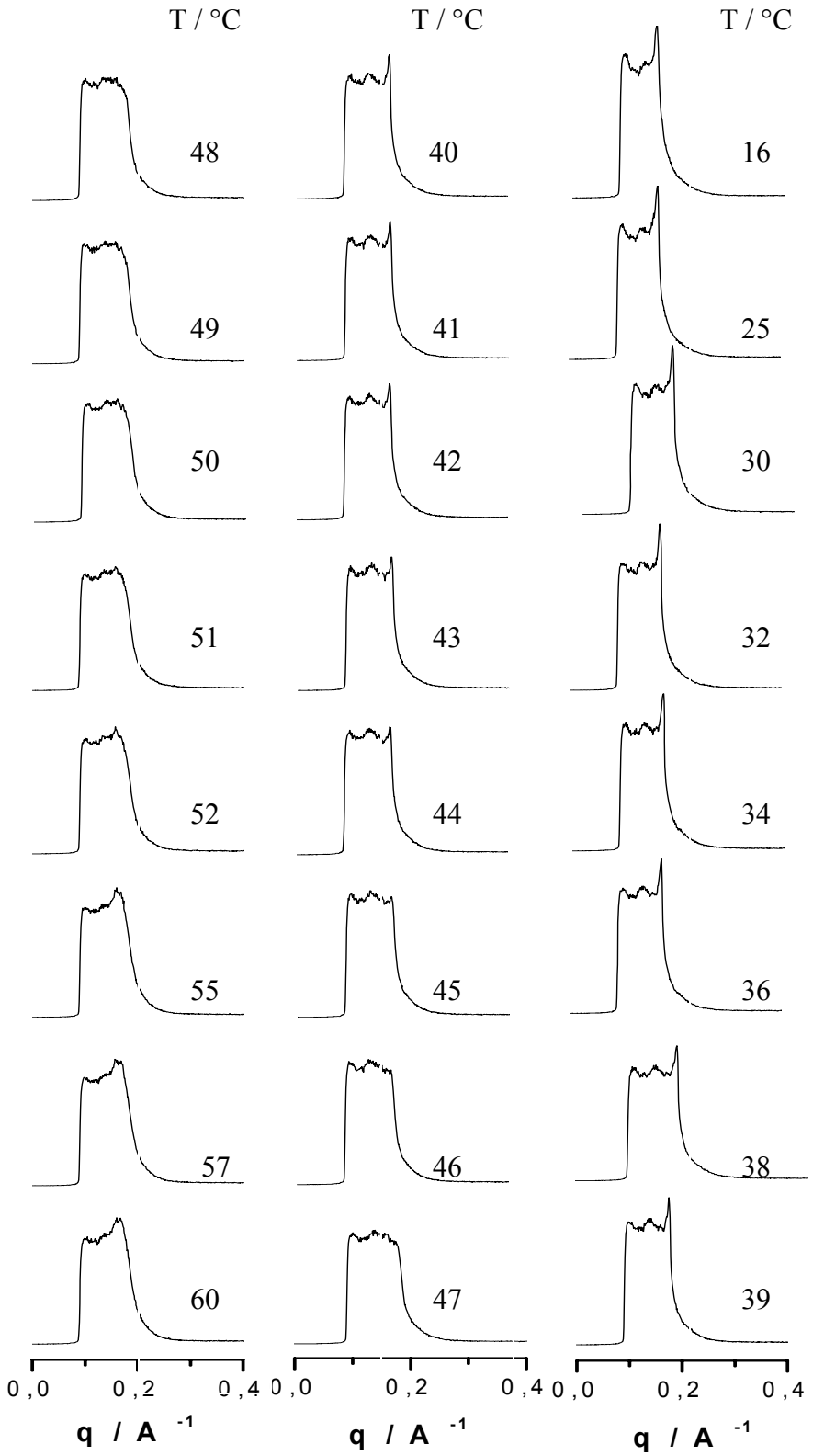

Figure 4.7 SAXS diffraction patterns obtained by scanning temperatures for sample 17 (n_w = 5.5) of the system lecithin/D_2O/n-decane in Lund University.

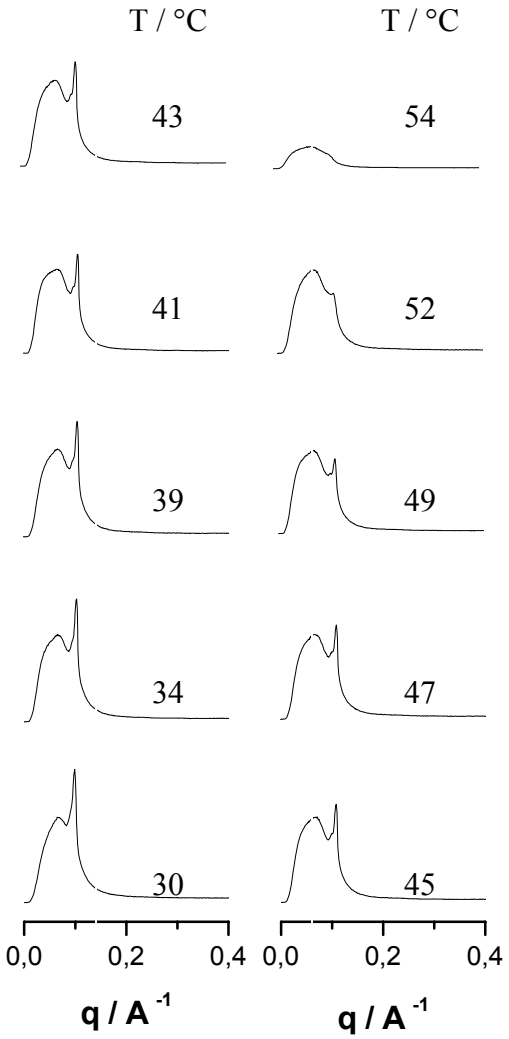

Figure 4.8 SAXS diffraction pattern obtained by scanning temperatures for sample 13 (n_w = 5.5) of the system lecithin/D_2O/n-decane at Paderborn University. Two different peaks in the SAXS pattern give evidence of the coexistence of Lα and N_D phases.

At 54 °C there is only the single broad peak of the nematic phase. Its low intensity could be due to a coexistence with the isotropic phase which may have lower scattering intensity. SAXS measurements give structural information about the distance between the lattice planes. Table 4.1 shows the average distances between bilayers and discs in the lamellar and nematic phases for samples with

n_w = 4 and n_w = 5.5, respectively. The results obtained for the measurement in Lund (Figures 4.6 and 4.7) and Paderborn (Figure 4.8) are shown. For the former experiment the exact position of the primary beam is not known any more. Therefore, two calculations for two different values for the channel of the primary beam were performed. The results for a beam position at channel 236 are closer to the ones obtained in Paderborn, for which a calibration had been carried out. Therefore, the correct values are 60 and 95 Å for the lamellar and nematic phase, respectively. The average distance between the discs in the nematic phase is larger compared to the bilayer period in the lamellar phase.

Table 4.1 The average period of the bilayer and discs in lamellar and nematic phases for samples with n_w = 5.5 and n_w = 4 of the system lecithin/D_2O/n-decane obtained by SAXS measurements.

Measurement Place	**Primary beam**	**D /Å**		
		Sample n_w = 5.5		**Sample n_w = 4**
		L_α	**N_D**	**L_α**
Lund University	119	35.6	46	31.4
	236	72.2	133.6	57.8
Paderborn University	-	60	95	-

4.3 Identification of Phase Transitions by ^{2}H NMR

The NMR spectrum from the deuterated water is dominated by the interaction of the deuteron quadrupole moment with the electric field gradient at the nucleus. In anisotropic liquid crystalline samples, the quadrupole interaction generates an NMR spectrum with two peaks of equal intensity, while for an isotropic LC phase or a solution a single sharp peak is obtained because of the rapid and isotropic molecular motions which average the interactions to zero.[111,112] The deuterium NMR technique is thus applicable in phase behaviour studies of amphiphile-water systems such as the system of AOT/brine (see appendix, Figure A.2) and the lecithin system investigated here. For a system containing more than one phase, the ^{2}H NMR spectra are superimposed unless there is fast ^{2}H exchange between the phases. For the mixture of lamellar and nematic liquid crystalline phases, two splittings can then be observed with the one originating from the lamellar phase being of larger magnitude than that obtained for the nematic phase.

In the following, the ^{2}H NMR study of the phase behaviour of lecithin/D_2O/n-decane is presented. Sample 11 was filled in 4 cm long glass tubes of 5 mm diameter, which were sealed with a Teflon plug and epoxy glue. The tube was inserted in a goniometer probe with the tube axis perpendicular to the static magnetic field. Spectra were obtained with a quadrupole echo pulse sequence, typically 128 scans were averaged. To obtain well-aligned lyotropic phases, the sample was pre-equilibrated in the isotropic phase at temperatures above 54 °C before cooling. Slow cooling from the isotropic to the anisotropic phase is sufficient to achieve uniform alignment of the anisotropic phase by the magnetic field. In figure 4.9 spectra as a function of the temperature are shown. The evolution of the phases is clearly seen: spectra with splittings characteristic of an anisotropic phase exist from 24 °C up to 52 °C indicating a large amount of the L_α phase. A small shoulder on the inner side of the right peak of the spectra at low temperature indicates the existence of another phase (probably a nematic one). An additional spitting is clearly seen at 44 °C and above, showing the co-existence of two anisotropic phases. The two anisotropic phases coexist with an

isotropic phase at 50 to 52 °C.

To elucidate the structure of the second phase which appears to exist in larger amount at elevated temperature, a rotation experiment, in which the line shape is measured in dependence of the sample orientation with respect to the magnetic field, was carried out. Changing the sample orientation by rotating it by 90° about an axis perpendicular to the magnetic field, one observes a change of the line shape. The new line shape corresponds to the superposition of doublets according to the distribution of director orientations in the sample. For a lamellar phase, after rotation the spectrum extends over the range of frequencies corresponding to the range of director orientations from θ = 90° to 0°. To distinguish L_α and N_D phases by the rotation experiment, the relaxation time of the samples needed to realign in the initial orientation was measured.

Rotation experiments carried out at two different temperatures, 30 and 49°C, for the presented system are shown in Figure 4.10. At 49 °C (right side of Figure 4.10), where a large fraction of nematic phase is expected, the first spectrum recorded after rotation of the sample by 90°, exhibits a line shape, which shows different orientations of the director with respect to the magnetic field. All orientations from 0° (edges of the shoulders) to 90° (maximum peaks) occur. The line shapes change in a way indicating that a partial relaxation towards the initial state occurs on the time scale of the rotation of the samples which takes about 30 s. This experiment was repeated at 30°C for the same sample. As can been seen in the left side of Figure 4.10 the line shapes immediately after rotation shows an additional splitting twice as big as the initial splitting but also intensities at an frequencies between the peaks of the outer doublet. This indicates a distribution of orientations of the normal vectors in a plane parallel to the magnetic field. Such a distribution is expected for a lamellar phase, the directors of which are aligned in the plane perpendicular to the magnetic field before the sample rotation and in a plane parallel to the magnetic field after sample rotation if no realignment occurs during the rotation. The relaxation time of director alignment for this sample with a large amount of lamellar phase at this temperature was found to be larger than 138 min. These results indicate that

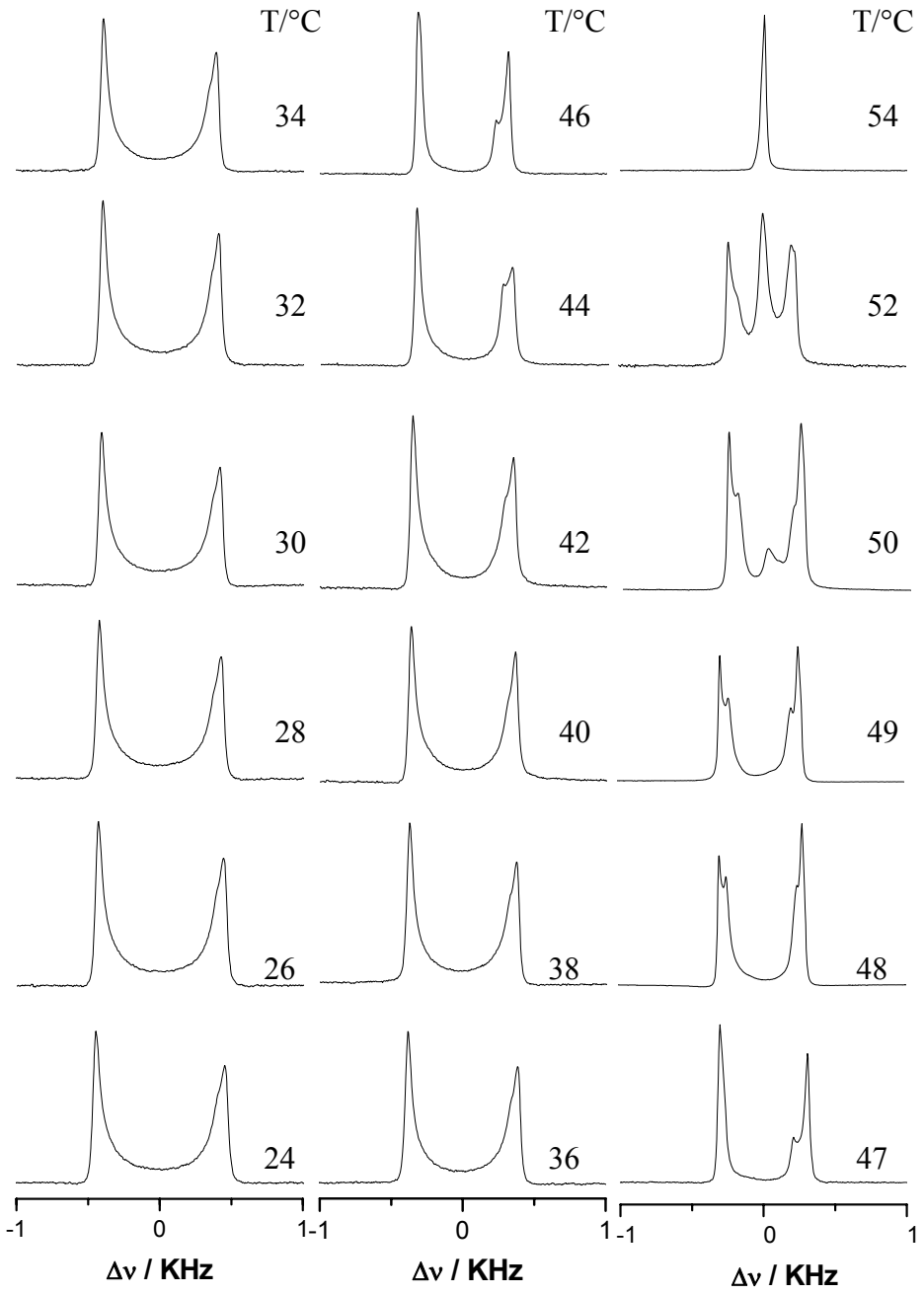

the

Figure 4.9 ^{2}H NMR spectra obtained by scanning temperatures for sample 11 (n_w = 5.5) of the system lecithin/D_2O/n-decane. For the lamellar phase (L_α) a quadrupole splitting $\Delta\nu$ is observed (spectra at 24 to 40 °C), whereas an additional nematic phase (N_D) gives an additional doublet with a small splitting at 42 to 49 °C. At 50 °C and 52 °C anisotropic and isotropic phases coexist. The single peak at 54 °C shows an isotropic phase.

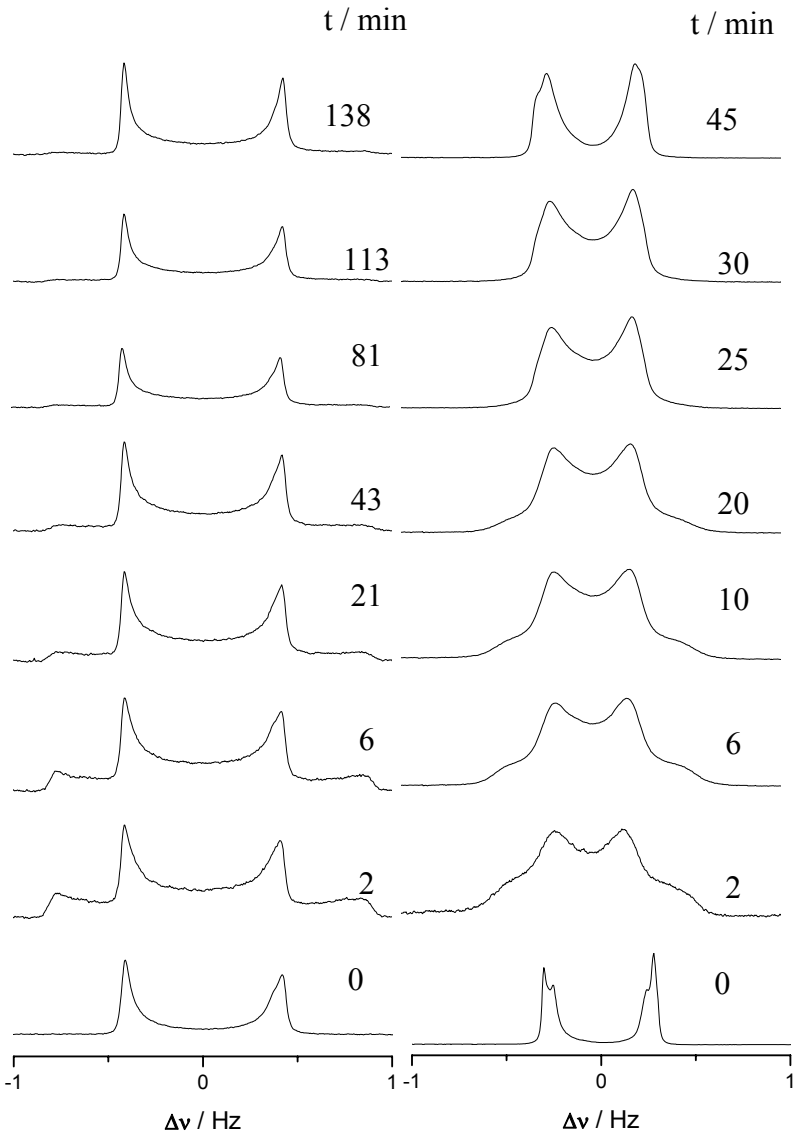

Figure 4.10 ^{2}H NMR spectra obtained before and after a sample rotation by 90° at two different temperatures 30 °C (left) and 49 °C (right) for sample 11 of the system lecithin/D_2O/n-decane. The relaxation of the director orientation at 49 °C is faster compared to 30 °C.

the relaxation at higher temperature, where a large amount of the nematic phase is present, is much faster due to the lower viscosity than the relaxation at low temperature with a large amount of the lamellar phase.
indicate that the

4.4 Identification of Phase Transitions by Rheological Experiments

The rheological signatures of the various liquid crystalline phases were determined using a Physica UDS 200 rheometer in stress-controlled mode. The measurement cell had cone-and-plate geometry with a cone angle of 1°. To determine the phase transition temperatures sweeps were performed for a sample of lecithin/D_2O/n-decane with n_w = 5.5 (sample 17) and a heating rate of 0.5 °C/min. The stress amplitude was 1 Pa (linear regime) and the angular frequency 1 rad/s.

Measurement of the storage and loss moduli as a function of temperature reveals different regions. Figure 4.10 shows an example of a temperature scan of G' and G" for the system lecithin/D_2O/n-decane. At 60 °C G' is lower than G" which indicates that the system is more liquid (existence of isotropic phase). By slow cooling of the sample to about 50 °C, the storage and loss moduli increase, G" remaining larger than G'. This is consistent with a sample consisting of some amount of lamellar phase in coexistence with a large portion of other phases (isotropic and nematic phases). Further decrease of the temperature to around 42 °C causes an approach of G' and G" and a crossing point between G' and G", at about 40 °C. Below 40 °C the sample is more elastic than viscous. At about 37 °C a discontinuity in the slopes of both G' and G" is observed. This may be the temperature, above which the lamellar phase coexists with nematic one in this sample. The behaviour is reversed as the temperature increases, in agreement with the changing proportions of lamellar and nematic phase observed by ^2H NMR and other techniques.

This experiment was repeated by scanning the temperature from 25 to 60 °C for a similar sample as shown in Figure 4.11. After equilibrating the sample in the isotropic phase, the temperature was lowered to 25 °C and the measurement was started upon increasing temperature. As shown in Figure 4.11 curves qualitatively similar to those of Figure 4.10 were obtained.

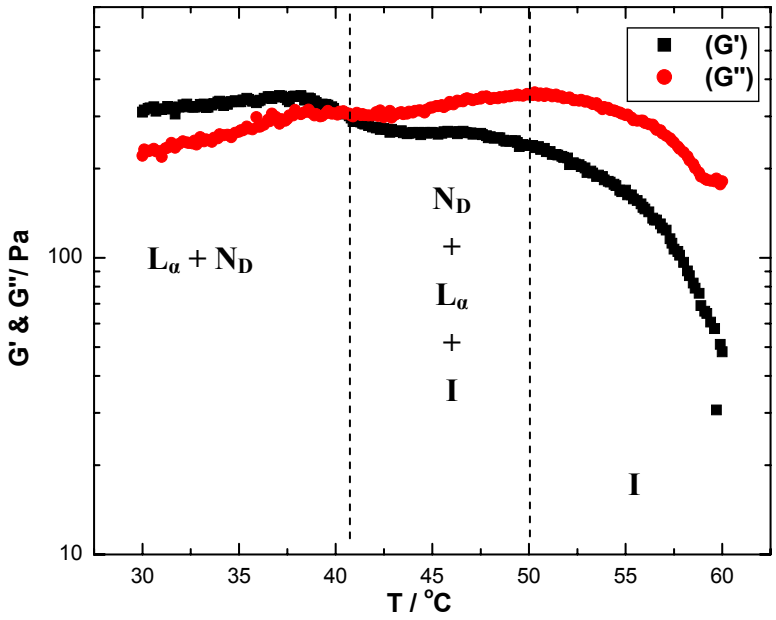

Figure 4.10 Storage, G', and loss, G", moduli as a function of temperature for the system lecithin/D_2O/n-decane with n_w = 5.5. The measurement was performed with decreasing temperature. The vertical lines indicate the temperatures were phase transitions where observed by ^2H NMR.

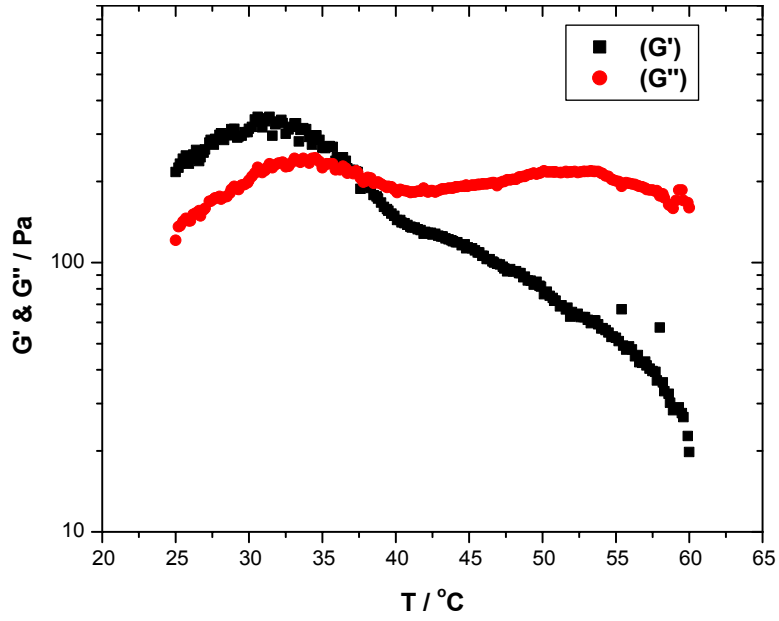

Figure 4.11 Storage, G', and loss, G", moduli as a function of temperature for the system lecithin/D_2O/n-decane with n_w = 5.5, measured at increasing temperatures from 25 to 60 °C.

4.5 Phase Diagram

The temperature dependence of many properties of surfactant solutions provides a convenient way to examine phase structures as a function of temperature. The phase transition temperatures of the system lecithin/D_2O/n-decane in a small region of the phase triangle were obtained by ^2H NMR measurements. The phase transitions were determined for a limited number of samples, 22–33 as listed in Table 3.3. The samples were prepared according to the standard procedure which is described in section 3.2. Figure 4.12 shows the complete pseudo ternary phase triangle of lecithin/D_2O/n-decane at 25 °C (top) and a sub-section of the phase triangle showing our samples investigated (bottom).

Figure 4.13 shows the transition temperatures between different regions of lamellar, nematic, biphasic and isotropic phases as a function of the mole ratio of deuterium per lecithin (n_w). Three different types of phase transitions are obtained: a) a lamellar phase to an isotropic one via a narrow two-phase region at low concentration of water ($n_w \leq 4$), b) a lamellar phase to the coexistence of the lamellar and nematic phases and c) the phase transition from this biphasic region to the isotropic phase, passing a three-phase region at high concentrations of water ($n_w > 4$).

The curves shown in Figure 4.13 were obtained by analyzing the quadrupole splittings of ^2H NMR spectra. Addition of more water (D_2O) to a system of lecithin–n-decane/D_2O increases the temperature of the transition to the isotropic phase. A large part of the phase diagram is occupied by a lamellar phase. The nematic phase could not be distinguished for samples with $n_w \leq 4$. For sample with $n_w > 4$ above a certain temperature two different anisotropic phases, a lamellar one and a nematic one, could be distinguished. Because the quadrupole splitting of these two phases are very similar at low temperatures the location of the boundary between the regions of pure L_α and $L_\alpha + N_D$ remains somewhat uncertain.

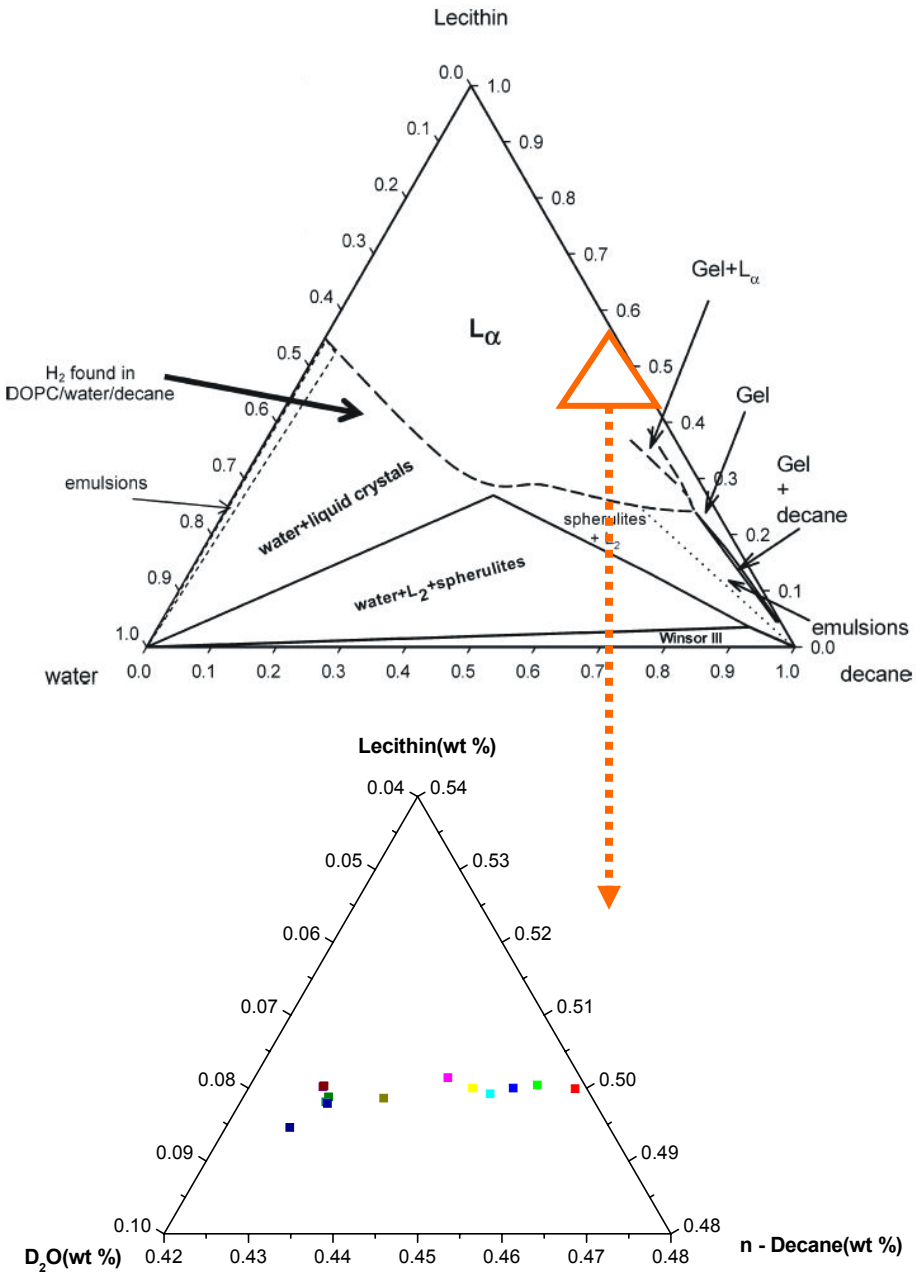

Figure 4.12 Phase diagram for the system lecithin/water/decane at 25 °C with single and multiphase areas which has been obtained by Angelico and co-workers (top)[12]. The samples with different compositions investigated by ^{2}H NMR are mapped in the phase diagram as shown at the bottom.

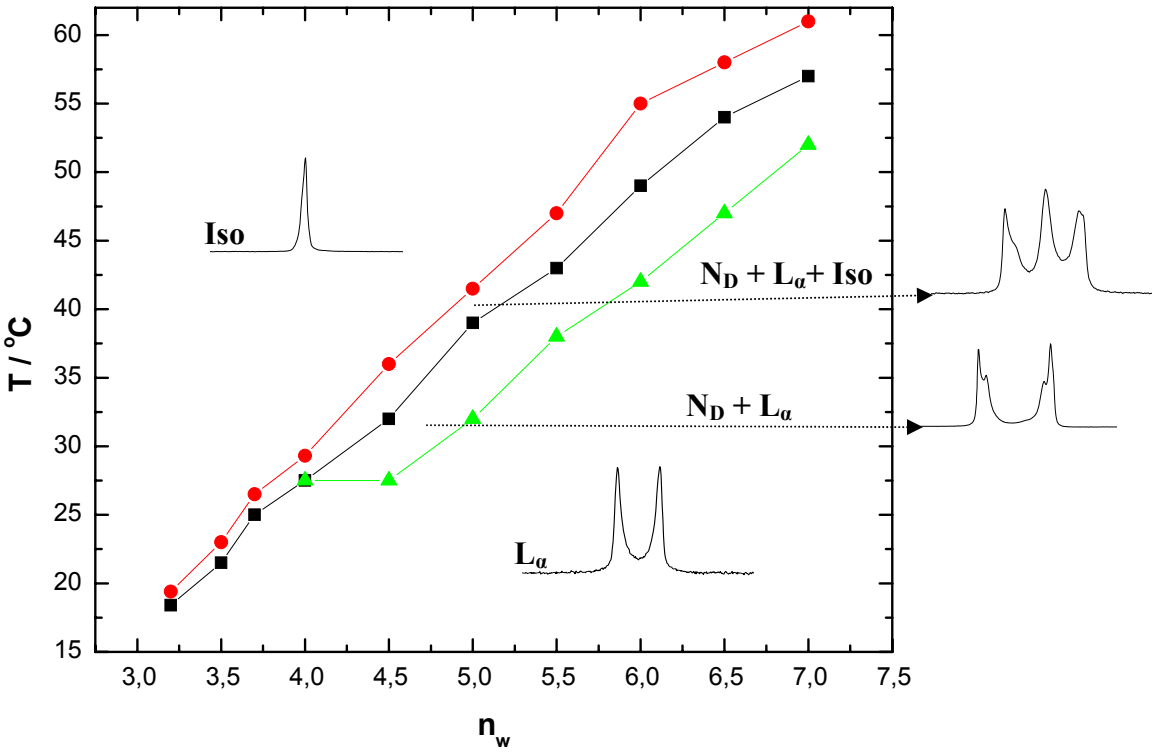

Figure 4.13 Temperature dependence of phase equilibria as a function of mole ratio of water to lecithin (n_w) for the system lecithin/water/decane. The curves indicate the phase transitions from L_α to biphasic $L_\alpha + N_D$ to $L_\alpha + N_D$ + isotropic to isotropic.

5 Synthesis of Colloidal Particles

A colloidal dispersion consists of colloidal particles dispersed in a medium. Both the particle and the dispersion medium can be in the gas, liquid or solid state. Colloidal dispersions are found in food, paint, foam, toothpaste etc. One specific type of colloidal dispersions is a sol, where solid particles are dispersed in a liquid. The liquid can be either polar or non-polar depending on the nature of the colloidal particles.[80]

The stability of a colloidal dispersion is determined by the interactions between the colloidal particles in the dispersion medium. As the colloidal particles are continuously moving around in the medium, they will sooner or later meet. If the colloidal particles attract each other, aggregates will form. An aggregation of colloidal particles that is reversible is termed flocculation, while an irreversible aggregation is called coagulation. Separation of the colloidal particles from the dispersion medium concentrates the particles, by sedimentation at the bottom or by creaming at the top, depending on the density of the particles compared to the dispersion medium. On the other hand, if the particles do not attract each other, the dispersion remains stable. Commonly, a difference between thermodynamically stable and kinetically stable dispersions is made, where a kinetically stable dispersion is only stabilized by an energy barrier between the particles. Stabilization of a colloidal dispersion is created either by electrostatic repulsion between the colloidal particles or by steric stabilization.[42]

The preparation of spherical particles via hetero-phase polymerization has developed into a mature technique in macromolecular chemistry.[28] The control of the particle size, size distribution and shape, or the incorporation of functional groups in the particles or on their surfaces is a central topic in preparative colloid chemistry. The result is an ever-growing number of new functional materials. The accessibility of highly monodisperse colloids within a tunable size range is a crucial prerequisite for the generation of photonic band gap materials.[29] Dye-labelled spherical particles[113] are used as calibration kits for optical methods e.g. confocal microscopy[30] or flow-cytometry.[31]

Three different kinds of spherical particles were synthesized throughout this work. Silica particles were prepared by condensation polymerization of tetraethoxysilane following Stöber.[114] Epoxy-functionalized acrylate colloids were synthesized according to the basic procedure of a surfactant-free emulsion polymerization which has been reported by Zentel and coworkers,[115,116] and the surface of these particles was modified by dodecylamine and dyes.[113] Finally micrometer-sized spherical melamine-formaldehyde resin particles were prepared according to a slightly modified procedure as described in a patent by Merck GmbH.[117]

5.1 Experimental Description

The materials used for the experiments in this section have been previously described in Chapter 3. All solvents were of technical grade, if not noted otherwise. Particle characterization was performed with a combination of scanning probe microscopy (Model Alpha, WiTec), light scattering, light microscopy and ^{13}C NMR techniques. Centrifugations were done using an Eppendorf centrifuge 5810 at speeds that never exceeded 200 rpm.

5.2 Synthesis and Characterization of SiO_2 Particles

Monodisperse colloidal silica can be prepared by a simple procedure from tetreaethoxysilane in alcoholic solutions:

$$Si(OC_2H_5)_4 + 4\,H_2O \xrightarrow[EtOH]{NH_3} Si(OH)_4 + 4\,C_2H_5OH \quad (1)$$

$$Si(OH)_4 \xrightarrow[EtOH]{NH_3} SiO_2\downarrow + 2\,H_2O \quad (2)$$

Hydrolysis, eq. (1), and condensation, eq. (2), of the monomers are base-catalyzed by ammonia, which also provides the particles with negative stabilizing surface charge. The general procedure for the synthesis of monodisperse silica particles is described in section 3.1.2.1.

Monodisperse, spherical particles were obtained by condensation polymerization. Figure 5.1 shows a nearly hexagonal periodic pattern of the SiO_2 particles which

was obtained by AFM (WiTEC type α-SNOM) indicating their spherical shape and size uniformity. Diameters in the range from 380 to 410 nm were realized.

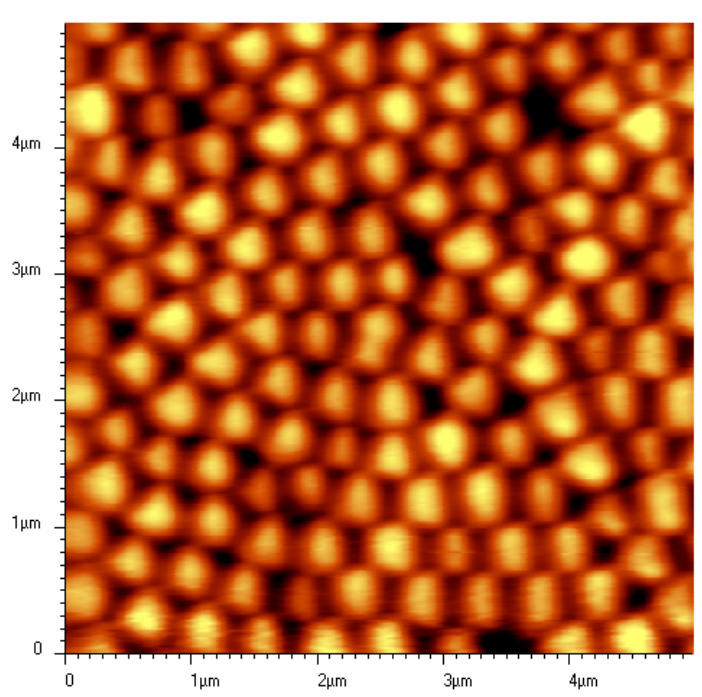

Figure 5.1 AFM picture of the monodisperse silica particles. The particle diameter was determined to be between 380 and 410 nm.

5.3 Synthesis and Characterization of PMMA Particles

The basic procedure is a surfactant-free emulsion polymerization, described in detail in the section 3.1.2.2. Particle synthesis is carried out by emulsion co-polymerization of MMA, cross-linker and epoxy-functionalized comonomer. In Figure 5.2 AFM pictures of a sample of epoxy-functionalized particles and of the same particles after modification with dodecylamine are shown. It can clearly be seen that a hexagonal close packed structure is formed, which is typical for monodisperse spheres. The particles retain their size and shape after surface modification. Light scattering experiments confirmed the particle size and narrow size distribution, with a polydispersity index *PDI* ≤ 1.05 for the epoxy-functionalized PMMA particles and *PDI* > 1.2 for the surface-modified sample. The results of the particles characterization are summarized in Table 5.2. The

values for the ratio of radius of gyration, R_g, and hydrodynamic radius, R_h, of the particles exceed the expected hard sphere value of around 0.86. To verify the incorporation of the epoxy-functionality, ^{13}C-NMR spectra of redissolved particles were recorded showing the expected signals in the epoxy regime at 65 ppm. Since no signals occur in this part of the spectrum for poly (methyl methacrylate), no disturbing signals from the main polymer component have to be considered. ^{13}C-NMR measurements were also carried out on the particles after surface modification with dodecylamine, but the amount of bound nucleophile is too small to be detectable by NMR.

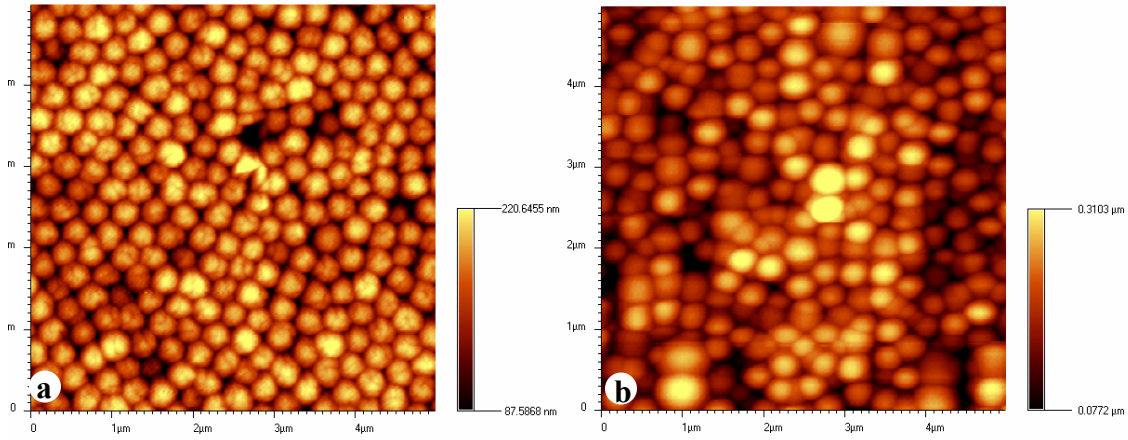

Figure 5.2 Topography of dried samples obtained by AFM measurements. The pictures show (a) epoxy-functionalized PMMA particles and (b) PMMA with dodecylamine.

Table 5.2 Results of particle characterization: AFM measurements were performed on dried samples, SLS/DLS was carried out in water and toluene. E-PMMA1: PMMA with epoxy groups, D-PMMA1: epoxy-functionalized PMMA particles surface-modified with dodecylamine.

Sample	R_{solid} [AFM] (nm)	R_g [SLS] (nm)	R_h [DLS] (nm)	PDI	R_g/R_h	Solvent
E-PMMA1	180	189	220	1.05	0.86	Water
D-PMMA1	186–197	177	222	1.2	0.80	Toluene

5.4 Synthesis and Characterization of Melamine-Formaldehyde Particles

Amino resins, also called aminoplast resins, are major cross-linking agents for baked thermosetting coatings. The amino resins most commonly used are derived from melamine (2,4,6-triamino-1,3,5-triazine).

The first step in the synthesis of melamine-formaldehyde (MF) resins is methylolation, the reaction of melamine with formaldehyde under basic conditions. With excess formaldehyde, the reaction can be driven to form predominantly hexamethylolmelamine (1), where R is H (see Figure 5.3). A mixture of partially methylolated derivatives, including species such as symmetrical trimethylolmelamine (2), is formed with less than the stoichiometric 6 mol of formaldehyde per 1 mol of melamine.

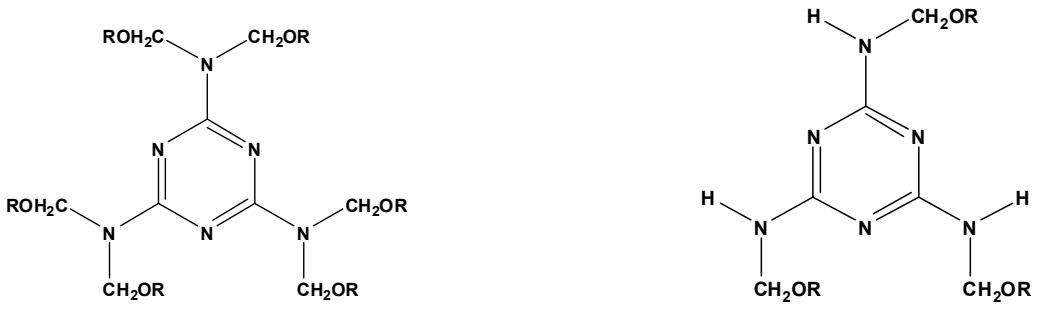

(1) (2)

Figure 5.3 The chemical structure of hexamethylol melamine (1) with R = H and trimethylolmelamine (2) with R = H.

The probable mechanism for the base-catalyzed reaction of melamine with formaldehyde is shown in Figure 5.4. The first step involves the nucleophilic attack by the amino group on the electrophilic C of formaldehyde, which is facilitated by the removal of a proton from N by the base (B^-). This is followed by proton transfer from the resulting B−H to the negative oxygen atom, which yields the methylolated product and regenerates the base catalyst. Both steps are reversible.

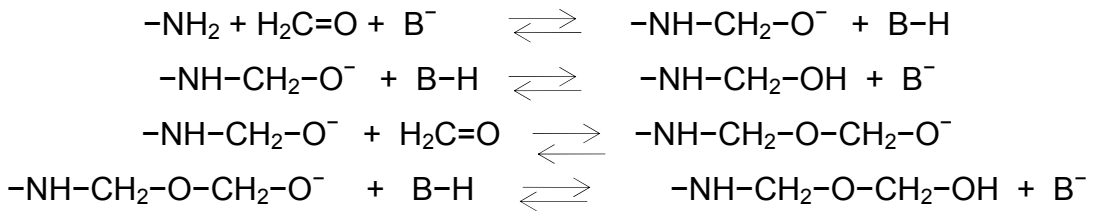

Figure 5.4 The probable mechanism for the base-catalyzed reaction of melamine with formaldehyde.

Studies of the kinetics of the reaction indicate that the presence of one methylol group on N deactivates the group for a second reaction by a factor of 0.6. On the other hand substitution on one amino group has little effect on the reactivity of the other amino groups. These kinetic factors favor formation of the symmetrical trimethylolmelamine (TMMM). However, the preference is not strong enough to overcome the thermodynamic tendency to produce mixtures of products. Thus, at equilibrium, the reaction of 6 mol of formaldehyde with 1 mol of melamine yields a mixture of products including all levels of methylolation and free formaldehyde.[118]

Details of the synthesis of M-F particles are given in section 3.1.2.3. As for the other types of particles the characterization was performed with scanning probe microscopy (SPM) and light microscopy. The SPM was operating in pulsed force mode using silicon cantilevers (pointprobe-FM, nanosensors). All samples were prepared on glass substrates. NMR spectra were recorded on a Bruker AMX 300 spectrometer. Chemical shifts are reported in ppm from tetramethylsilane (TMS). Dispersed melamine-formaldehyde micro-particles in water and aggregated particles as observed by light microscopy are shown in Figure 5.5 (a) and (b), respectively. The micro-particles attract each other, and after 24 hours aggregation occurs. This aggregation is reversible which means that a flocculation of the M-F particles occurred. In Figure 5.6 a dispersion of M-F micro-particles of M-F in n-dodecane is shown. The micro-particles can easily be resuspended in apolar liquids such as n-dodecane by mild sonication. The pictures shown were observed between parallel polarizers immediately after

sonication (a) and after 24 hours (b), respectively.

Figure 5.7 shows an AFM image of the M-F particles indicating their spherical shape and size uniformity. Diameters in the range from 1 to 1.8 μm were measured.

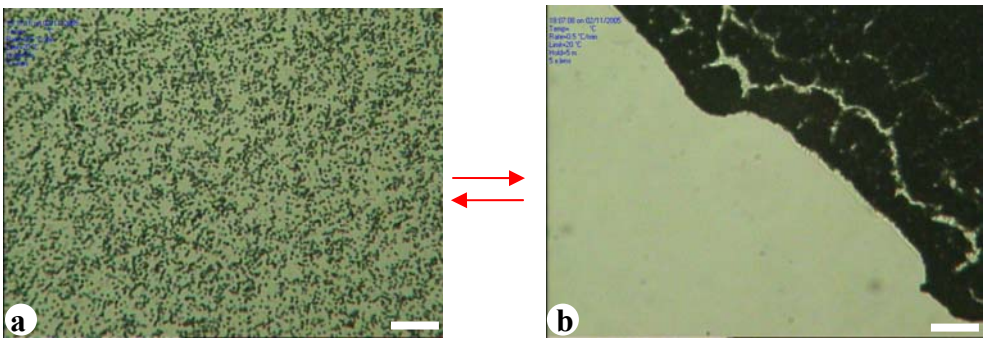

Figure 5.5 Pictures obtained by light microscopy of the micro-particles of melamine-formaldehyde in water. Pattern (a) shows a dispersion of monodisperse M-F particles in water. Pattern (b) shows the aggregation of M-F particles in water after 24 hours. Bar = 100 μm.

To verify the mechanism of M-F particles, ^{13}C NMR and FTIR spectroscopy were performed. An ether bridge in the micro-particles was found at 78 pmm in ^{13}C NMR and 1160 cm^{-1} to confirm the mechanism of M-F reaction.

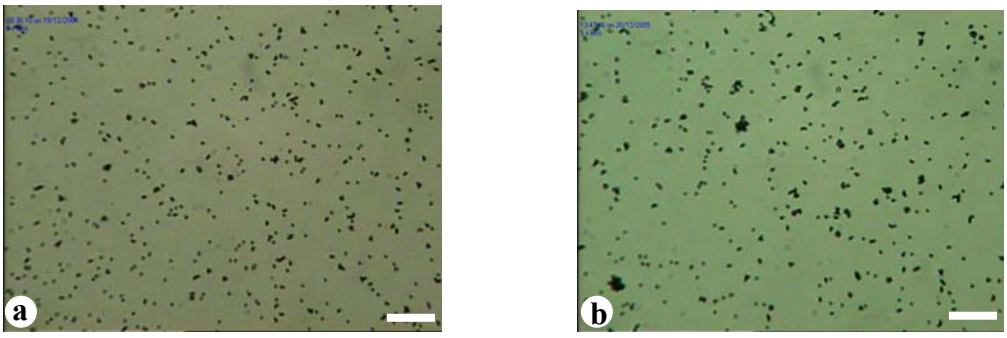

Figure 5.6 Pictures obtained by light microscopy of the micro-particles of melamine-formaldehyde in n-dodecane. Patterns show the dispersion of monodisperse particles in n-dodecane after dissolving the particles and mild sonication (a) and after 24 hours (b), respectively. Bar = 100 μm.

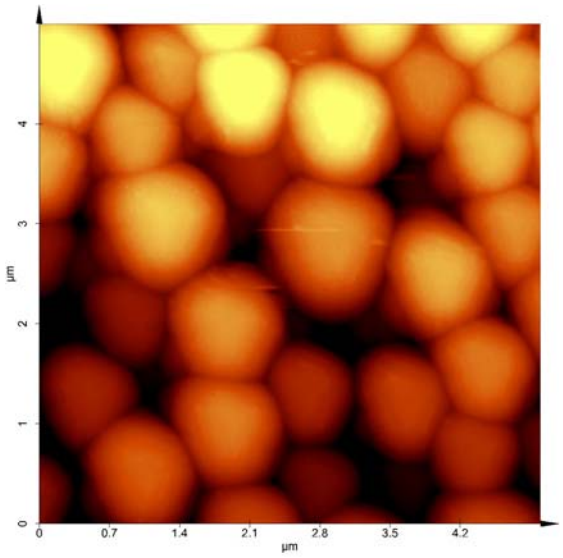

Figure 5.7 Topography of a dried sample of M-F particles obtained by AFM, covering a 5 × 5 µm square.

6 Influence of Micro-Particles on the L_α Phase under Shear

Liquid crystalline phases used as solvent for colloidal particles provide new methods to control the spatial organization of colloidal systems. Well defined anisotropic structures and new phases have been recently observed in several systems such as mixtures of rodlike viruses and colloid,[119] molecular nematic or cholesteric emulsions[39,120,121] and suspensions of latex particles in discotic micellar nematics.[122-125] The behaviour of lamellar phases under shear is a subject that has been receiving a lot of attention in recent years.[54-57] In fact, many different shear effects have been reported such as transformation from lamellar phase to MLVs, changes in lamellar orientation,[15,61,62] reduction in lamellar spacing[126] and transitions from MLVs to unilamellar vesicles.[67] The most interesting shear effect is the formation of MLVs in the presence of micro-particles. In the mixture, topological defects and distortions of layers around the particles are generated due to the incompatibility of particle size (μm) and the interlamellar space (5 nm). These defects also generate inter-particle elastic forces that govern the stability and the ordering of the particles.[38]

The aim of this work is to clarify whether defects in the layer structure of lyotropic lamellar phases generated by the incorporation of micro-particles enhances the nucleation of vesicles under shear. Regarding our goal, we have studied the kinetics of the MLV formation, the influence of spherical micro-particles on the shear-induced orientation states and the reversibility of size changes of the MLVs.

6.1 Experimental Description

The system investigated is the pseudo-ternary mixture of soybean lecithin in D_2O and n-decane. The PMMA particles used were provided by Dr. A. Imhof from Utrecht University. They are surface-modified with poly(12-hydroxystearic acid) and labelled with the fluorescent dye (Rodamine RITC) and had a diameter of 2 μm. The particles synthesized in this work either were too small to be observed by light microscopy or could not be well dispersed in the liquid crystal. Some of

them showed aggregation and poor miscibility with a lamellar phase (see appendix, Figure A.5). The D_2O to lecithin mole ratio was kept constant at $n_w \approx 5.5$ for all experiments. The composition of the samples is shown in Table 3.3. Samples 9, 16, 17 and 19 (without particles) and samples 10, 14, 15 and 20 (with particles of PMMA) have been used. These samples were all prepared according to a standard procedure as described in section 3.1.1.

The influence of micro-particles on the shear-induced orientation states in a lamellar system is studied by polarizing microscopy, deuterium rheo-NMR spectroscopy and rheological experiments. Detailed descriptions of these methods are given in chapter 3.

6.2 Results and Discussion

This section is divided into three subsections. These subsections correspond to groups of experiments that have been conducted to examine: (1) influence of micro-particles on the shear-induced orientation states of the lamellae, (2) influence of micro-particles on the formation process and size of MLV formation and (3) influence of micro-particles on the reversibility of shear-induced formation of the MLVs.

6.2.1 Influence of Micro-Particles on Shear-Induced Orientation States of the Lamellae

This subsection presents results from experiments in which the different orientation states of the lamellar phase of lecithin/water/n-decane under constant shear rate is investigated at various temperatures for two samples, one without particles and another one with 5 % particles. From the comparison of these results the influence of micro-particles on the shear-induced orientation states will be understood.

Figure 6.1 shows deuteron NMR spectra of the lamellar phase during shear. The spectra reflect the sequence of orientation states with increasing temperatures for a sample with $n_w = 5.5$ (n_w is mole ratio of D_2O/Lecithin). The spectra were recorded at a constant shear rate of 20 s^{-1} in the steady-state. For each series of NMR measurements the samples were heated up to temperatures slightly above

the transition into the isotropic phase. After alignment of the samples in the magnetic field by slow cooling through the biphasic regime of the isotropic/lamellar phase transition, the temperature was set to the initial value of the series, a spectrum at rest ($\dot{\gamma}$ = 0 s^{-1}) was measured and measurement of the temperature series under shear was started. The samples were sheared for 30 minutes at each temperature before measurements were started. The first spectrum depicted in Figure 6.1 (bottom left) corresponds to the magnetically aligned lamellar phase, which shows a director orientation perpendicular to the magnetic field. At T = 14 °C, upon the start of shear (20 s^{-1}) in the Couette cell the NMR line shape changes to a broad featureless spectrum which indicates the formation of multi-lamellar vesicles. The line shapes do not change until 18 °C but the line width of the spectra becomes smaller during the shear. With further increase of the temperature, a gradual transformation to a new line shape with a doublet splitting is observed. At 22°C the line shape resembles a powder pattern, which indicates that layers with all directions are present in the sample. At 24 °C a doublet grows from the outer edges of the powder line shape which indicates a preference of the director orientation parallel to the magnetic field, that is, a preference of the perpendicular orientation in the flow field. At 34 °C the layers show the best alignment with their normal axes parallel to the vorticity axis (parallel to magnetic field) in this so-called perpendicular orientation. This type of alignment gives rise to a doublet with almost twice the initial splitting. With increasing temperature once more the inner splitting is observed in the spectra showing a change to the parallel (a) orientation. With increasing temperature, however, the splitting decreases and finally vanishes due to transition to the isotropic phase at 40 °C.

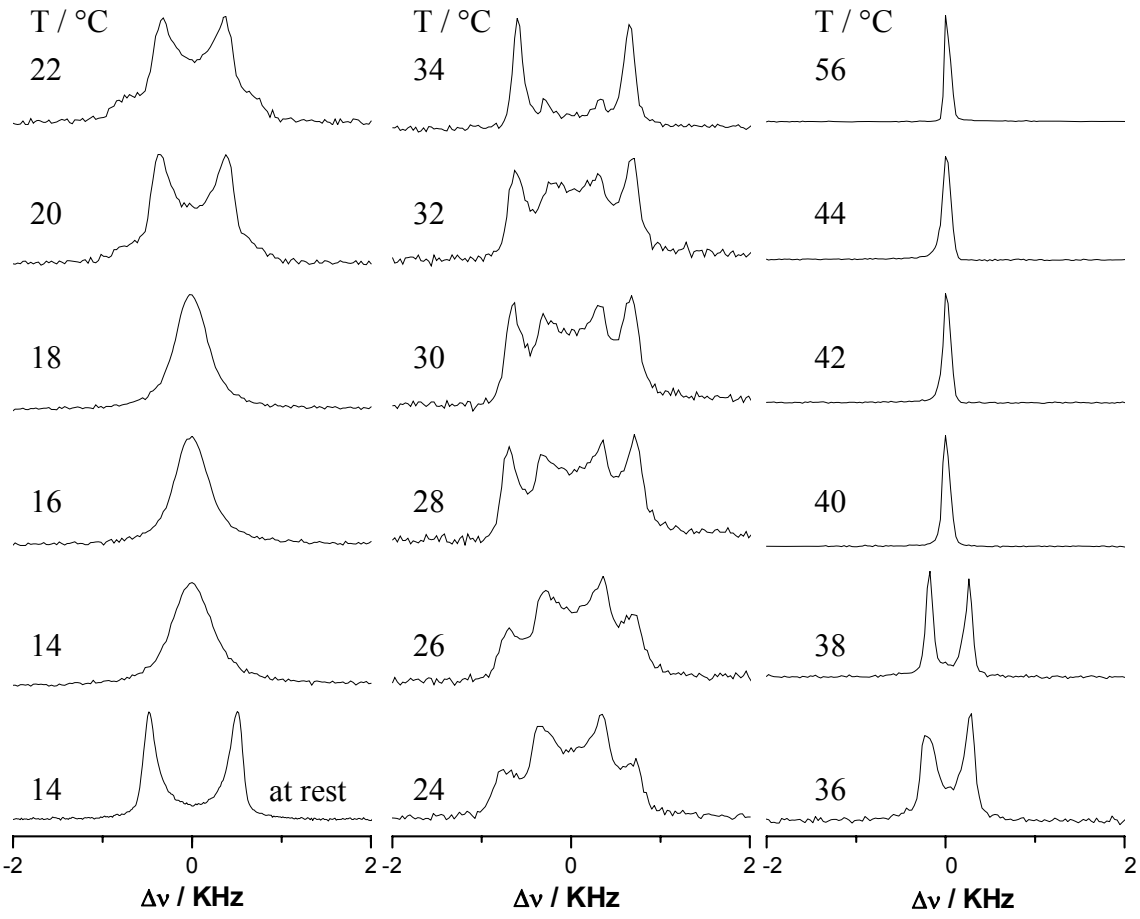

Figure 6.1 Deuteron NMR spectra obtained at different temperatures (30 min for each temperature) for sample 19 (containing no particles) with n_w = 5.5 of the system lecithin/D_2O/n-decane at a constant shear rate of 20 s^{-1}. The first spectrum (bottom left) was obtained at rest.

Deuteron NMR spectra of the lamellar phase of lecithin/water/n-decane during shear (20 s^{-1}) are shown in Figure 6.2 for a sample with surfactant concentration of 50 wt %, 43 wt % n-decane and 7 wt % D_2O mixed with 5 % micro-particles of PMMA (sample 20). The experiment was carried out in the same way as for the sample without particles. By increase of the temperature during constant shear rate for the sample with particles, different orientations of the director are observed as well. As can be seen in figure 6.2 at low temperatures a state of shear-induced MLV occurs. The spectra between 34 °C to 38 °C exhibit just

shoulders corresponding to the perpendicular flow orientation which indicates that only a small amount of the layer normals is parallel to the magnetic field, in contrast to the sample without particles. It might take more than 30 min for complete alignment or the state of perpendicular orientation does not exist in the presence of particles.

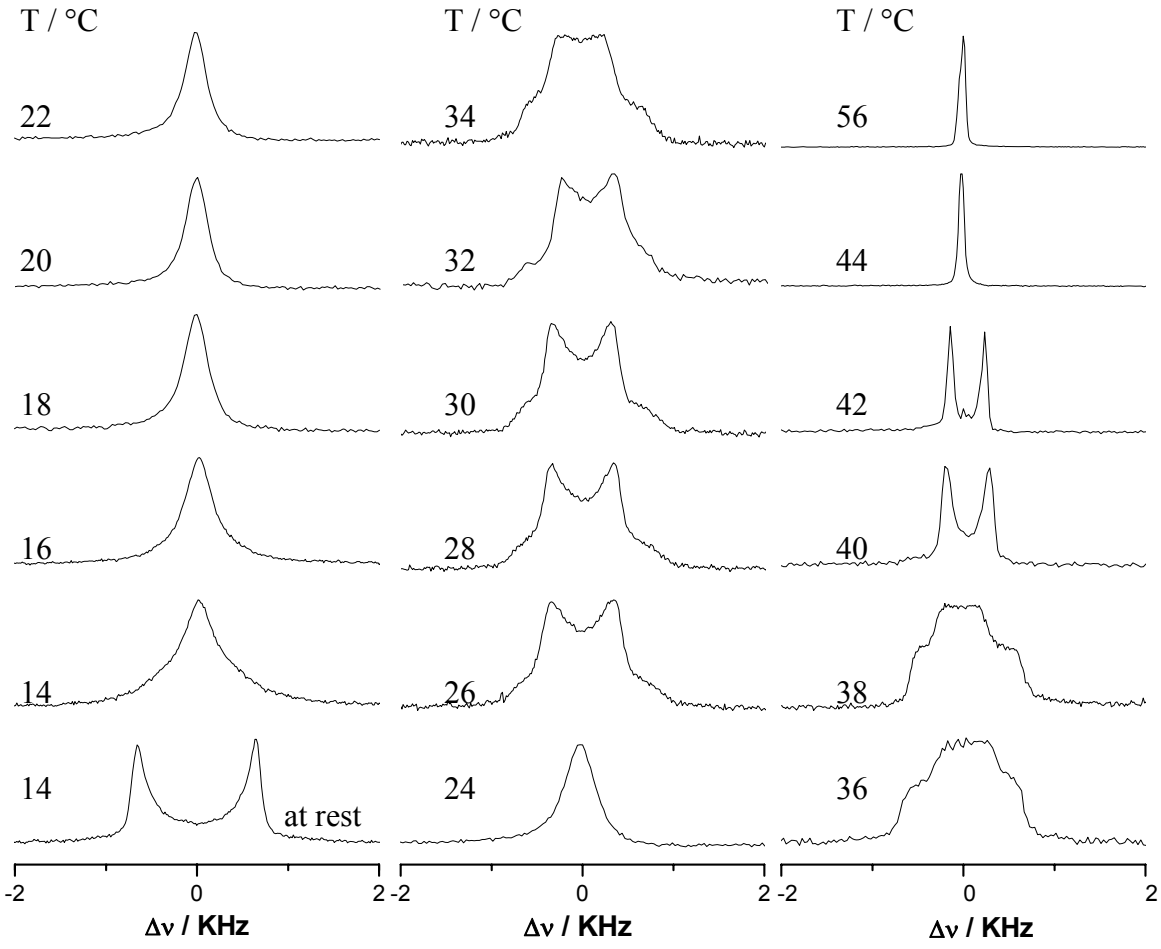

Figure 6.2 Deuteron NMR spectra obtained at different temperatures (30 min for each temperature) for sample 20 with n_w = 5.5 of the system lecithin/D_2O/n-decane at mixed with 5 % micro-particles of PMMA at a constant shear rate of 20 s^{-1}. The first spectrum (bottom left) was obtained at rest.

A comparison of the single broad spectra in Figures 6.1 and 6.2 shows that the MLVs were formed between 14 °C to 24 °C for a sample with 5 % particles, while

they exist between 14 °C to 18 °C for a sample without particles. This means that the temperature range where MLVs exist is larger for a sample containing particles, which indicates that the stability of MLVs (in comparison to planar layers) is increased when particles are present.

As can be seen in Figure 6.2 the perpendicular orientation was not observed during shear for a sample with 5 % particles, however, it appears clearly for a sample without particles at 34 °C. One may conclude from these results that not only a change in temperature but also adding micro-particles to an L_α system, changes the orientation state of the layers during shear.

At last, the temperature of the transition to the isotropic phase under shear for the two samples of Figures 6.1 and 6.2 is different. For the sample without particles it is around 40 °C while it is around 44 °C for the sample with 5 % particles. If we consider that the composition of the lamellar system, the duration of shear and the temperature applied for the two samples are similar, it is possible that additional micro-particles increase the stability of MLVs under shear.

6.2.2 Influence of Micro-Particles on MLV Formation Process and Vesicle Size

In this section, we will present the results from experiments, in which the kinetics of MLV formation is investigated by using ^2H rheo-NMR technique and rheology measurement. The following of these results the size dependence of MLV as a function of time at various shear rates will be presented.

6.2.2.1 The Results of ^2H NMR

Deuteron NMR spectra of the lamellar phase of lecithin/water/n-decane during shear are shown in figure 6.3 for two samples, one without particles and the other one with 5 % particles. The spectra were recorded at 16 °C at a constant shear rate $\dot{\gamma}$ = 1 s^{-1}. The number at each pair of spectra gives the shear strain $\gamma = \dot{\gamma} t$. The spectra at the bottom of each column were obtained at zero shear rate after aligning the samples in the magnetic field by slow cooling through the biphasic regime of the isotropic/lamellar phase transition. The quadrupole

splittings of the doublet spectra are 1191 Hz, and 1075 Hz for samples without particles and with 5 % particles, respectively. As can be seen from Figure 6.3, the transition from the aligned lamellar phase (characterized by the quadrupole splitting) to MLVs (broad single peak) started with a clear decrease of the quadrupole splitting until it vanishes at γ = 12540 and γ = 2640 for samples without and with particles, respectively. The line widths (full width of half height) for the samples as mentioned are 1198 Hz and 1104 Hz.

Figure 6.4 shows the quadrupole splitting, $\Delta\upsilon$, of the NMR spectra of the samples without particles and with 5 % particles as a function of time under a constant shear rate of 1 s^{-1}. In this plot, the transition regions from lamellar to MLVs are characterized by a rapid decrease of $\Delta\upsilon$ for the sample with 5 % particles. However, it decreases slowly for a sample without particles. In this diagram, t_c is defined as the time at which formation of vesicles has proceeded to the point where the splitting cannot be recognized any more. A comparison of the two curves in figure 6.4 shows that the formation of MLVs for a sample with 5 % particles is faster compared to the sample without particles.

The NMR spectra were recorded also at shear rates of 2, 5, 10, 20, 50 s^{-1} at constant temperature (16°C). The results of these experiments are in agreement with the results from the experiments at a shear rate of 1 s^{-1} at 16 °C. Figure 6.5 depicts the critical times where the splitting has vanished as a function of the shear rate for samples without and with 5 % particles. A comparison of the two curves in figure 6.5 shows that the addition of the particles is found to accelerate the formation of multi-lamellar vesicles compared to the system without particles.

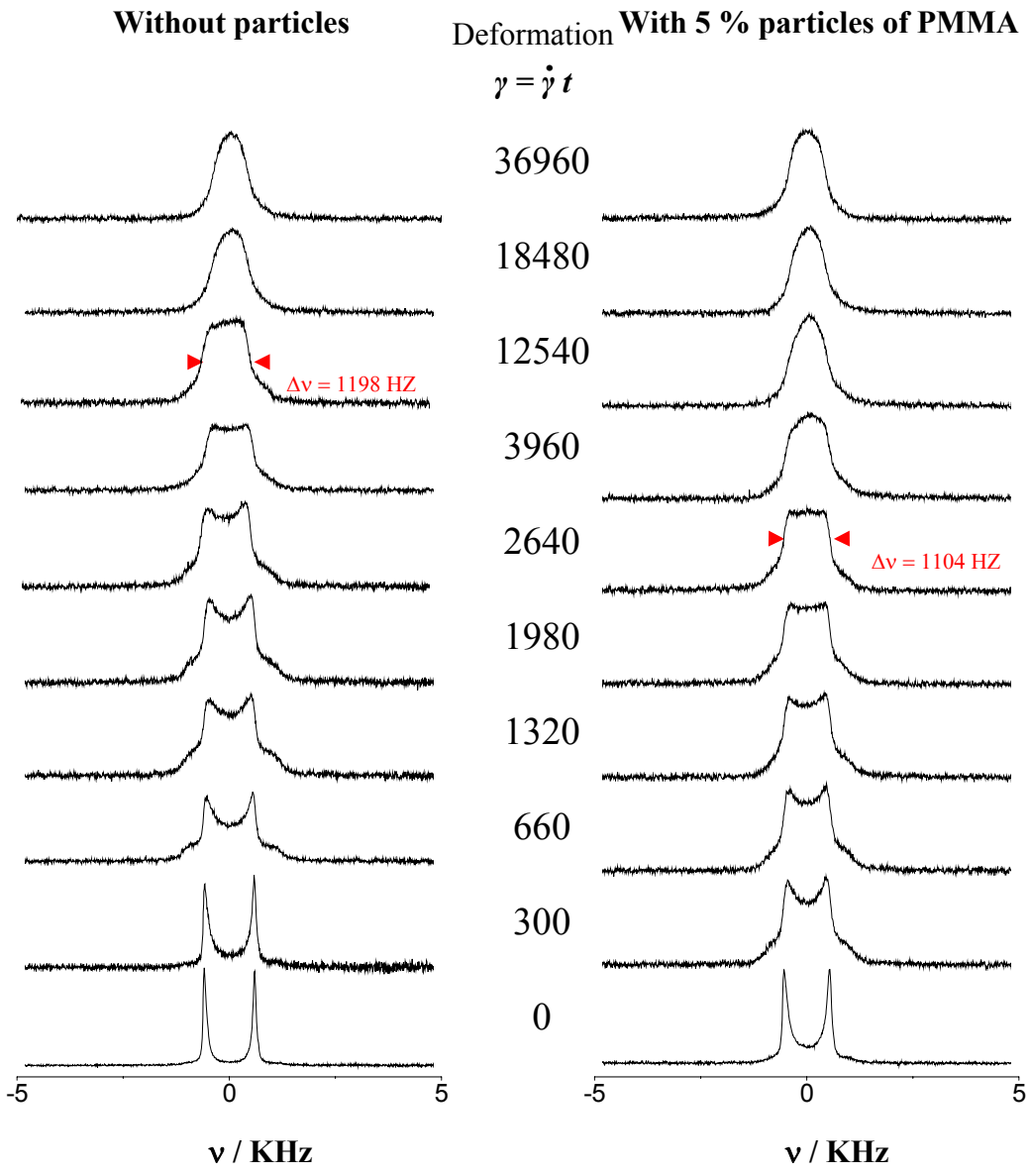

Figure 6.3 Deuteron NMR spectra obtained at different deformations for samples 9 (left) and 10 (right) of the system lecithin/D_2O/n-decane at a constant shear rate of 1 s^{-1} and T = 16 °C.

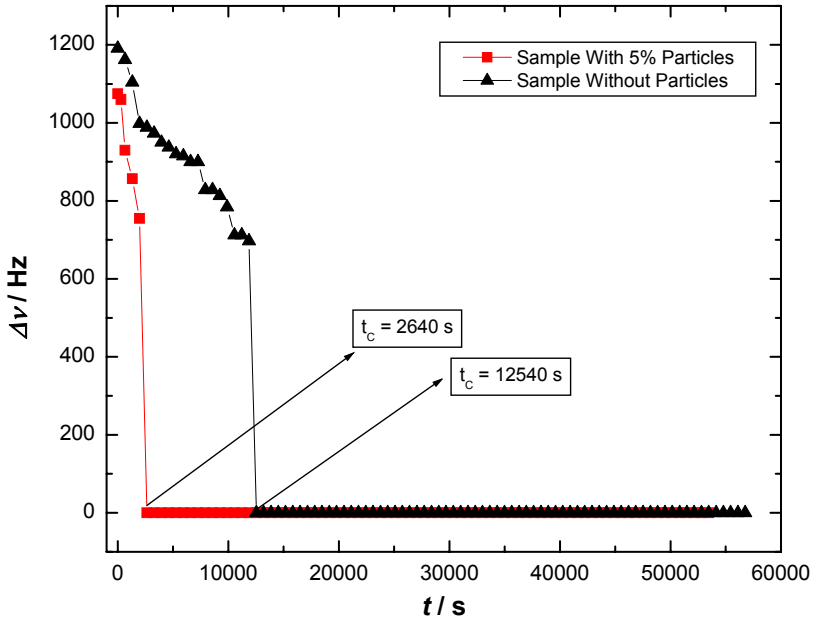

Figure 6.4 Quadrupole splitting as a function of time for the spectra shown in figure 6.3. t_c is the critical time when the splitting can no longer be determined.

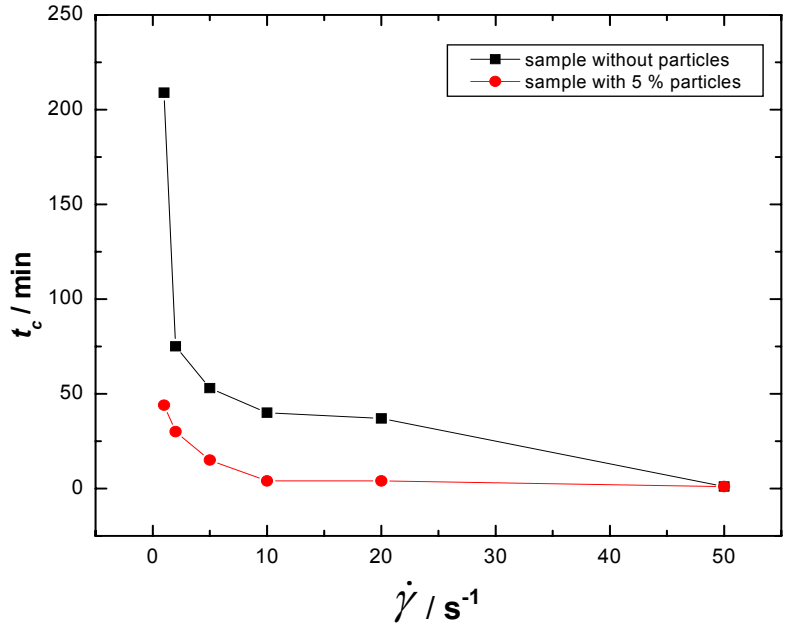

Figure 6.5 Critical time t_c as a function of shear rate for samples 9 and 10 of the system lecithin/D_2O/n-decane at T = 16 °C.

In Figures 6.6 and 6.7 the different line shapes of NMR spectra at various shear rates (1, 2, 5, 10 s^{-1}) for samples without particles and with 5 % particles are presented. The numbers at each pair of spectra give the shear strain (deformation). At rest the samples are aligned with the director perpendicular to the magnetic field, resulting in the doublet spectra seen in the first spectra (bottom). Upon applying shear, the director orientation changes and the NMR line shapes change to the single broad peaks characteristic of MLVs. Only the spectra obtained at large strain are shown in Figures 6.6 and 6.7. A close inspection of the spectra in Figures 6.6 and 6.7 indicates that not only the shear rate but also the presence of micro-particles can change the size of the multi-lamellar vesicles. This is seen even better in Figures 6.8 to 6.11, in which the line widths of the spectra in Figures 6.6 and 6.7 are shown as a function of time and strain.

Figure 6.8 shows the full line width at half height, L_W, of the NMR spectra of the sample without particles as a function of time at different shear rates. In this plot, the region I is characterized by a rapid decrease of L_W. The beginning of region II can be identified as the point where the slope of the curves becomes zero. Within region I, L_W decreases, until in region II a constant plateau is reached, indicating that the MLVs have reached their steady-state size. The decrease of the line width to lower values at higher shear rates reflects the dependence of the steady-state MLV size on the shear rate, well known from other lamellar systems. A comparison of the curves in figures 6.8 demonstrates not only that the MLVs are smaller at higher shear rates but also that the transition to the steady-state with MLVs of constant size occurs faster at high shear rates.

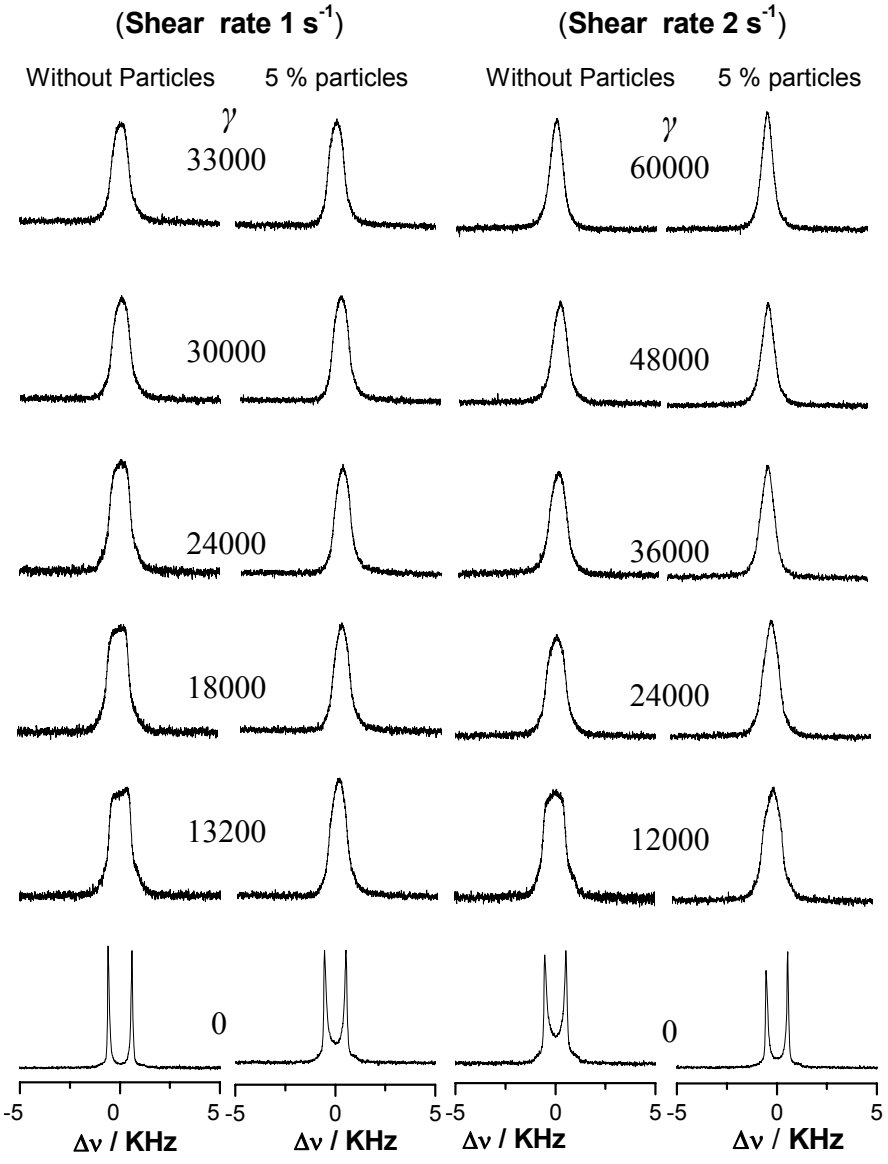

Figure 6.6 Deuteron NMR spectra obtained at different deformations for samples 9 and 10 of the system lecithin/D_2O/n-decane at shear rates of 1and 2 s^{-1} and T = 16 °C. Spectra at rest and at large stain are shown.

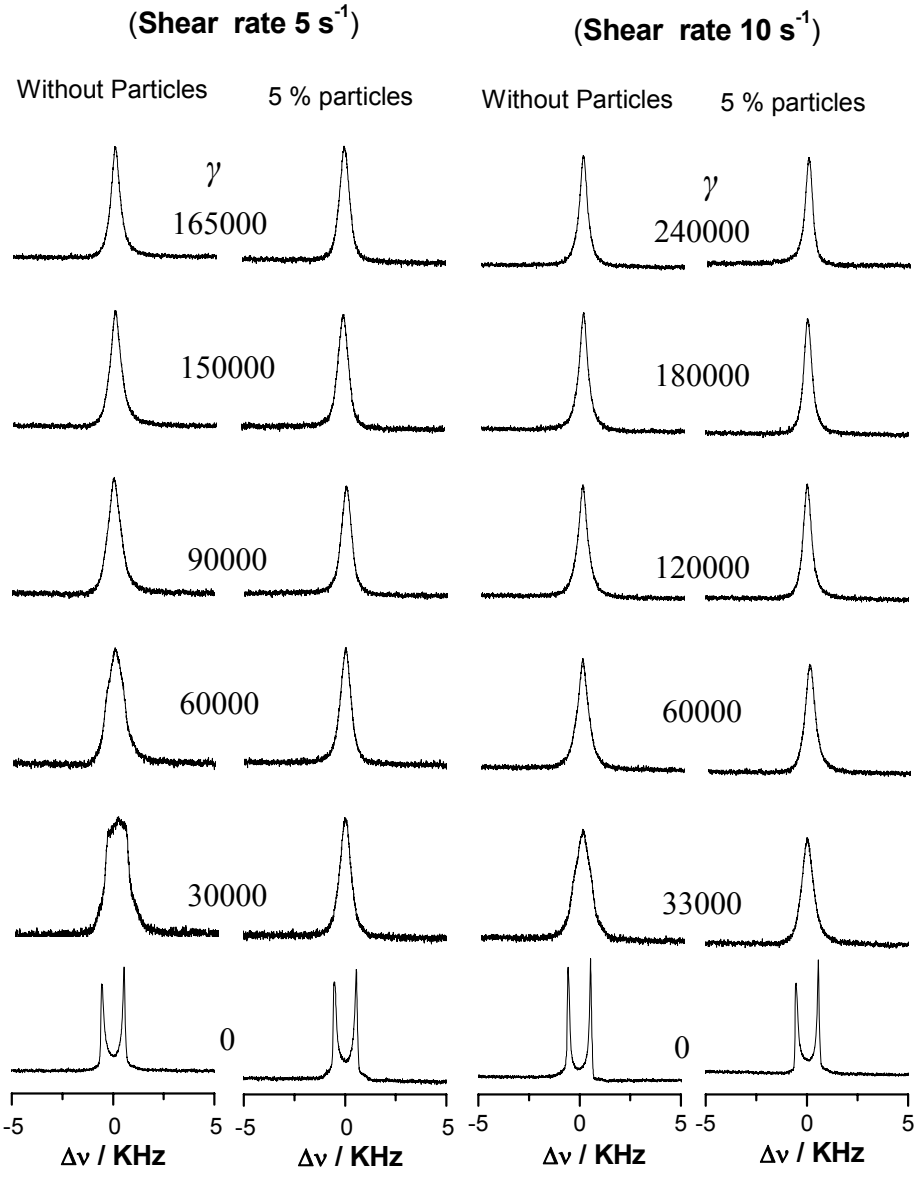

Figure 6.7 Deuteron NMR spectra obtained at different deformations for samples 9 and 10 of the system lecithin/D_2O/n-decane at shear rates of 5 and 10 s^{-1} and T =16 °C.

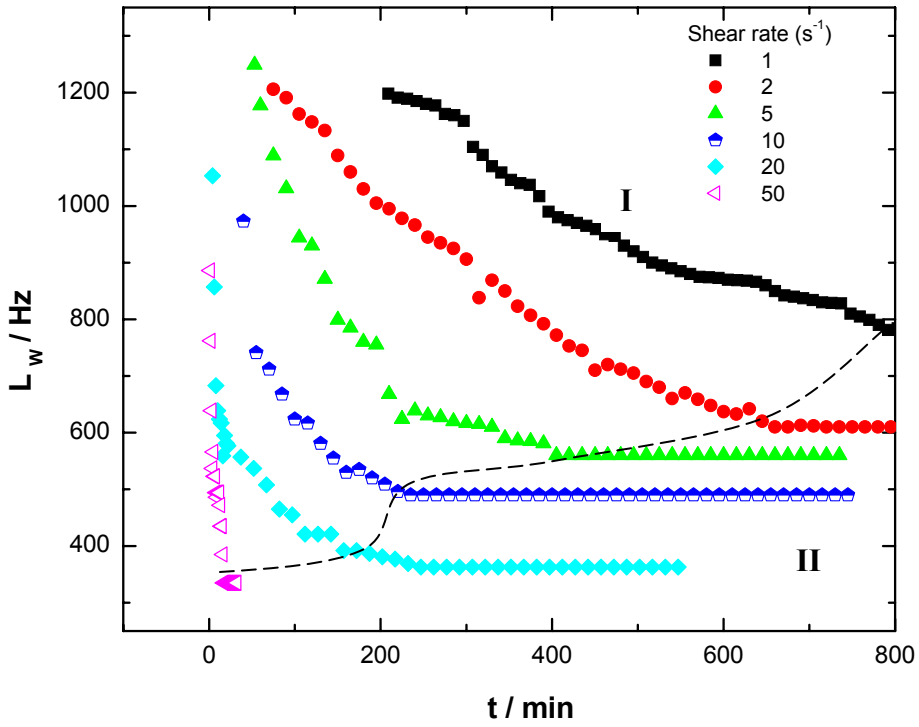

Figure 6.8 Full line width at half height of the NMR spectra of sample 9 of the system lecithin/D_2O/n-decane as a function of the time at T = 16 °C.

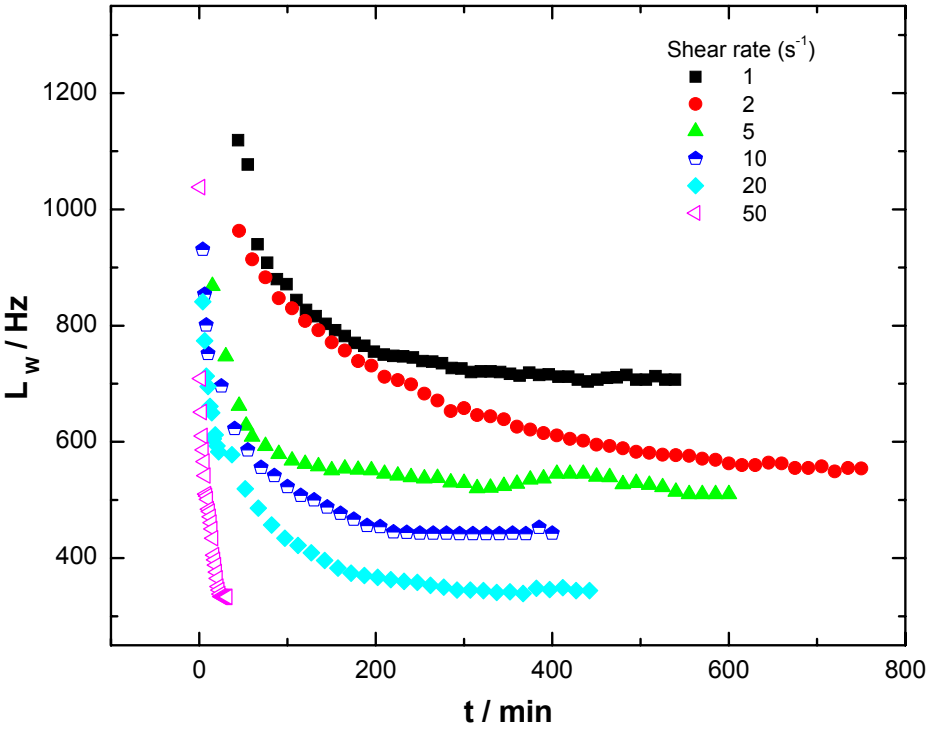

Figure 6.9 Full line width at half height of the NMR spectra of sample 10 (with 5 % particles) as function of the time at T = 16 °C.

Figure 6.9 depicts the line width L_W of the NMR spectra of the sample with 5 % particles as a function of time at different shear rates. As in Figure 6.8 the transition to the steady-state of MLVs is identified by a sharp decrease of L_W. A comparison with Figure 6.8 shows that the plateau values reached are lower in the presence of particles, indicating that the size of the MLVs is smaller.

In Figures 6.10 and 6.11 the same data as in Figures 6.8 and 6.9 are plotted but as a function of strain instead of time. Although there is no perfect scaling with the strain it becomes obvious that strain and not time is the important parameter for the MLV formation. The comparison of the curves in Figures 6.8 and 6.9 or in Figures 6.10 and 6.11 shows that in the presence of particles the size of onions is smaller compared to the system without particles under the same conditions. There are energetic reasons for this: the stability of multi-lamellar vesicles can be described as an equilibrium between large strain energies (drag force) at the interstices between onions which are strongly deformed and large curvature energies (thermodynamic force) of bilayers in the core. If we consider that the presence of a particle in the onion core reduces the elastic part of the stress, equilibrium with the drag force can be reached at a smaller onion size. However, this is rather speculative.[35,73]

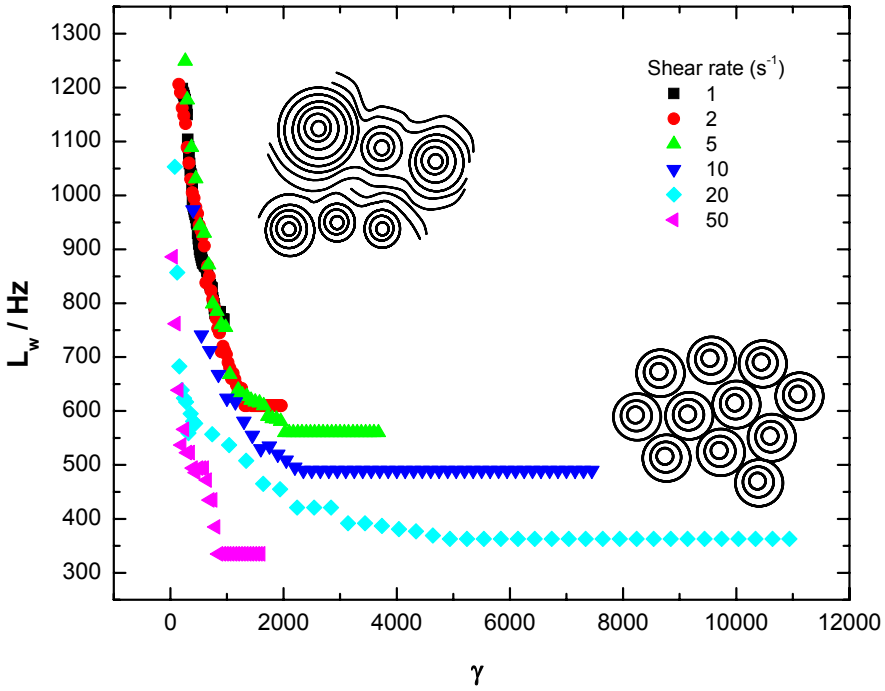

Figure 6.10 Full line width at half height of the NMR spectra of sample 9 of the system lecithin/D_2O/n-decane as a function of the deformation at T = 16 °C.

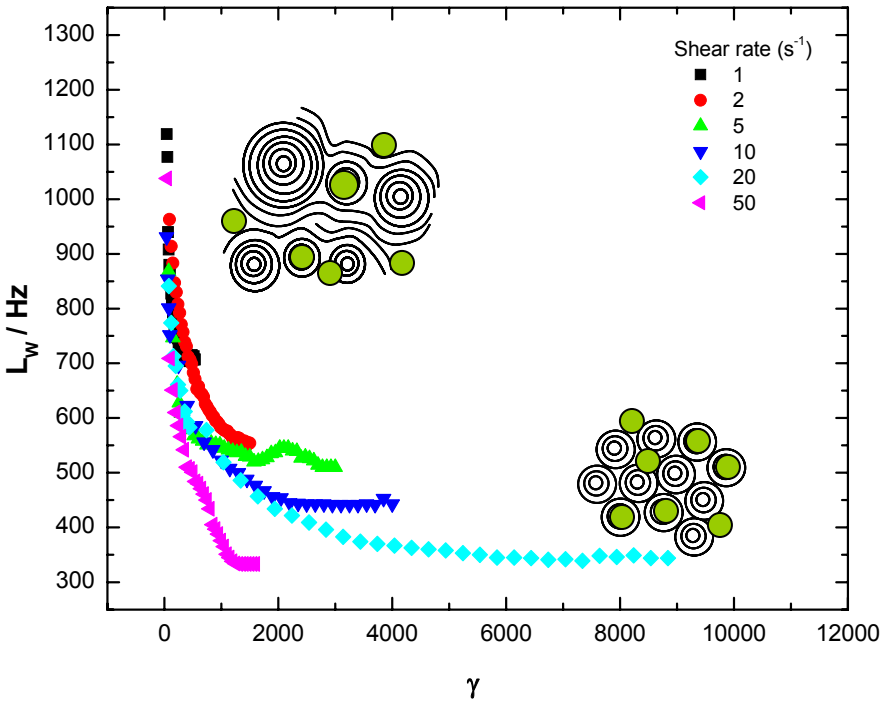

Figure 6.11 Full line width at half height of the NMR spectra of sample 10 (with 5 % wt micro-particles of PMMA) of the system lecithin/D_2O/n-decane as a function of the deformation at T = 16 °C.

6.2.2.2 The Results of Rheology

The kinetics of onion formation from the lamellar phase and the influence of micro-particles on the formation of MLVs as shear proceeds can be investigated by using rheological techniques. In this section flow experiments (transient viscosity η(t) under constant shear rate), and viscoelastic properties (storage and loss moduli, G' and G") of the lyotropic lamellar phase composed of lecithin/D_2O/n-decane for a sample without particles and a sample with PMMA micro-particles will be presented. Detailed descriptions of the equipment and the sample preparation used for these experiments are given in chapter 3.

In Figure 6.12 the steady-state viscosity as a function of shear strain at constant shear rate of 5 s^{-1} and constant temperature of 16 °C is shown. After pre-shearing the sample for 10 min at 5 s^{-1} and 35 °C for alignment of the lamellar phase, the sample was cooled to 16 °C and a constant shear rate of 5 s^{-1} was applied for 1 hour. During the pre-shear (not shown) the viscosity for the three samples 14, 15 and 17 (see Table 3.3) decreases indicating the alignment of the lamellar phase. Figure 6.12 shows the viscosity as a function of strain for samples 14(A), 15(B) and 17(C) which indicates that the orientation or the structure of the L_α phase changes. In the beginning, the viscosities of the samples are $\eta_C > \eta_B > \eta_A$ which indicates that by adding micro-particles of PMMA to the lamellar phase the system becomes more viscous. The constant plateau is reached at 1250 s for sample (C), while for sample (B) and sample (A) a plateau or maximum indicating the formation of MLVs is reached at later times. The decrease of the curves in the end region of the diagram for samples (C) and (B) indicates that the size of MLVs becomes smaller.

A comparison of the curves for the three samples in Figure 6.12 indicates not only that adding 5 % micro-particles of PMMA to a lamellar system accelerates the formation of MLVs compared with samples containing only 1 % or no particles but also that the size of MLVs become smaller resulting in lower viscosity, if the particles are incorporated into the core of the onions.

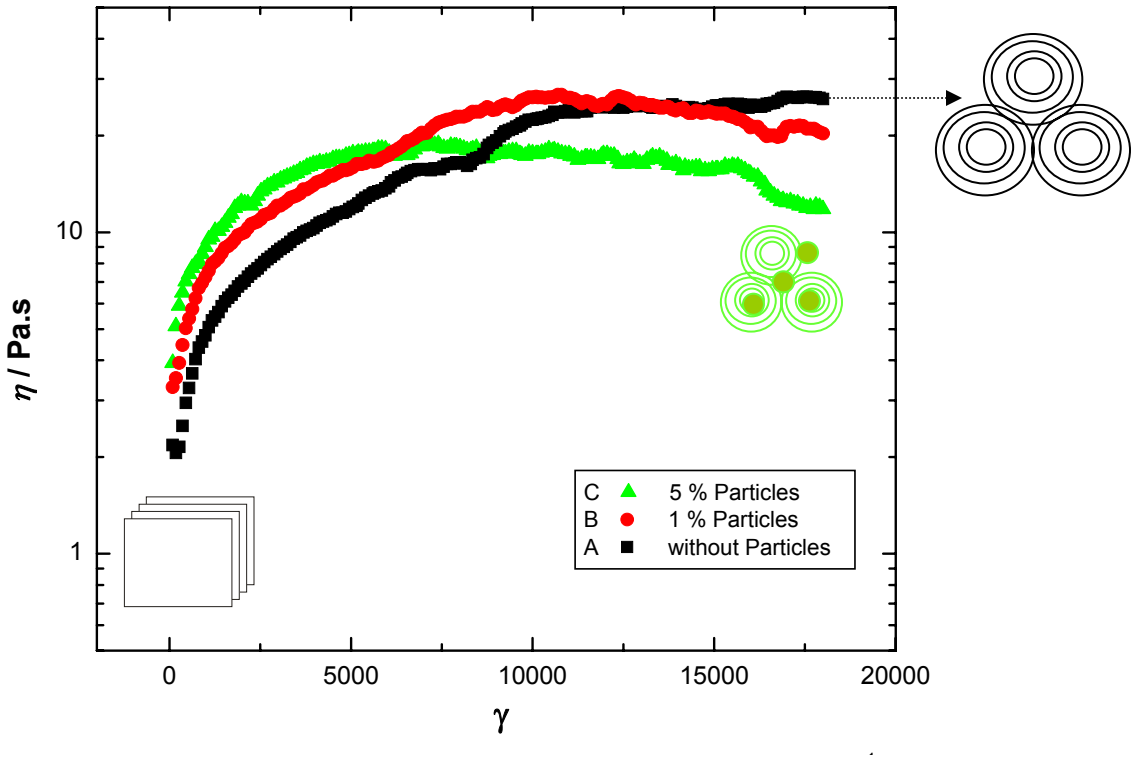

Figure 6.12 Viscosity versus deformation for samples 17 (A), 15 (B) and 14 (C) of the system lecithin/D_2O/n-decane at $T = 16$ °C under constant shear rate $\dot{\gamma} = 5\ s^{-1}$.

Figure 6.13 shows the viscosity of samples with lecithin/water/n-decane filled with 5 %, 1 % and without micro-particles as a function of strain at constant shear rate of 1 s^{-1} and constant temperature of 16 °C. In this plot, the viscosity for sample 14 (C) is higher than for the other samples. Upon application of shear to an aligned lamellar phase, a steep increase of the viscosity is observed which is evidence of the reorganization of the lamellar phase into MLVs. A gradual increase of viscosity at about 1800 s might indicate the formation MLVs. With continued shear a constant plateau can be reached which is not shown in the diagrams.

A comparison of the curves for the three samples in figure 6.13 shows that the viscosity of the sample with 5 % particles is higher than for the other samples, and also the formation of MLVs for samples with particles is faster than for the sample without particles. Those results, at low shear rate (1 s^{-1}) are in agreement

with results at high shear rate (5 s^{-1}).

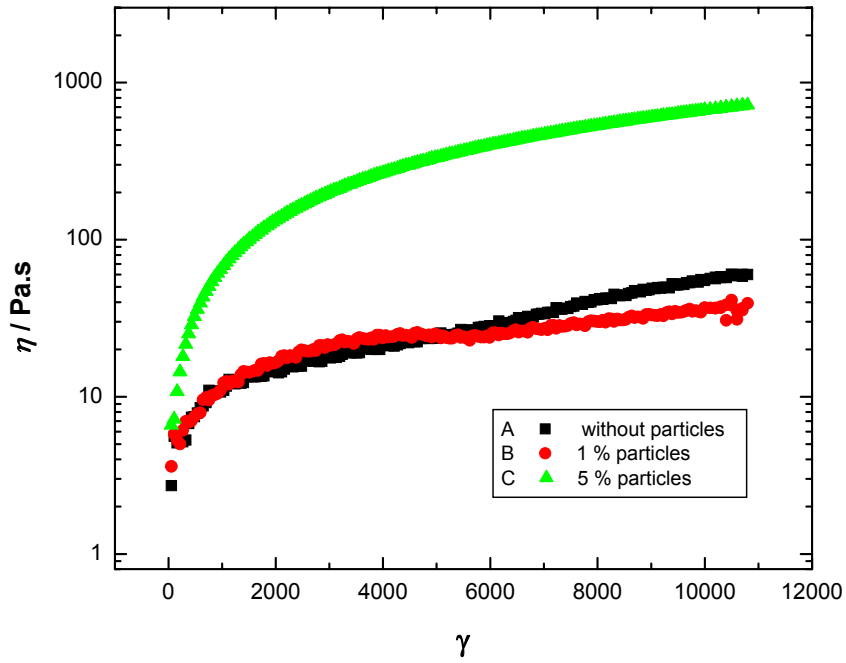

Figure 6.13 viscosity versus deformation for samples 17 (A), 15 (B) and 14 (C) of the system lecithin/D_2O/n-decane at T = 16 °C under constant shear rate $\dot{\gamma}$ = 1 s^{-1}.

Dynamic or oscillatory tests were also performed to study the influence of particles on the viscoelastic properties of the lamellar phase and multi-lamellar vesicles formed by lecithin/D_2O/n-decane for two samples, one without particles and another one with particles of PMMA. Three experiments are performed at different temperatures of 16, 25, 35 °C. First a pre-shear treatment was applied at 35°C during 10 minutes (lamellar phase orientation). Then the temperature was decreased and MLVs were formed at 16 °C, where a constant shear rate of 5 s^{-1} was applied. Before any dynamic test, a stress sweep test was done at the desired temperatures in order to check the linear viscoelastic regime (both for the oriented lamellar phase and MLVs). Finally, the frequency sweep test was done in a frequency range between 10 and 0.1 Hz.

Figure 6.14 shows the typical frequency scans (mechanical spectrum) for the oriented lamellar phase at different temperatures for sample 17. The values of G' and G" at various temperatures show different behaviour when the frequency

increases. At all temperatures G' is larger than G" showing the elastic character of the sample. Both G' and G" decrease with increasing temperature. At 16 °C (temperature were the MLVs are stable) a considerable difference between G' and G" is observed. MLVs present a dramatic elastic behaviour (solid material). When the frequency is increased, both storage and loss moduli increase for all temperatures as shown in the diagram.

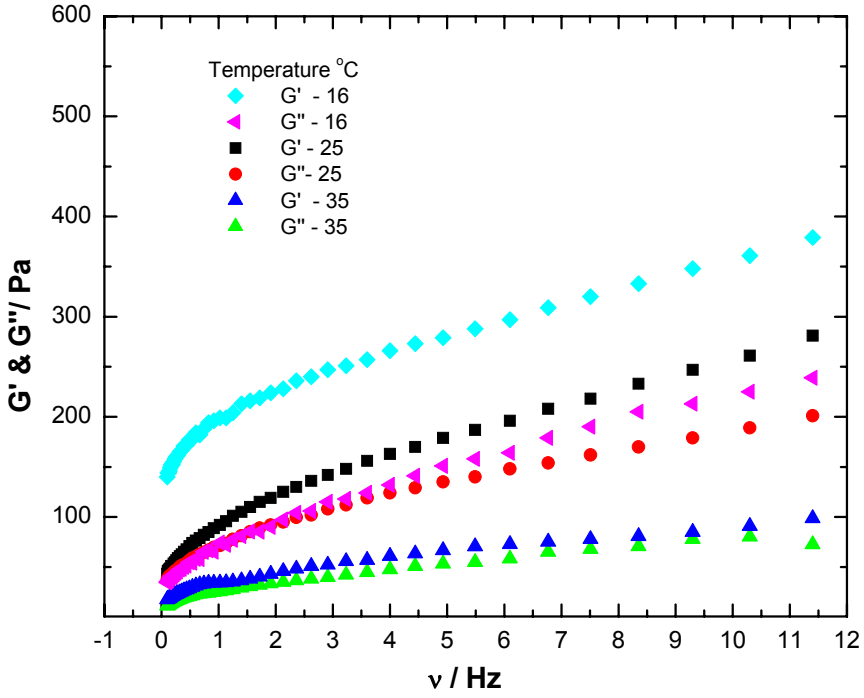

Figure 6.14 Storage, G', and loss, G", moduli as a function of frequency for sample 17 (without particles) at 16, 25, 35 °C and constant shear stress amplitude of 1 Pa.

At low temperature (16°C), MLVs are stable and due to their volume fraction, they occupy all the space. We do not have data to confirm this, but the spherical shape is probably deformed to a more polyhedral array to fill all the available space as observed in related systems. The MLVs space disposition increases the magnitude of the storage modulus. At higher temperatures (25 and 35 °C), MLV are no longer stable and the zero curvature structure, planar lamellae in coexistence with a nematic phase, appears. As we saw, the elastic modulus is dramatically lower at 35 °C compared to the MLV solid system.

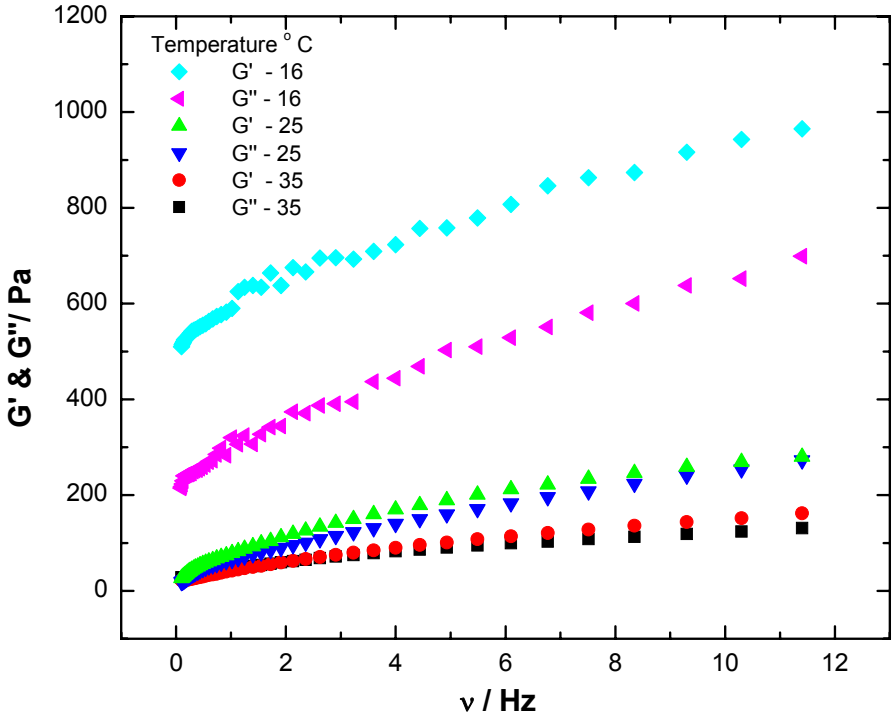

Figure 6.15 Storage, G', and loss, G", moduli as a function of frequency for sample 14 (with 5 % particles) at 16, 25, 35 °C and constant shear stress of 1 Pa.

The influence of particles on the viscoelastic properties of the system was also studied. The G' and G" were determined as a function of various temperatures for a sample of lamellar phase formed by lecithin/D_2O/n-decane filled with 5 % micro-particles of PMMA. Note that the viscoelastic properties have a strong dependence on the orientation states of the bilayers in the lamellar phase mixed with spherical micro-particles. The results are shown in figure 6.15. They clearly show that at 16 °C where MLVs or stuffed onions are formed the value of G' is higher than G" in the whole frequency range. Moreover, G' is almost three times higher in the doped system. Similar results can be observed at 25 °C and 35 °C. The doped planar lamellae or coexistence of the lamellar phase with nematic one present a higher elastic behaviour when compared to the system without particles. The latter can be explained by an increase of structural defects in the lamellae where different layers can be connected giving rise to the observed elastic behaviour. In the former case (MLVs), the increase of elasticity is related

to the increase of the number density of MLVs caused by the particles (higher polydispersity).

Table

6.1 summarizes the G' and G" values at a constant frequency of 10.3 Hz for the lecithin/water/n-decane system with and without particles. At 16 °C MLVs are stable and, on the other hand, at 25 and 35 °C planar lamellae or coexisting phases (lamellar and nematic) are stable.

Table 6.1 Values of the storage, G', and loss, G", moduli at various temperatures and constant frequency of 10.3 Hz for two samples, one without particles and the other one with 5 % micro-particles of PMMA.

	With particles		**Without particles**	
T / °C	**G'/Pa**	**G"/Pa**	**G'/Pa**	**G"/Pa**
16	943	652	361	225
25	269	251	261	189
35	152	124	90.8	80.3

6.2.2.3 The Results of Polarizing Microscopy

The polarized microscopy experiments were performed in transmission mode in the Linkam plate-plate shear cell for samples 4 and 8 of the system lecithin/D_2O/n-decane.

The lamellar phase develops a typical oily-streaks texture at rest. This texture occurs only in lamellar phases. An example for sample 4 is shown in Figure 6.16 (a). This texture was obtained after loading the fresh sample in the plate-plate shear cell with 500 µm gap, at 16 °C. The PMMA micro-particles aggregated at the network nodes are clearly seen in Fig 6.16 (b).

An example of the multi-lamellar vesicle texture observed by polarizing light microscopy in the system lecithin/D_2O/n-decane with n_w = 5.5 is shown in Figure 6.17. The sample was sheared at 5 s^{-1} for 20 min and diluted by D_2O. The structure of a mixture of lecithin/D_2O/n-decane with PMMA micro-particles observed under shear of 1 s^{-1} at 16 °C is shown in Figure 6.18. The fine dispersion of the micro-particles can be recognized, but the portion of particles in the onion core or around the onions can not be distinguished. Therefore, this microscopic texture may represent a phase with stuffed onions or decorated onions. A similar feature has been observed by Arrault et al.[36] for the system AOT/ brine mixing with polystyrene spheres.

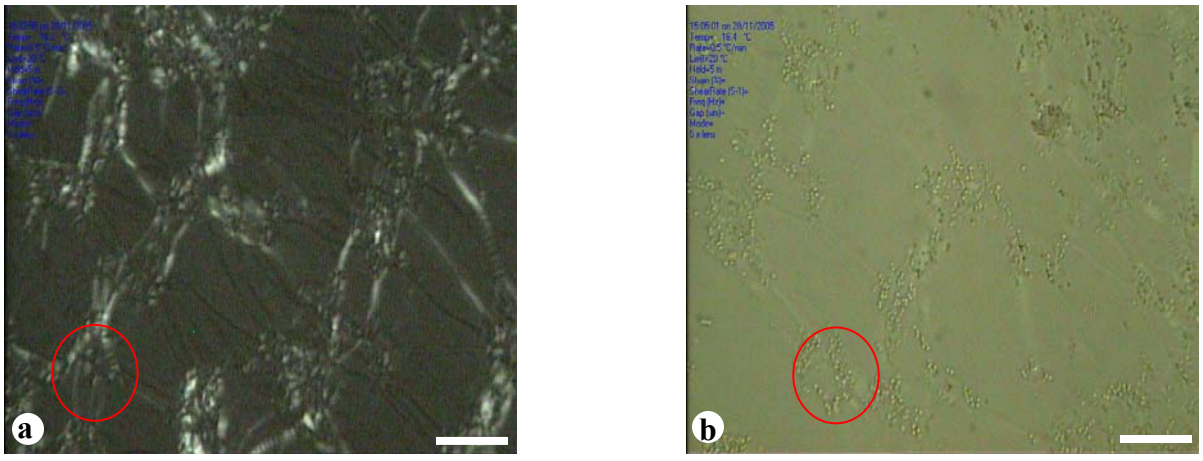

Figure 6.16 Light microscope textures of the system lecithin/D_2O/n-decance with n_w = 5.5. The lamellar oily-streaks texture of a sample containing PMMA micro-particles, observed between crossed polarizers (a) and parallel polarizers (b) at 16 °C. The particles aggregated at the network nodes are shown by the circles. Bar = 100 µm.

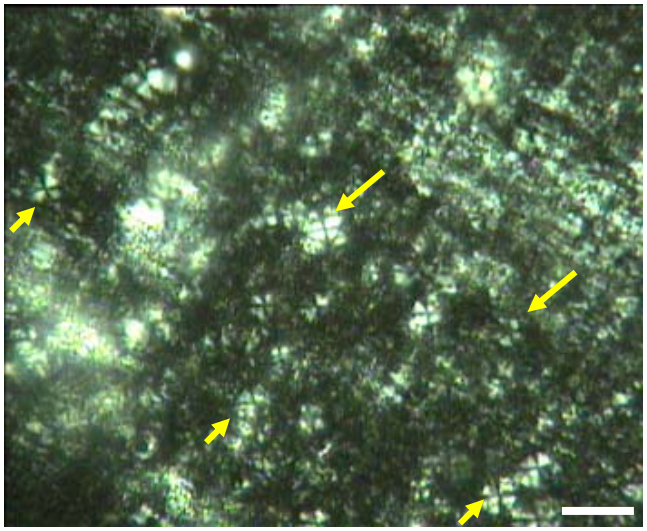

Figure 6.17 A vesicle texture is observed for system of lecithin/D_2O/n-decance with n_w = 5.5 taken in polarized light. The texture was observed after 20 min with a shear rate of 5 s^{-1}.The sample was diluted by D_2O. The arrows show the MLVs. Bar = 100 μm.

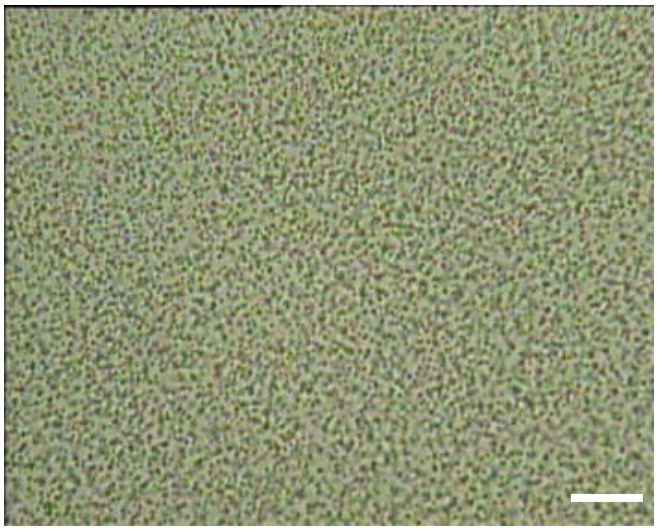

Figure 6.18 Optical micrograph of lecithin/D_2O/n-decance with n_w = 5.5 and 5 % wt of PMMA. The sample was sheared at 1 s^{-1} for 1 hour at 16 °C. Bar = 100 μm.

6.2.3 Influence of Micro-Particles on Vice Versa Shear-Induced of MLVs Formation

In this section the stability of shear-induced MLVs and the reversibility of the MLV size changes under shear for a lamellar phase of lecithin/D_2O/n-decane and for the same system but including micro-particles will be presented.

Figure 6.19 shows the NMR spectra of D_2O in the lamellar phase during stepwise cycling of the shear rate. Spectra were recorded at shear rates of 1, 5, 10, 20, 50, 100, 50, 20, 10, 5 and 1 s^{-1}, for a sample with n_w = 5.5 at T = 16 °C. The samples were sheared for 25 min at each shear rate. At rest the sample is aligned with the director perpendicular to the magnetic field by slow cooling through the biphasic regime of the isotropic/lamellar phase transition. Upon increasing the shear rate (left column of Figure 19.6), a gradual transformation to a new line shape is observed: The splitting decreases while, at the same time, a powder-like spectrum develops, the features of which become less distinct. At last, the splitting coalesces and a broad single peak appears. The single broad peak first observed at $\dot{\gamma}$ = 10 s^{-1} can be assigned to the state of close-packed vesicles. Upon further increase of the shear rate, the total line width of the spectra becomes smaller which indicates that the vesicles become smaller. The right part of Figure 6.19 shows the spectra during the decrease of the shear rate from 100 to 1 s^{-1}. The total line width of the spectra at first decreases when the shear rate is reduced to 50 s^{-1} but then it slightly increased by decreasing the shear rate. After the spectrum at $\dot{\gamma}$ = 1 s^{-1} had been recorded the shear was stopped and the sample kept at T = 16 °C. After one day an NMR spectrum was measured. This spectrum, which can be seen in the last row of Figure 6.19, shows that a splitting reappears, indicating a coexistence with an aligned L_α structure. In Figure 6.20 the line width of the spectra during the cycle of shear rates is shown. The line width decreased by increasing the shear rate while it is only very slightly increased by decreasing the shear rate as shown in Figure 6.20. It is possible, however, that the MLVs will return to their initial size when shear is applied for long times.

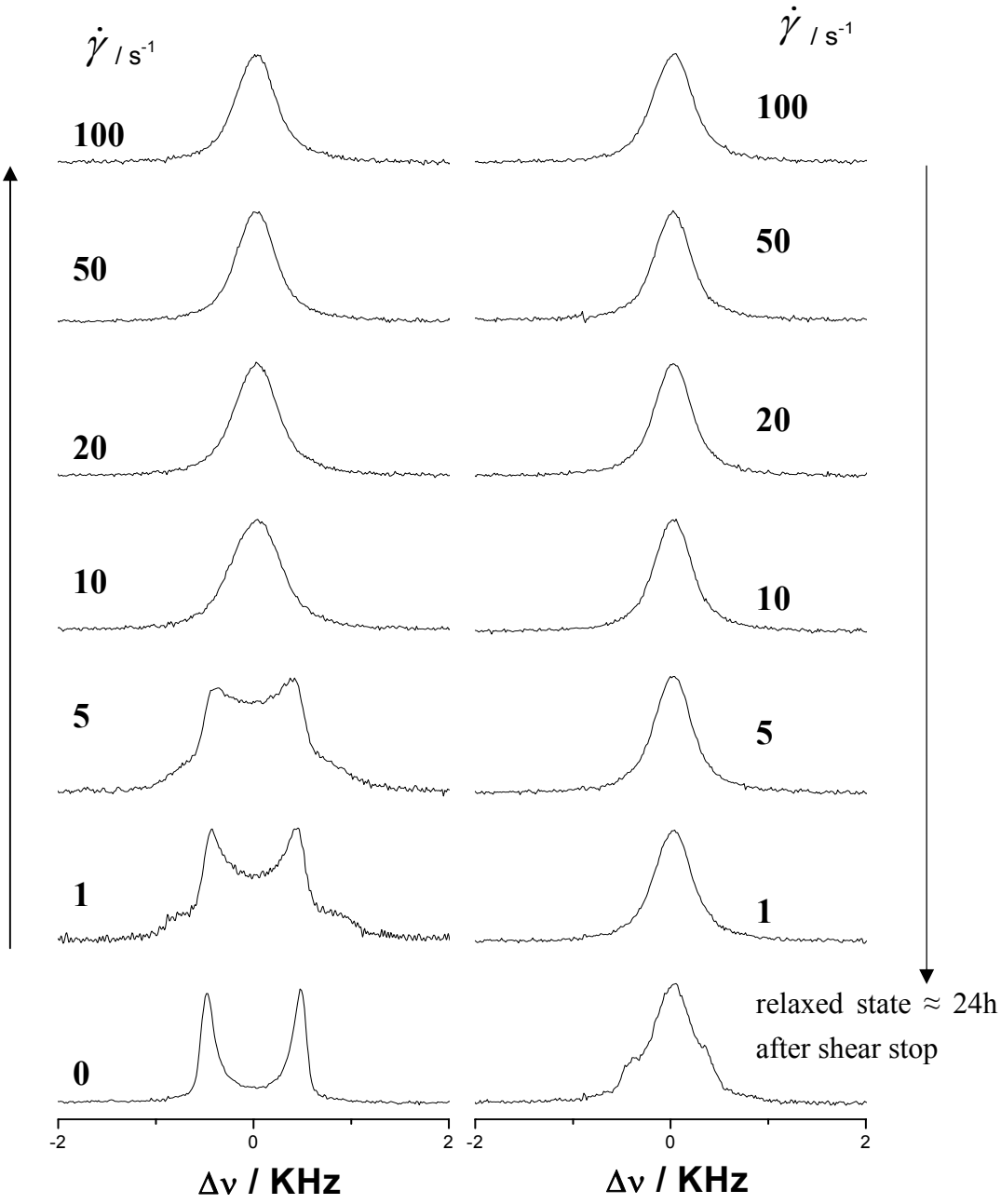

Figure 6.19 Deuteron NMR spectra obtained at different shear rates (25 min for each shear rate) for sample 19 with n_w = 5.5 of the system lecithin/D_2O/n-decaneat at T = 16 °C.

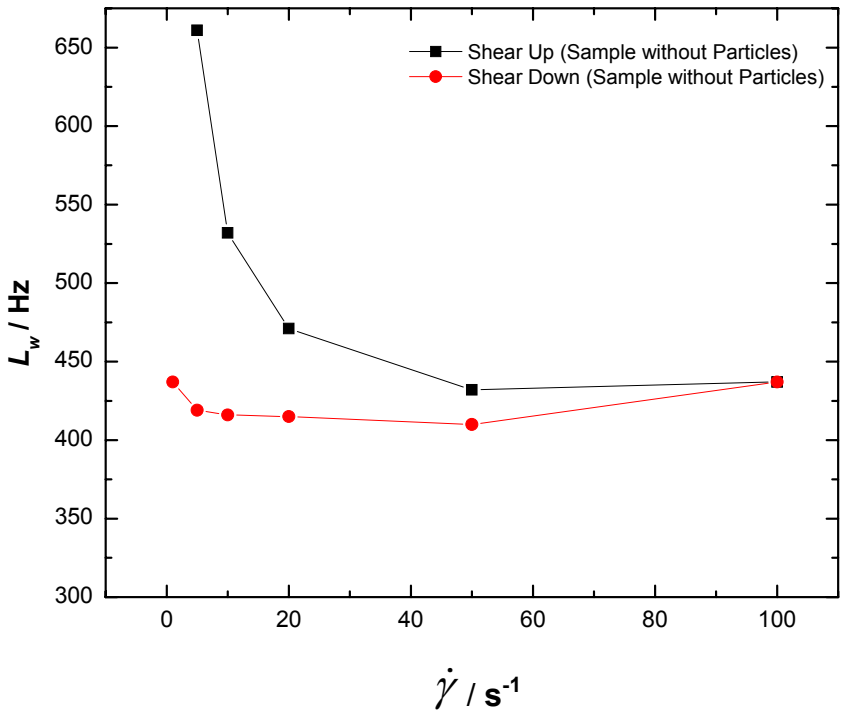

Figure 6.20 The full line width, L_w, of the NMR spectra shown in figure 6.19 as function of vice versa shear rate at a constant $T = 16$ °C.

The experiments were repeated for a sample with lecithin/D_2O/n-decane mixed with 5 % PMMA micro-particles under the same conditions. We thus address the question whether the spherical micro-particles have an effect on the size and stability of MLVs during stepwise cycling of the shear rate. As can be seen in Figure 6.21 the formation of MLVs now occurs already at $\dot{\gamma}$ = 5 s^{-1}. The line width of the spectra is shown in Figure 6.22. With increasing shear rate up to 100 s^{-1} the line width of the spectra becomes smaller, in agreements with other systems. Interestingly, with decreasing shear rate from 100 to 1 s^{-1} the line width of the spectra becomes broader which indicates an increase in the size of the MLVs. The NMR measurement recorded one day after shear was stopped at T = 16 °C, shows a similar result as for the sample without particles. As can be seen for the last spectrum of Figure 6.21 the NMR line shape becomes broader after one day which shows that the size of MLVs has changed.

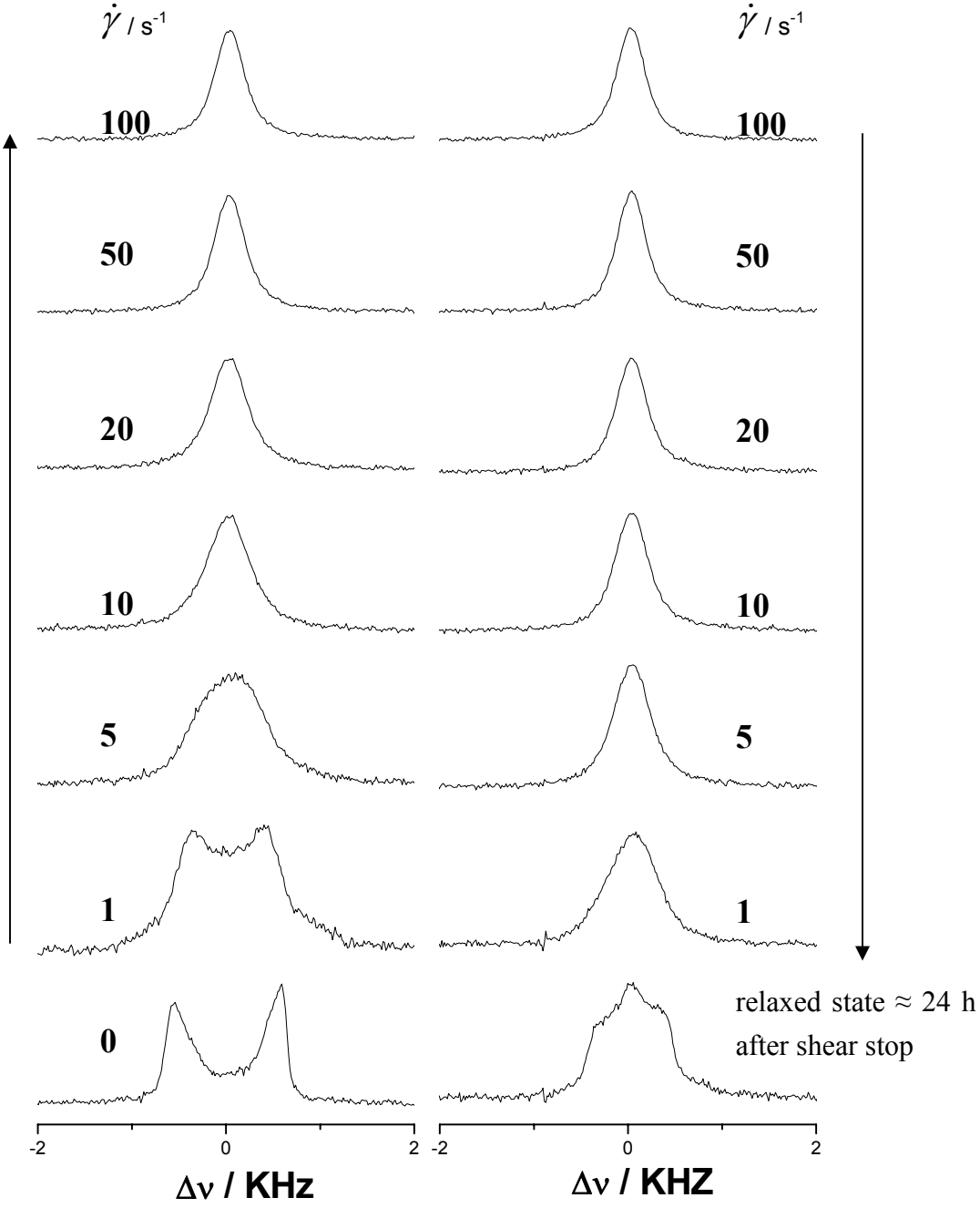

Figure 6.21 Deuteron NMR spectra obtained at different shear rates (25 min for each shear rate) for sample (20) with n_w = 5.5 of the system lecithin/D_2O/n-decane at mixed with 5 % PMMA micro-particles at a constant T = 16 °C.

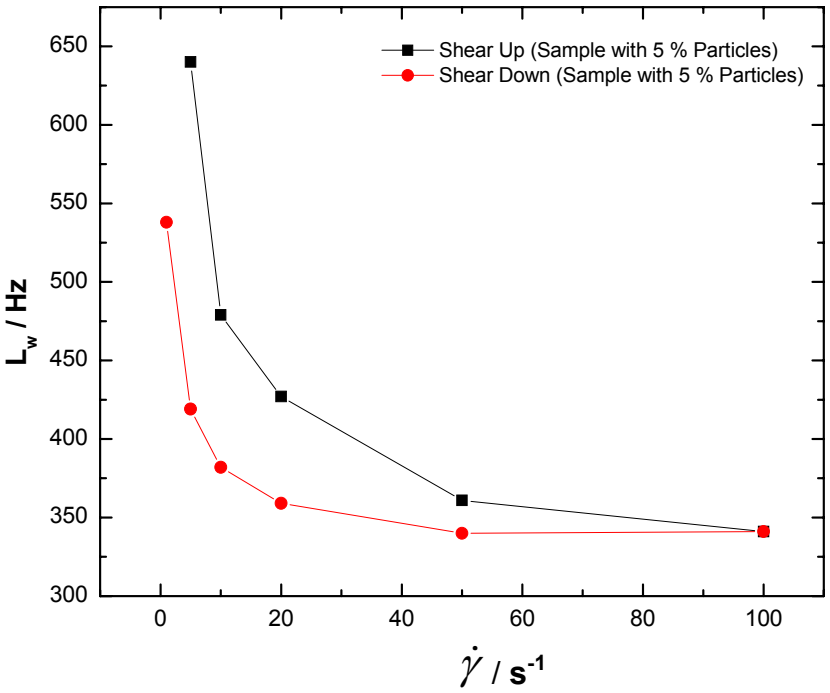

Figure 6.22 The full line width, L_w, of the NMR spectra shown in figure 6.21 as function of vice versa shear rate at a constant $T = 16$ °C.

7 Conclusions and Outlook

7.1 Conclusions

The present work consists of a study of the lamellar phase in the pseudo-ternary system formed by lecithin/D_2O/n-decane. The investigation of the phase behaviour as a function of the temperature in a narrow range of compositions and of the influence of spherical micro-particles on the shear-induced orientation states of the lamellar phase, in particular, on the formation of multi-lamellar vesicles were the main research topics. The major conclusions of this thesis are summarized below.

We have investigated a previously unidentified phase in the organogel system lecithin/D_2O/n-decane by using different techniques including polarizing microscopy, ^2H NMR, SAXS, and rheological measurements on samples containing 50 w/w % lecithin and 5.5 mole water per mole lecithin. Polarizing microscopy shows different optical textures as a function of temperature. The typical oily-streaks of the lamellar phase are found at 16 °C. At temperatures above 25 °C the textures are consistent with a coexistence of a lamellar phase with a discotic nematic phase. An isotropic phase is observed above 50 °C. The existence of these phases is confirmed by ^2H NMR spectroscopy. A second doublet in the NMR spectra appears as a shoulder at 24 °C and its peaks grow on increasing temperature. This additional doublet indicates the coexistence of the lamellar phase with another liquid crystalline phase. To obtain information on the rotational viscosity of the LC phases rotation experiments were performed by ^2H NMR. The relaxation time required for the director realignment by the magnetic field, following a 90° rotation of the sample, by which a non-aligned state is generated was measured at two different temperatures. At 45 °C realignment occurs fast due to a low viscosity, but at 30 °C orientational relaxation is slow. This can be explained by a large amount of lamellar phase at low temperature and a large amount of nematic phase at high temperature. The

coexistence of two phases is confirmed by the presence of two peaks in the SAXS pattern. The additional broad peak that grows as temperature is increased occurs at lower scattering angle (q vector) than the narrow peak of the L_α phase. Finally, the rheology results show the existence of three different regions: (i) a region of coexistence of a large amount of lamellar phase and a small amount of nematic phase from 25 to around 37 °C, where the storage modulus (G') is larger than the loss modulus (G") and the system becomes semi-solid (highly elastic) consequently, (ii) a region from around 37 to around 50 °C, where G" is larger than G' and the system becomes semi-liquid (low viscous), which means that the amount of nematic phase has increased, and (iii) the existence of the isotropic phase above 50 °C, where G" >> G'. The second anisotropic phase, coexisting with the lamellar phase thus has been confirmed by different experimental techniques. It was expected to be a discotic nematic phase and not a calamitic nematic one because of its proximity to the L_α phase. This was proven by the ^2H NMR line shapes following a 90° rotation of aligned samples.

Several types of particles, based on SiO_2, PMMA, and M-F, were synthesized and characterized using AFM, polarizing microscopy, light scattering and ^{13}C NMR techniques. We have successfully synthesized monodisperse spherical particles of SiO_2 with diameters of 380 to 410 nm by the base-catalyzed condensation of monomers ($Si(OH)_4$) with ammonia.

Monodisperse colloidal particles of PMMA with diameters of 260 to 850 nm were obtained by the reaction of MMA, a crosslinker and an epoxy-functionalized comonomer. The size of the particles was controlled by observing the interference colour of samples taken from the reaction vessel and dried on a glass plate. The investigation of the reaction with amino-substituted compounds confirms that functional components can be covalently attached to the surface of particles.

Larger micro-particles of melamine formaldehyde were realized with diameters of 1 to 1.8 μm as determined by AFM. The size of the particles depends on the kind of solvent, initiator, temperature and reaction time of the process. Flocculation was observed for the M-F particles; however, the micro-particles can be

resuspended in apolar liquids such as n-dodecane by mild sonication and the suspension is stable for 24 h.

The influence of spherical particles on the shear-induced orientation states of the lecithin organogel system was studied using the rheo-^{2}H NMR technique. Different orientation states of the lamellar phase were observed when the temperature was increased from 14 to 56 °C at a constant shear rate of 20 s^{-1}. Without particles the following sequence of orientation states occurs with increasing temperature: MLVs, parallel and perpendicular orientations. When micro-particles were added the sequence of orientation states is roughly the same. However, the perpendicular orientation was not detected in the particle-doped system. An additional and important observation is the fact that the presence of particles indeed stabilizes the temperature range of multi-lamellar vesicles. It is increased from ΔT = 2 °C (without particles) to ΔT = 10 °C (with particles).

Concerning the shear-induced MLVs we conclude that the presence of particles increases the rate of onion formation. We think that the local order of the lamellae is greatly disrupted by adding large external objects such as micron-sized particles. The flow of this defected lamellar system is irregular and tumbling processes may occur, speeding up the onions formation. This conclusion is supported mainly by the rheo-^{2}H NMR data where the broad singlet spectrum (characteristic fingerprint of these MLVs systems) was observed earlier when particles are present, comparing with the case without particles. Moreover, the rheological flow curves also show that the steady state is reached faster (less strain units needed) when the system is doped with particles. Concerning the dimensions of the shear-induced MLVs it seems that the presence of particles decreases the size of onions. This conclusion is supported by a clear decrease of the line width of the MLV broad singlet spectrum and also from the observation of the rheological mechanical spectra where the elastic modulus drastically increases when particles are added. The elastic modulus, G', can be related to the number density of onions and so an increase of this parameter reflects an increase of the number of onions and consequently a decrease of their size.

7.2 Outlook

The phase diagram of the system lecithin/D_2O/n-decane, especially in the region of the lamellar and its neighbouring phase, is still incomplete. Therefore, the elucidation of the phase transition temperatures of this system for various samples with different amount of oil and different mole ratio of water per lecithin will be interesting to determine the boundary of the lamellar phase with the discotic nematic one and to identify possible other phase transitions in this region.

Using particles of different size, e.g., nano-particles or other kinds of micro-particles, also at high volume fraction, mixed into different types of lyotropic liquid crystalline systems such as non-ionic surfactant solutions will be a large research field to address the question of how these particles have an effect on the size, stability and formation of MLVs under shear.

Furthermore, the influence of the concentrations of the different components, lecithin, water and oil, on the shear-induced orientation states of the lamellar phase, in particular, on the formation of multi-lamellar vesicles, which has been investigated only partly, is an interesting research topic worthwhile to be completed in the future.

Appendix

A.1 The System of AOT/brine

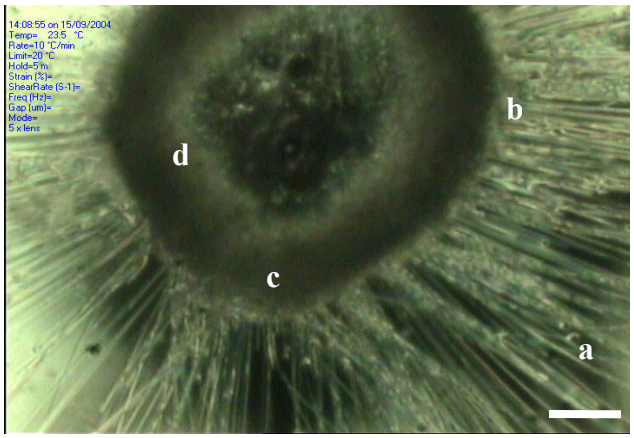

Figure A.1 Optical micrograph of a contact preparation of AOT (centre) and brine (15 g/l of NaCl) observed between crossed polarizers. The different textures correspond to myelin (a), lamellar phase (b), cubic phase (c), hexagonal phase (d). Bar = 10 μm.

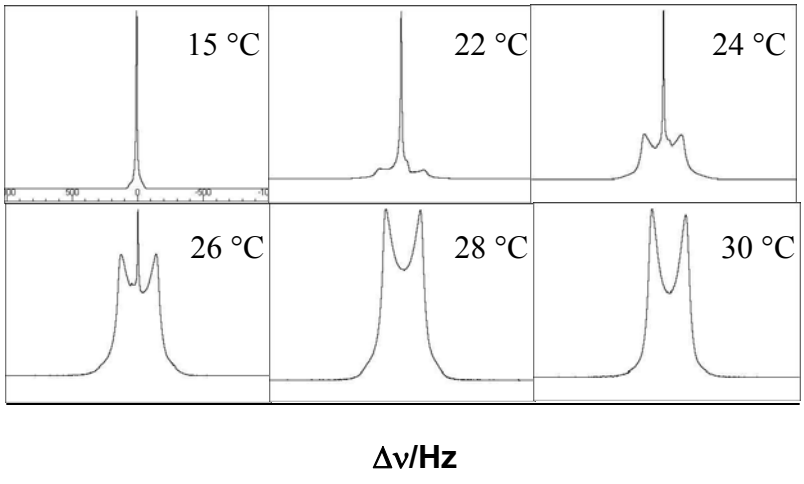

Figure A.2 ^{2}H NMR spectra for a sample with 25 w/w % AOT in brine (15 g/l of NaCl). For the lamellar phase (L_α) a quadrupole splitting $\Delta\nu$ is observed. At 22 to 26 °C the lamellar phase and the isotropic one coexist. The single peak at 15 °C shows the pure isotropic phase.

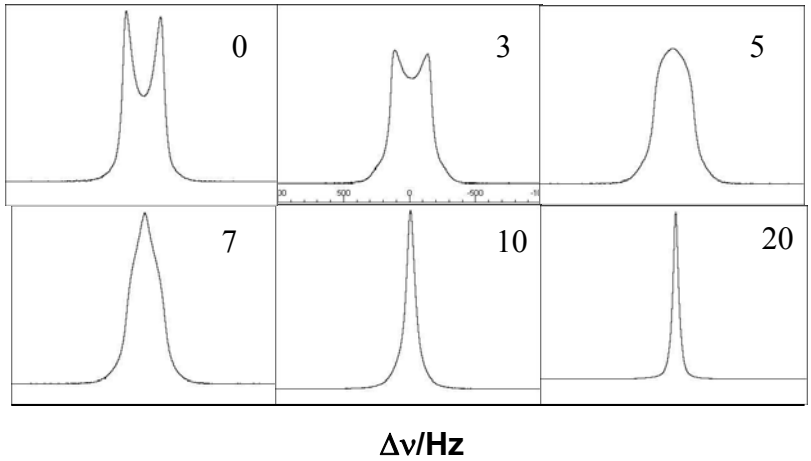

Figure A.3 ^{2}H NMR spectra obtained at different shear rates (15 min for each shear rate), given to the right of each spectrum in s^{-1} for a sample with 25 w/w % AOT in brine (15 g/l of NaCl) at 30 °C.

A.2 Characterization of PMMA Particles

Table A.1 The different sizes of PMMA particles obtained by AFM measurements.

Sample	*Size of epoxy-functionalized PMMA (nm)*	**Size of modified PMMA (nm)*	*Comment-Remark*
PMMA1	400–600	400–850	
PMMA2	320–340	500–1400	
PMMA3	270–300	400–800	The surface functionalized groups were analyzed by FT-IR
PMMA4	290–320	260–410	Synthesis of PMMA without Cross-linker, the surface functionalized groups were analyzed by FT-IR
PMMA5	aggregation	aggregation	Synthesis of PMMA without functionalized comonomer
PMMA6	270–350	370–800	The surface functionalized groups were analyzed by FT-IR and NMR-^{13}C/MAS
PMMA7	-	-	AFM was detected, PMMA was modified at different conditions, the surface functionlazed groups Were analyzed by NMR-^{13}C/MAS

* Surface was modified with dodecylamine

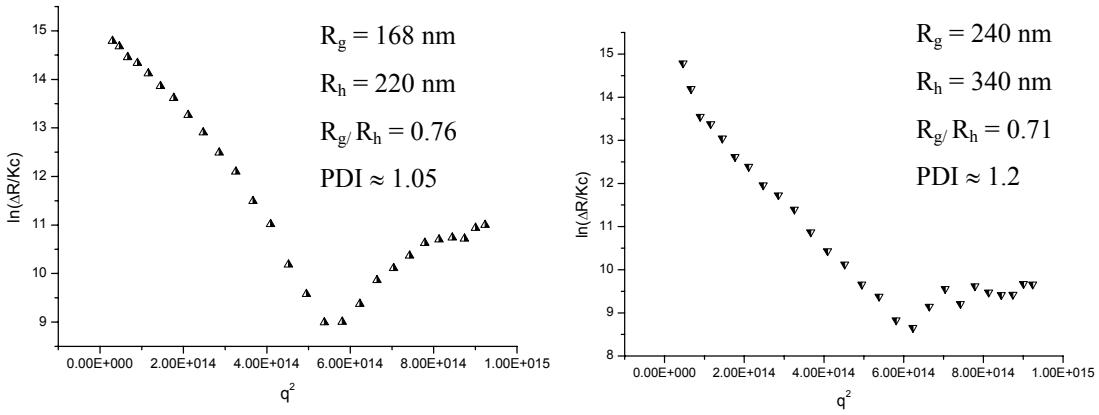

Figure A.4 Scattering curves as a function of scattering vector q for samples of epoxy-functionalized PMMA particles before (left) and after (right) surface modification with dodecylamin.

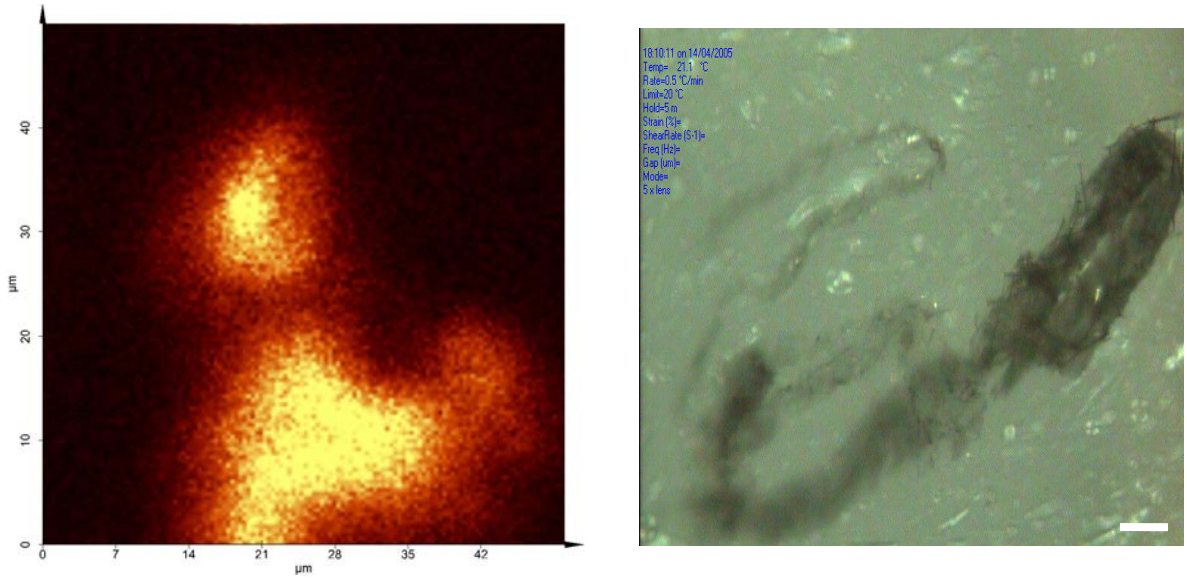

Figure A.5 Miscibility of spherical PMMA particles of a few hundred nanometres diameter in the lamellar phase of the system AOT/brine. Left: image obtained by confocal microscopy of the particles labelled with Rhodamine 6G (360 nm) in lamellar phase of 25 w/w % AOT in brine (15 g/l of NaCl) at 25 °C. Right: image obtained by polarizing microscopy of the particles labelled with Coumarin 120 (280 nm) in the similar system at 28 °C. Bar = 100 μm. Aggregation is observed in both cases.

A.3 The System of Lecithin/water/n-decane

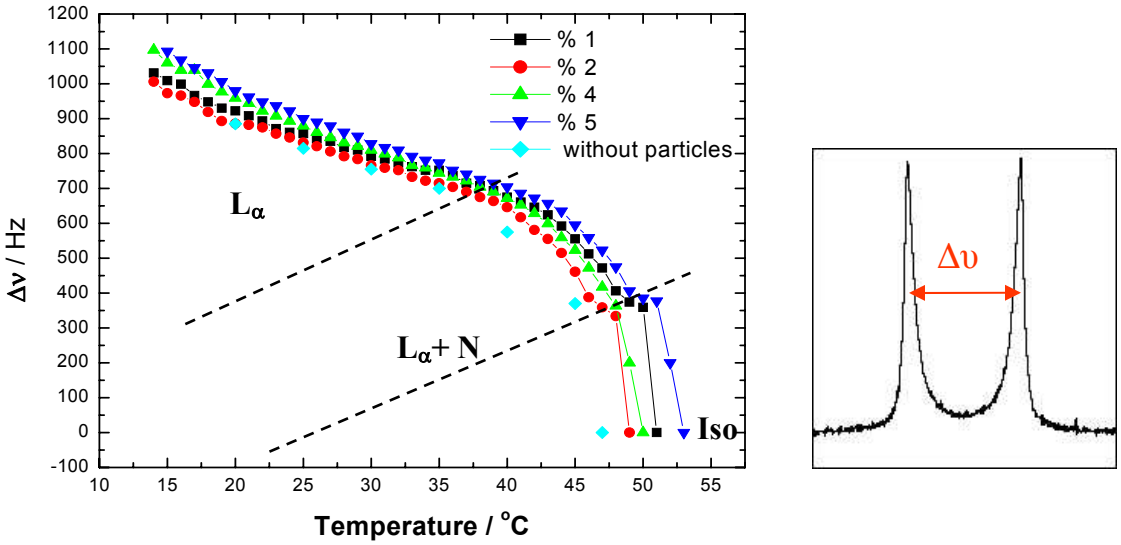

Figure A.6 Quadrupole splitting of NMR spectra as function of temperature for samples 7, 5, 6 and 4 (see Table 3.3) with 1 %, 2 %, 4 % and 5 % particles of PMMA (2 µm) respectively, and sample 29 without particles of the system lecithine/D2O/n-decane.

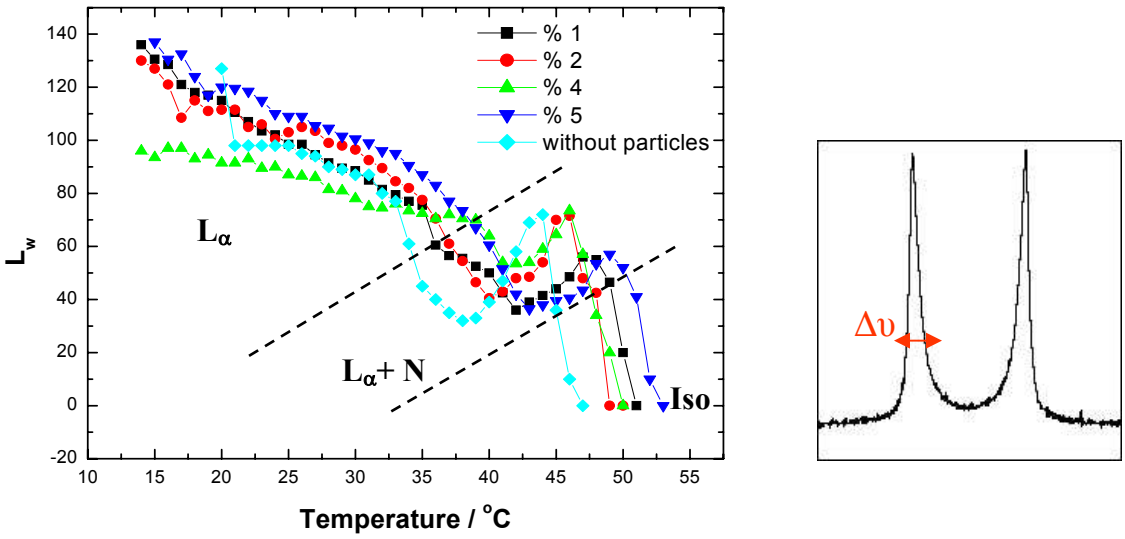

Figure A.7 Full line width at half height of the NMR spectra of samples 7, 5, 6 and 4 (see Table 3.3) with 1 %, 2 %, 4 % and 5 % particles of PMMA (2 µm) respectively, and sample 27 without particles of the system lecithine/D_2O/n-decane as function of temperature.

A.4 Calibration of SAXS

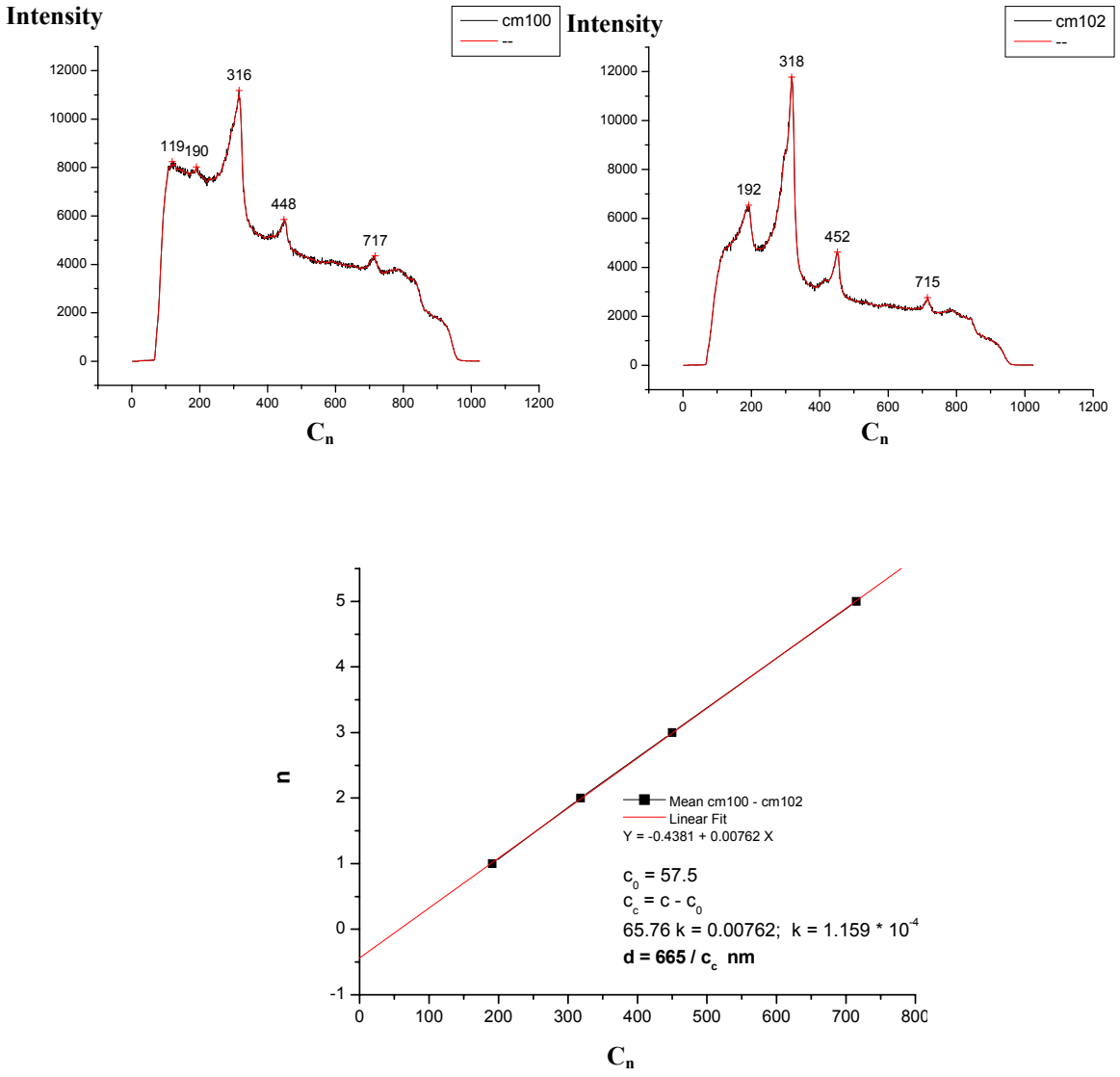

Figure A.8 X-ray scattering of cholesterylmyristate (top) used for calibrating the Kratky camera and calibration curve (peak order (n) as a function of channel number (C_n)) (bottom).

Abbreviations

AFM	Atomic force microscopy
AOT	Aerosol-OT
a_0	Area per head group
B_0	Static magnetic field
CMC	Critical Micelle Concentration
CPP	Critical Packing Parameter
$\nabla\vec{V}$	Velocity gradient
$\Delta\nu$	Quadrupole splitting
δ	Quadrupolar coupling constant
δ	Phase angle
EFG	Electric field gradient
eQ	Quadrupole moment
EtOH	Ethanol
FT	Fourier transform
G'	Elastic or storage modulus
G"	Viscous or loss modulus
γ	Strain or deformation
$\dot{\gamma}$	Shear rate
H	Mean curvature
h	hour(s)
H_D	Hamiltonian of dipole-dipole interaction
H_σ	Chemical-shift Hamiltonian
H_z	Zeeman Hamiltonian
hex.	Hexagonal phase
iso.	Isotropic phase
κ	Bending modulus

k_B	Boltzmann constant
l	Length of the hydrocarbon chain
lam.	Lamellar phase
L_α	Lamellar phase
L_w	Line width
I_z	Operator for the total z component of I
M-F	melamine-formaldehyde
MMA	Methyl methacrylate
MLV	Multi-lamellar vesicle
η	Asymmetry parameter
η	Viscosity
$\vec{n}$	Director
n_c	Number of carbon atoms
N_C	Nematic calamitic phase
N_D	Nematic discotic phase
N_{ex}	Nematic biaxial phase
n_{Me}	Number of methyl groups
NMR	Nuclear magnetic resonance
N_s	Surfactant number or Surfactant parameter
n_w	Mole ratio of water to lecithin
PDI	Poly dispersity index
PMMA	Poly methyl methacrylate
ω	Frequency
ω_o	Larmor frequency
υ	Volume of the hydrocarbon chain
R_1, R_2	Principal radii of curvature
Ref.	Reference
R_g	Radius of gyration
R_h	Hydrodynamic Radius
rpm	Rotation per minute
SAXS	Small angle X-ray scattering

σ	Shear stress
σ_0	Yield stress
t	time
t_c	critical time
TMMM	trimethylol melamine
T	Temperature
T_k	Krafft Temperature
τ	Time between two pulses
$\vec{V}$	Velocity
v_x	Velocity in the *x* direction
$\vec{Z}$	Vorticity or neutral axis

References

(1) V. Degiorgio; M. Corti. *Physics of Amphiphiles: Micelles, Vesicles and Microemulsions.Italian Physical society* **1985**, *Course XC*.
(2) J. N. Israelachvilli; D. J. Mitchell; B. W. Ninham. *J. Chem. Soc. Faraday Trans. II* **1976**, *72*, 1525.
(3) W. Helfrich. *Z. Naturforsch.* **1973**, *28c*, 693.
(4) R. G. Laughlin. *The aqueous Phase Behaviour of Surfactants.Academic press: London,* **1994**.
(5) C. Ocak; M. Acimish; E. Akpinar; A. Gök. *Phys. Chem.Chem.Phys.* **2000**, *2*, 5703.
(6) A. H. Alexopulus; J.E. Puig; E. I. Franses. *J. Colloid Interface Sci.* **1989**, *128*, 26.
(7) E. Jahns; H. Finkelman. *Colloid polym Sci.* **1987**, *265*, 304.
(8) G. J. T. Tiddy. *Physics Report (Review Section of Physical Letters)* **1980**, *57*, 1.
(9) H. Hoffmann; H. Löbl; H. Rehange; I. Wunderlich. *Tenside Deterg.* **1985**, *22*, 290.
(10) U. Olsson; O. Söderman; P. Guering. *J. Phys. Chem.* **1986**, *90*, 5223.
(11) A. Onuki; K. Kawasaki. *Ann. Phys.* **1979**, *121*, 456.
(12) R. Angelico; A. Ceglie; G. Colafemmina; F. Delfine; U. Olsson; G. Palazzo. *Langmuir* **2004**, *20*, 619.
(13) D. Roux; F. Nallet; O. Diat. *J.physics II france* **1993**, *3*, 1427.
(14) J. Bergenholtz; N. J. Wagner. *Langmuir* **1996**, *12*, 3122.
(15) J. Berghausen; J. Zipfel; P. Lindner; W. Richtering. *Europhys. Lett.* **1998**, *43*, 683.
(16) S. Müller; C. Börschig; W. Gronski; C. Schmidt. *Langmuir* **1999**, *15*, 7558.
(17) D. Roux; F. Nallet; O. Diat. *Europhys. Lett.* **1993**, *24*, 53.
(18) J. Zipfel; P. Lindner; W. Richtering. *Prog.Colloid Polym.Sci.* **1998**, *110*, 139.
(19) O. Diat; D. Roux. *J.physics II france* **1993**, *3*, 9.
(20) J. Zipfel; P. Lindner; W. Richtering. *J. Phys. Chem. B* **1999**, *103*, 2841.
(21) W. Richtering. *Prog.Colloid Polym.Sci.* **1997**, *104*, 90.
(22) J. Penfold. *J. Phys. Chem. B* **1997**, *101*, 66.
(23) J. I. Escalante; M. Gradzielski; H. Hoffmann; K. Mortensen. *Langmuir* **2000**, *16*, 8653.
(24) P. Panizza; A. Colin; C. Coulon; D. Roux. *Eur. Phys. J. B* **1998**, *4*, 65.
(25) B. Medronho; S. Fujii; W. Richtering; M. G. Miguel; U. Olsson. *Colloid polym Sci.* **2005**, *284*, 317.
(26) D. Burgemeister. *PhD thesis, Universität Freiburg* **2003**.
(27) M.Blaschke. *Deploma thesis, Universität Paderborn* **2006**.
(28) M. Antonietti; K. Tauer. *Macromol. Chem. Phys.* **2003**, *204*, 207.
(29) T. Röder; T. Kramer; K. Huber; H.S. Kitzerow. *Macromol. Chem. Phys.* **2003**, *204*, 2204.
(30) J. B. Pawley. *Handbook of Biological Confocal microscopy. Plenum Press:New York* **1995**.
(31) A. Radbruch. *Flow Cytometry and Cell Sorting. Springer:Darmstadt* **1999**.

(32) N. Kern; B. Fourcade. *Europhys. Lett.* **1997**, *38*, 395.
(33) C. Quilliet; P. Fabre; V. Cabuil. *J. Phys. Chem.* **1993**, *97*, 287.
(34) P. Fabre; C. Casagrande; M. Veyssie; V. Cabuil; R. Massart. *Phys. Rev. Lett.* **1990**, *64*, 539.
(35) J. Arrault; C. Grand; W. C. K. Poon; M. E. Cates. *Europhys. Lett.* **1997**, *38*, 625.
(36) J. Arrault; W. C. K. Poon; M. E. Cates. *Physical Review E* **1999**, *59*, 3242.
(37) L. E. Nielsen; R. F. Landel. *Mechanical Properties of Polymers and Composites.* **1994**, *Dekker, New York, ed. 2*, chapter 7.
(38) O. Mondain-Monval; P. Poulin. *J. Phys.:Condens. Matter* **2004**, *16*, S1873.
(39) M. Zapotocky; L. Ramos; P. Poulin; T. C. Lubensky; Weitz, D. A. *Science* **1999**, *283*, 209.
(40) G. Basappa; V. Kumaran; P. R. Nott; S. Ramaswamy; V. M. Naik; Rout, D. *Eur. Phys.J. B* **1999**, *12*, 269.
(41) B. Lindman; B. Jönsson; K. Holmberg; B. Kronberg. *Surfactants and Polymers in Aqueous Solution. John Wiley & Sons: Chichester, England,* **1998**.
(42) I. M. Hamley. *Introduction to Soft Matter. Wiley-VCH New York,* **2000**.
(43) C. Tanford. *The Hydrophobic Effect. Wiley-Intersciece, New York.* **1980**.
(44) D. F. Evans; H. Wennerström. *The Colloidal Domain: Where Physics, Chemistry, Biology and Technology meet; John Wiley & Sons: New York,* **1999**.
(45) G. Burducea. *Romanian Reports in Physics,* **2004**, *56*, 66.
(46) C. Safinya; D. Roux; G. Smith; S. Sinha; P. Dimon; A. Clark; Bellocq, A. *Phys. Rev.Lett.* **1986**, *57*, 2718.
(47) F. Larche; J. Appel; G. Porte; P. Bassereau; J. Marignan. *Phys. Rev. Lett.* **1986**, *56*, 1700.
(48) K. D. Lawson; T. J. Flautt. *J. Am. Chem. Soc.* **1967**, *89*, 5489.
(49) S. Chandrasekhar. *Liquid Crystals. Cambridge University Press: Cambridge, England,* **1992**.
(50) Yu. A. Shchipunov. *Encyclopedia of Surface and Colloid Science* **2002**, 2997.
(51) J. B. F. N. Engberts; D. Hoekstra. *Biochim, Biophys. Acta* **1995**, *1241*, 323.
(52) D. D. Larsic. *J. Liposome Res.* **1993**, *3*, 257.
(53) D. D. Larsic. *Biochem. J.* **1988**, *256*, 1.
(54) W. Richtering. *Curr.Opin. Colloid Interface Sci.* **2001**, *6*, 446.
(55) K. Mortensen. *Curr.Opin. Colloid Interface Sci.* **2001**, *6*, 140.
(56) P. Butler. *Curr.Opin. Colloid Interface Sci.* **1999**, *4*, 214.
(57) M. G. Berni; C. J. Laurence; D. Machin. *Curr.Opin. Colloid Interface Sci.* **2002**, *98*, 217.
(58) F. Nettesheim; J. Zipfel; U. Olsson; F. Renth; P. Lindener; w. Richtering. *Langmuir* **2003**, *19*, 3603.
(59) C. Oliviero; L. Coppola; R. Gianferri; I. Nicotera; U. Olsson. *Coll. Surf. A* **2003**, *228*, 85.
(60) U. Wiesner. *Macromol. Chem. Phys.* **1997**, *198*, 3319.
(61) J. Zipfel; J. Berghausen; G. Schmidt; P. Lindener; P. Alexandridis; M. Tsianou; W. Richtering. *Phys. Chem.Chem.Phys.* **1999**, *1*, 3905.
(62) O. Dhez; F. Nallet; O. Diat. *Eur. phys. Lett.* **2001**, *55*, 821.
(63) D. Maring; U. Wiesner. *Macromolecules* **1997**, *30*, 660.
(64) J. Berghausen; J. Zipfel; O. Diat; J. Naranayan; W. Richtering. *Phys.*

Chem.Chem.Phys. **2000**, *2*, 3623.
(65) T. D. Le; U. Olsson; K. Mortensen; J. Zipfel; W. Richtering. *Langmuir* **2001**, *17*, 999.
(66) T. Gulik-Krzywicki; J. C. Dedieu; D. Roux; C. Degert; R. Laversanne. *Langmuir* **1996**, *12*, 4668.
(67) M. Bergmeier; M. Gradzielski; H. Hoffmann; K. Mortensen. *J. Phys. Chem. B* **1999**, *103*, 1605.
(68) P. Partal; A. J. Kowalski; D. Machin; N. Kiratzis; M. G. Berni; C. J. Lawrence. *Langmuir* **2001**, *17*, 1331.
(69) J. Läuger; R. Weigel; K. Berger; K. Hiltrop; W. Richtering. *J. Colloid Interface Sci.* **1996**, *181*, 521.
(70) R. Weigel; J. läuger; W. Richtering; P. Lindener. *J. Phys. II* **1996**, *6*, 529.
(71) A. Leon; D. Bonn; J. Meunier. *J. Phys. Condens. Metter* **2002**, *14*, 4785.
(72) L. Soubiran; E. Staples; I. Tucker; J. Penfold; A. Creeth. *Langmuir* **2001**, *17*, 7988.
(73) O. Diat; D. Roux; F. Nallet. *J. Phys. II* **1993**, *2*, 1427.
(74) A. Onuki. *J. Chem. Phys.* **1987**, *87*, 3692.
(75) G. H. Fredrickson; F. S. Bates. *Ann. Rev. Mater. Sci.* **1996**, *26*, 501.
(76) M. E. Cates; S. T. Milner. *Phys. Rev.Lett.* **1989**, *62*, 182.
(77) C. M. Marques; M. E. Cates. *J. Phys. France* **1990**, *51*, 1733.
(78) A. G. Zilman; R. Granek. *Eur. Phys. J. B* **1999**, *11*, 593.
(79) G. Auernhammer; H. Brand; H. Pleiner. *Phys. Rev. E* **2002**, *66*, 1707.
(80) D. J. Shaw. *Introduction to Colloid and Surface Chemistry, 4th ed. Butterworth-Heinemann* **1992**.
(81) D. Urban; K. Takamura. *Polymer Dispersions and Their Industrial applications, Wiley-VCH.* **2002**.
(82) P. Diehl; E. Fluck; H. Günther; R. Kosfeld; J. Seelig. *NMR: Solid-State NMR III, Springer-Verlag* **1994**.
(83) J. Keeler. *Understanding NMR Spectroscopy, John Wiley & Sons* **2006**.
(84) F. Keinschmidt. *PhD thesis, Universität Freiburg* **2005**.
(85) R. A. Komoroski; L. W. Jelinski. *High Resolution NMR Spectroscopy of Synthetic Polymers in Bulk.* **1986**, *VCH, Chapter 10.*
(86) R. L. Thurmond; G. Lindblom; M. F. Brow. *Biochemistry* **1993**, *32*, 5394.
(87) C. Leal. *PhD thesis, University of Lund,* **2006**.
(88) H. A. Barnes; J. F. Hutton; K. Walters. *An Introduction to Rheology, Elsevier,* **1993**.
(89) L. Antl; J. W. Goodwin; R. D. Hill; R. H. Ottewill; S. M. Owens; S. Papworth. *Collodis and Surfaces,* **1986**, *17*, 67.
(90) J. Balogh. *PhD thesis, University of Lund,* **2006**.
(91) K. Berger. *PhD thesis, Universität Paderborn,* **1995**.
(92) T. Kramer. *PhD thesis, Universität Paderborn,* **2005**.
(93) J. F. Nagle; H. L. Scott. *Physics Today* **1978**, *10*, 38.
(94) A. M. Donald; A. H. Windle. *Liquid crystalline polymers. Cambridge University Press: Cambridge, England,* **1992**.
(95) P.G. de Gennes. *The physics of liquid crystals. Oxford University Press:Oxfored, England,* **1974**.

(96) W. Hemker. *J. Am. Oil Chem. Soc.* **1981**, *58*, 114.
(97) T. N. Kumar; Y. S. R. Sastry; G. Lakshminarayana. *J. Am. Oil Chem. Soc.* **1989**, *66*, 153.
(98) S. Paash; F. Schambil; M. J. Schuwuger. *Langmuir* **1989**, *5*, 1344.
(99) P. Mariani; F. Rustichelli; L. Saturni; L. Cardone. *Eur. Biophys. J.* **1999**, *28*, 294.
(100) L. de Campo; A. Yaghmur; L. Sagalowicz; M. E. Leser; H. Watzke; O. Glatter. *Langmuir* **2004**, *20*, 5254.
(101) K. Larsson. *Curr.Opin. Colloid Interface Sci.* **2000**, *5*, 64.
(102) F. Caboi; J. Borne; T. Nylander; a. Khan; A. Svendsen; S. Patkar. *Colloids Surf., B* **2002**, *26*, 159.
(103) R. Angelico; A. Ceglie; U. Olsson; G. Palazzo. *Langmuir* **2000**, *16*, 2124.
(104) M. Blaschke. *Deploma thesis, Universität Paderborn,* **2005**.
(105) A. Saupe. *J. Colloid Interface Sci.* **1977**, *58*, 583.
(106) C. A. Rang; C. A. Miller. *J. Colloid Interface Sci.* **1999**, *209*, 179.
(107) D. Tezak; N. Jalsenjak; N. Ljubesic. *Prog. Colloid Polymer Sci.* **1998**, *110*, 204.
(108) H. P. Lin; C. Y. Mou; S. B. Liu. *Adv. Matt.* **2000**, *12*, 103.
(109) M. Buchanan; M.E. Cates. *Langmuir* **1998**, *14*, 7371.
(110) H.P. Lin; C.Y. Mou; S.B. Liu. *Adv. Matt.* **2000**, *12*, 103.
(111) N.O. Persson; K. Fontell; B. Lindman; G.J.T. Tiddy. *J. Colloid Interface Sci.* **1975**, *53*, 461.
(112) H. Wennerström; N.O. Persson; B. Lindman. *Adv. Chem.Ser.* **1975**, *9*, 253.
(113) T. Kramer; T. Röder; K. Huber; H.S. Kitzerow. *Polym. Adv. Technol.* **2005**, *16*, 38.
(114) W. Stöber; A. Fink; E. Bohn. *J. Colloid Interface Sci.* **1968**, *26*, 62.
(115) P.A. Lovell; M.S. El-Asser. *Emulsion Polymerization and Emulsion Polymers. Wiley-VCH:New York* **1997**.
(116) M. Müller; R. Zentel; T. Maka; S.G. Romanov; Torres, C. M. S. *Polymer Preprints* **2000**, *41*, 811.
(117) Merck Patent GmbH. *DE 10209357 A1* **2003**.
(118) J. O. Santer. *Prog. Org. Coat.* **1984**, *12*, 309.
(119) M. Adams; Z. Dogic; S. L. Keller; S. Fraden. *Nature* **1998**, *393*, 349.
(120) P. Poulin; D. A. Weitz. *Phys. Rev. E* **1998**, *57*, 626.
(121) P. Poulin; H. Stark; T. C. Lubensky; D. A. Weitz. *Science* **1997**, *275*, 1770.
(122) P. Poulin; N. Frances; O. Mondain-Monval. *Phys. Rev. E* **1999**, *54*, 4384.
(123) V. A. Raghunatan; P. Richetti; D. Roux; F. Nallet; A. K. Sood. *Mol. Cryst. Liq. Cryst.* **1996**, *288*, 181.
(124) V. A. Raghunatan; P. Richetti; D. Roux. *Langmuir* **1996**, *12*, 3789.
(125) P. Poulin; V. A. Raghunatan; P. Richetti; D. Roux. *J. Physique II* **1994**, *4*, 1557.
(126) T. Kato; K. Minewaki; Y. Kawabata; M. Imai; Y. Takahashi. *Langmuir* **2004**, *20*, 3504.